STRUCTURAL ANALYSIS OF DDRB FROM *DEINOCOCCUS RADIODURANS*

STRUCTURAL ANALYSIS OF DDRB FROM *DEINOCOCCUS RADIODURANS*: INSIGHT INTO THE MECHANISM OF PROTEIN MEDIATED SINGLE-STRANDED DNA ANNEALING

By SEIJI N. SUGIMAN-MARANGOS, B.Sc.

A Thesis Submitted to the School of Graduate Studies in Partial Fulfillment of the Requirements for the Degree Doctor of Philosophy

McMaster University

DOCTOR OF PHILOSOPHY (2013) McMaster University
(Biochemistry and Biomedical Sciences) Hamilton, Ontario

TITLE: Structural analysis of DdrB from *Deinococcus radiodurans*: insight into the mechanism of protein mediated single-stranded DNA annealing.

AUTHOR: Seiji Nereus Sugiman-Marangos, B.Sc. (McMaster University)

SUPERVISOR: Dr. Murray S. Junop

NUMBER OF PAGES: xii, 177

ABSTRACT

Bacteria of the genus *Deinococcus* are perhaps the most resilient life forms ever discovered, demonstrating extreme resistance to ionizing radiation, ultraviolet radiation, desiccation, and a variety of mutagenic chemical agents. The most studied member of this genus, *D. radiodurans*, has been observed to rapidly reassemble its genome following severe fragmentation by hundreds of γ-radiation induced double-strand DNA breaks. Amongst the numerous factors contributing to DNA repair, a single-stranded annealing protein, DdrB, is believed to play an important role during the initial phases of recovery. The work described in this thesis represents the first structural characterization of DdrB, revealing a novel fold for single-stranded DNA binding. Together with biochemical data delineating the DNA-binding interface, two crystal structures of the DdrB/ssDNA complex were also solved, providing a comprehensive illustration of this interaction. Quaternary assemblies observed in these crystal structures also informed on the potential contribution of higher-order nucleoprotein complexes to the function of DdrB in single-stranded annealing. Most significantly, a face-to-face assembly of DdrB/ssDNA complexes provided insight into the mechanism by which DdrB mediates annealing of DNA, which may represent a common mechanism shared by other single-stranded annealing proteins.

ACKNOWLEDGEMENTS

I would like to start this thesis by thanking my supervisor, Dr. Murray Junop. The guidance and leadership that he has provided have been indispensable not only in carrying out the work presented in this thesis, but in my development as a scientist. His dedication to teaching, unwavering optimism, and extreme passion for science have served as an inspiration not only for myself, but also countless others that have spent time in his lab and his classrooms.

Thank you also to my committee members, Dr. Lori Burrows and Dr. Radhey Gupta, for their continued feedback and support throughout this voyage. Their careful criticisms and invaluable advice have contributed significantly to the direction that this project has taken. I would also like to thank Dr. Rodolfo Ghirlando for his expert contributions and meticulous attention to detail.

Thank you to the entire Junop lab, past and present. In particular, Dr. Sean Jackson and Dr. Sara Andres, thank you for your mentorship and friendship throughout the years. Special-thanks also to team *Deinococcus*: Matthew Czerwinski, Carly Willemsma, Chad Johnson, Joshua Chan, Erika Arseneau, Tana Shepherd, John Peel, Yoni Weiss, and Joey Laffradi. This work definitely would not have been possible without my army of undergraduate students.

Finally, I would like to thank my family: my parents Momoye Sugiman and Argyris Marangos; and my siblings Xenofon, Kiyoye, and Perseus. Your continuing love and encouragement to achieve my potential have molded me into the person I am today. Most importantly, thank you to my wife, Adrienne Li. Your love, patience and constant support throughout the entirety of this journey have been absolutely essential, and I am looking forward to our future together.

TABLE OF CONTENTS

FIGURES

Chapter 1 – Introduction

Chapter 2 – The structure of DdrB from *Deinococcus*: a new fold for single-stranded DNA binding proteins

Chapter 3 – Crystallization of the DdrB-DNA complex from *Deinococcus radiodurans*

Chapter 4 – Crystal structure of the DdrB/ssDNA complex from *Deinococcus radiodurans* reveals a DNA binding surface involving higher order oligomeric states

TABLES

ABBREVIATIONS

$^{\cdot}OH$ – hydroxyl radical
$^1O_2$ – singlet oxygen
3'-ssDNA – 3' ended strand of ssDNA
5'-ssDNA – 5' ended strand of ssDNA
6-4-PP – pyrimidine-(6-4)-pyrimidone photoproducts
6His – hexa-histidine
ASU – asymmetric unit
AUC – analytical ultracentrifugation
BER – base excision repair
BPP – bipyrimidine photoproducts
$c_{(s)}$ – sedimentation coefficient
CPD – cyclobutyl pyrimidine dimers
D_{10} – dose yielding 10% survival
D. radiodurans – *Deinococcus radiodurans*
DdrB – DNA damage response B
$DdrB_{Dg}$ – *Deinococcus geothermalis* DdrB
$DdrB_{Dr}$ – *Deinococcus radiodurans* DdrB
dG – deoxy-guanine
DNA – deoxyribonucleic acid
DSB – double-strand breaks
E. coli – *Escherichia coli*
EM – electron microscopy
EMSA – electrophoretic mobility shift assay

ESDSA – extended synthesis dependent strand annealing
FRET – Förster Resonance Energy Transfer
H2O2 – hydrogen peroxide
HR – homologous recombination
IPTG – isopropyl β-D-thiogalactopyranoside
IR – ionizing radiation
K_d – dissociation constant
MMC – mitomycin C
MMR – mismatch repair
Mn – manganese
NER – nucleotide excision repair
NHEJ – non-homologous end joining
NSLS – national synchrotron light source
$O2^-$ – superoxide
OB – oligonucleotide-binding
PC – protein carbonylation
PDB – protein databank
Pol I – DNA polymerase I
Pol III – DNA polymerase III
$RecA_{Dr}$ – *Deinococcus radiodurans* RecA
$RecA_{Ec}$ – *Escherichia coli* RecA
RMSD – root mean squared deviation
ROS – reactive oxygen species
SAD – single-wavelength anomalous diffraction
SeMet - selenomethionine
SSA – single-strand annealing pathway
SSB – single-stranded binding protein
SSB_{Dr} – *Deinococcus radiodurans* SSB
SSB_{Ec} – *Escherichia coli* SSB
ssDNA – single-stranded DNA
SSM – secondary-structure matching
T3SS – type III secretion system
T4P – type IV pilus
TBE - Tris/Borate/EDTA
UV – ultraviolet
vdW – van der Waals

CHAPTER 1 – INTRODUCTION

1.1 DNA Damage

The hereditary information essential to a cell's growth and maintenance is encoded in its deoxyribonucleic acid (DNA). Protecting this information from both exogenous and endogenous damage is therefore of utmost importance. The most common type of stress, oxidative damage, is generated through the action of reactive oxygen species (ROS), which are produced at a constant rate by both metabolic processes in a cell, and external stimuli such as ionizing radiation (Figure 1.1). Hydrogen peroxide (H_2O_2), superoxide (O_2^-), singlet oxygen ($^1O_2$), and hydroxyl radical ($^{\cdot}OH$) all possess sufficient reactivity to induce strand breakages and damage DNA bases. The majority of damage carried out by ROS occurs in the form of base modification, of which over 80 different types have been observed (Bjelland & Seeberg, 2003). Interaction with the sugar-phosphate backbone of DNA results in the formation of single-strand breaks, and clusters of lesions in close proximity can result in the formation of double-strand breaks (Kozmin *et al.*, 2009). As a single, unresolved double-strand break can be lethal to a cell, bacteria possess extensive mechanisms to detoxify ROS (e.g., catalase, superoxide dismutase, peroxidase, and Dps proteins) (Tian *et al.*, 2004) as well as to repair double-strand breaks, which takes place primarily through homologous recombination (HR).

Ultraviolet (UV) radiation in the far spectrum (UVB 290-320 nm; UVC <290 nm) damages DNA primarily through the induction of covalent linkages between

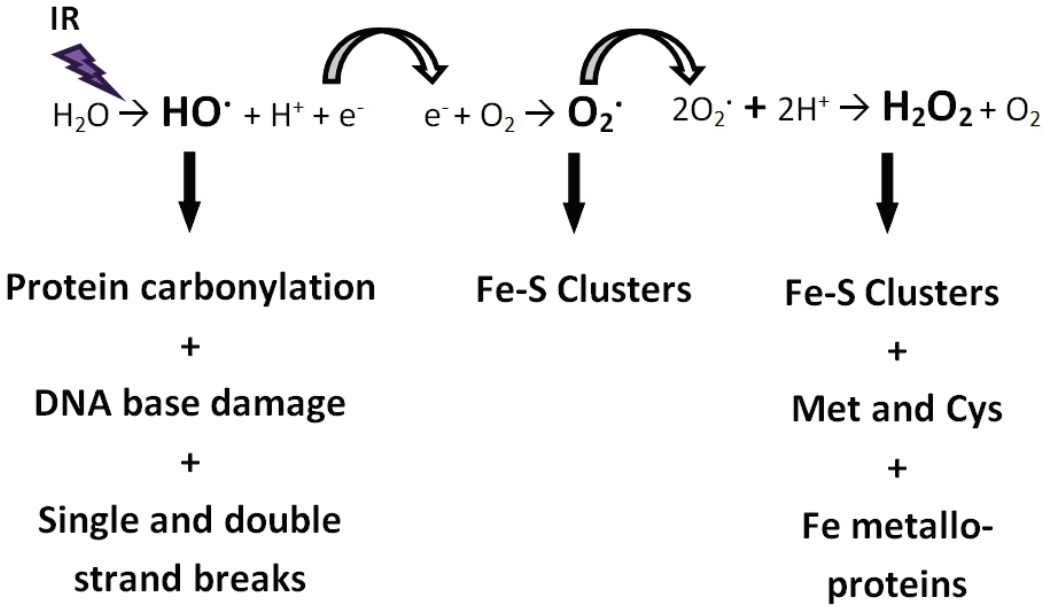

Fenton Reaction

$$Fe(II) + H_2O_2 \rightarrow Fe(III) + HO^{\cdot} + OH^-$$

Figure 1.1 Generation of ROS by radiolysis of H_2O. Cleavage of H_2O by ionizing radiation generates the short-lived, highly reactive hydroxyl radical ($HO^{\cdot}$), hydrogen (H^+) and a free electron (e^-). Free electrons generated by this reaction react with molecular oxygen (O_2) to form the superoxide radical ($O_2^{\cdot}$), which in turn react with hydrogen to generate hydrogen peroxide (H_2O_2). Oxidation of ferrous iron (Fe(II)) by hydrogen peroxide is a significant source of hydroxyl radical in proximity of iron metallo-proteins. Each type of ROS has differential effects on protein and DNA as discussed in Section 1.4.2.

DNA bases, producing cyclobutyl pyrimidine dimers (CPD) and pyrimidine-(6-4)-pyrimidone photoproducts (6-4-PP). These lesions can be lethal in bacteria if left unrepaired in large numbers, and are mutagenic if bypassed during replication or repaired incorrectly (Pfeifer, 1997). A number of different enzymes are involved in the repair of UV-induced lesions such as photolyases, DNA glycosylases, and nucleotide excision repair (NER) proteins. Additionally, UV radiation can produce ROS, and therefore is an indirect cause of strand breakages and base damage.

Adducts formed by the covalent linkage of chemical agents to DNA bases is another major form of damage that can be produced in a cell or introduced from the environment. Lipid oxidation is a significant source of potentially mutagenic agents such as acrolein and malondialdehyde, which result in disruption of Watson-Crick base pairing and therefore incorporation of incorrect bases during replication (De Bont & van Larebeke, 2004). These adducts, as well as clastogens such as Mitomycin C (MMC) and cisplatin, can also form covalent interstrand cross-links, blocking replication and transcription (Crooke & Bradner, 1976). Removal of DNA adducts and crosslinks in bacteria make use of base excision repair (BER) and NER proteins as well as the HR pathway.

1.2 Deinococcus

Of the countless organisms existing on this planet, bacteria of the genus *Deinococcus* are perhaps the most resistant to the effects of DNA damage. The first species isolated, *Deinococcus radiodurans* (*D. radiodurans)*, was discovered

in 1956 from a can of spoiled meat which had been treated with 4 kGy of γ-radiation (Anderson *et al.*, 1956). It wasn't until several years later that it was re-classified along with a number of other phylogenetically related bacteria into the phylum *Deinococcus* (Brooks & Murray, 1981). This genus now comprises 42 species which all share *D. radiodurans*' remarkable resilience to the effects of ionizing radiation. In addition to ionizing radiation, *Deinococcus* are also resistant to desiccation, UV, H_2O_2, MMC, and a variety of DNA base damaging agents (Battista, 1997).

1.2.1 General characteristics

D. radiodurans is red-pigmented, Gram-positive, mesophilic, and non-pathogenic. It has a doubling time of approximately 2 hours in TGY media at 30^{o}C. The genome of *D. radiodurans* is 3.28 Mb, consisting of 2 chromosomes (2.6 Mb and 0.4 Mb) and 2 plasmids (177.5 kb and 45.7 kb) (White *et al.*, 1999). All four of the genetic elements consist primarily of protein coding regions (80.9-93.5%), of which one-third of the predicted open reading frames had no database matches when the genome was first published. At all times, there are at least 2 complete copies of the genome present, with up to 10 copies dependent on the growth phase and media composition (Hansen, 1978, Harsojo *et al.*, 1981). Analysis of the genome of *D. radiodurans* revealed that it contains homologues to well characterized canonical DNA repair pathways, including BER, NER, HR, and mismatch repair (MMR) (Makarova *et al.*, 2001).

1.2.2 Ionizing radiation

Of all the stresses to which *D. radiodurans* is resistant, its tolerance to ionizing radiation remains the most impressive. An acute dose of ionizing radiation of 8 Gy is considered to be a lethal dose in humans, while *Escherichia coli* (*E. coli)* has a D_{10} (dose at which 10% of the population has survived) of ~82 Gy (Arrage *et al.*, 1993). *D. radiodurans* has a shoulder of resistance up to 5,000 Gy, experiencing no loss of viability, with a D_{10} of ~7,000 Gy (Battista, 1997). It is estimated that *D. radiodurans* accumulates DNA damage at approximately the same rate as non-radiation resistant organisms (Slade & Radman, 2011); a dose of 6,000 Gy results in the formation of approximately 200 double-strand breaks, 3,000 single-strand breaks, and a very large number of damaged bases per genome copy (Burrell *et al.*, 1971). Despite its DNA being shattered into hundreds of pieces, *D. radiodurans* is not only able to recover, but also do so rapidly (Zahradka *et al.*, 2006) and with high fidelity (Repar *et al.*, 2010). A number of factors have been proposed to be involved in this process which will be discussed in detail later (Sections 1.4 and 1.5).

1.2.3 UV-C radiation

D. radiodurans is approximately 20-fold more resistant to the effects of short-wave UV-C (254 nm) than *E. coli*, possessing D_{10} values of ~910 J/m^2 and ~40 J/m^2, respectively (Arrage *et al.*, 1993). UV damage in *D. radiodurans* is repaired by a combination of recombinational repair and NER, making use of two

independent endonucleases (UvrA and UvsE) (Minton, 1994), while notably lacking direct-damage reversal by photolyase and functional SOS-response machinery (Makarova *et al.*, 2001). A sub-lethal UV exposure of 500 J/m^2 results in the formation of tens of thousands of bipyrimidine photoproducts (BPPs), which are then excised by UvrA or UvsE (Moeller *et al.*, 2010) and released into the medium (Boling & Setlow, 1966). High doses of UV have also been observed to induce extensive genomic fragmentation (Bonura & Smith, 1975) attributed to a combination of collapsed replication forks as a result of encountering gaps from BPP excision, closely spaced BPPs on opposing strands, and oxidative damage from ROS. In fact, it has been reported that in total, 9% of the genomic content of the cells is released into the medium following exposure to 500 J/m^2, corresponding to approximately 50 bases of DNA per BPP (Varghese & Day, 1970). Mutations in recombinational repair proteins *recA (Tanaka et al., 2005)*, *recO* (Xu *et al.*, 2008), and *recF* (Chang *et al.*, 2010) all render *D. radiodurans* as sensitive to UV damage as mutations in *uvrA* and *uvsE* (Tanaka *et al.*, 2005). The extent of DNA degradation and fragmentation following excision of BPPs is thought to be the reason why recombinational repair is so essential to recovery following UV damage.

1.2.4 Mitomycin C

MMC is a chemotherapeutic agent that forms deoxy-guanine (dG) mono-adducts, dG-dG intrastrand cross-links (GG sites), and dG-dG interstrand cross-

links (GC sites) (Weng *et al.*, 2010). In addition to blocking transcription, excision of these adducts leads to the formation of double-strand breaks (Kitayama *et al.*, 1983). *D. radiodurans* is approximately 4-fold more resistant to the lethal effects of MMC than *E. coli* and immune to the mutagenic effects observed in *E. coli* following sub-lethal doses (Sweet & Moseley, 1976). Similar to *E. coli*, *D. radiodurans* is thought to remove MMC-related adducts via excision and recombinational repair, as demonstrated by the MMC-sensitivity of *recA* (Gutman *et al.*, 1994) and *uvrA* (Moseley & Evans, 1983) mutant strains.

1.2.5 Desiccation

The "desiccation adaptation hypothesis" is currently the most widely accepted explanation of the damage resistant phenotype of *Deinococcus*. As naturally occurring terrestrial sources of intense ionizing radiation are very few in number and desert environments have been present throughout the earth's history, it is thought that radiation resistance is a consequence of adaptation to periods of intense dehydration (Mattimore & Battista, 1996). To demonstrate this, 41 strains of *D. radiodurans* identified as "radiation-sensitive" were assayed for their tolerance to desiccation and all found to be equivalently sensitive (Mattimore & Battista, 1996). Furthermore, the correlation between resistance to ionizing radiation and desiccation holds true in unrelated bacteria outside of the *Deinococcus* genus (Shukla *et al.*, 2007).

While cultures of *E. coli* desiccated in a laboratory setting are reduced to less than 0.1% survival rate after only 2 days at <5% relative humidity, cultures of *D. radiodurans* survive 14 days under the same conditions with no loss of viability (Mattimore & Battista, 1996). The effects of desiccation on cellular components appear to be 2-fold: first, the decrease of available water causes proteins to denature and the levels of ROS in the cell to increase (Slade & Radman, 2011); and second, cellular processes are in stasis, allowing damage to accumulate until permissive growth conditions are restored (Potts, 1994). As a result, the types of damage observed in cells subjected to desiccation are similar to those observed in cells exposed to ionizing radiation. Transcriptome analysis of cultures of *D. radiodurans* recovering from exposure to ionizing radiation and desiccation revealed a sub-set of genes responding to both stimuli, including genes involved in DNA maintenance, ROS scavenging, and a number of conserved hypothetical proteins of unknown function (Tanaka *et al.*, 2004).

1.3 Damage response (Figure 1.2)

Damage response in *D. radiodurans* follows a systematic sequence of phases with durations dependent on the extent of damage incurred. Immediately following exposure to ionizing radiation, DNA synthesis is arrested and the cells enter a lag phase (Zahradka *et al.*, 2006, Driedger & Grayston, 1971). During this time, damaged bases are excised, and exposed DNA ends are digested by 5'->3' exonucleases (Lett *et al.*, 1967), yielding long stretches of

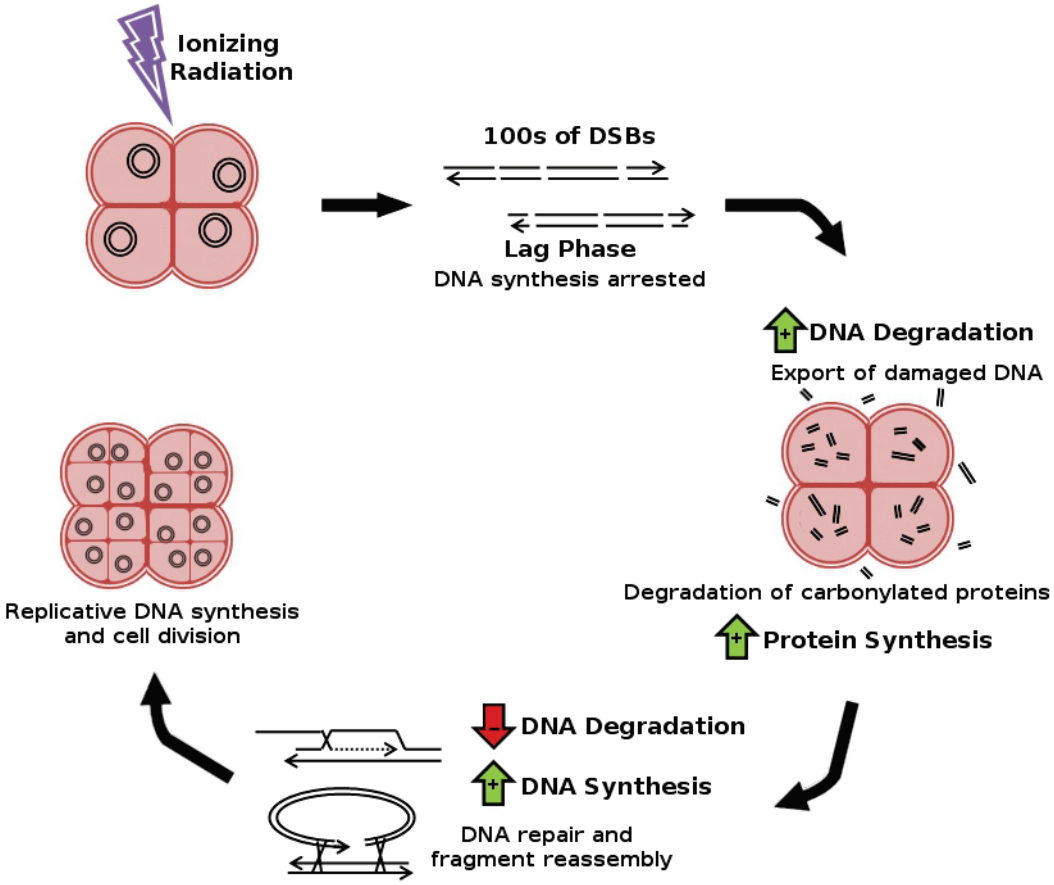

Figure 1.2 Damage response in *D. radiodurans*. Fragmentation of the genomic DNA by an acute dose of ionizing radiation results in a lag phase in which DNA synthesis is arrested. Damaged DNA is degraded and exported from the cell, carbonylated proteins are digested by proteases, and a damage response modulon is induced. Resumption of DNA synthesis is only initiated once degradation has subsided, and is absolutely required for DNA repair. Once the genome has been reassembled, replicative DNA synthesis and cell division resume.

single-stranded DNA (ssDNA) which serve as substrates to the single-stranded annealing pathway (SSA), RecA-mediated strand-invasion, and HR. The extent of DNA degradation increases linearly with the severity of the damage and is thought to be regulated in part by the activity of polymerase I (Pol I). UV17, a strain of *D. radiodurans* partially deficient in Pol I activity, degrades up to twice as much DNA as wild-type bacteria recovering from the same dose of ionizing radiation (Bonura & Bruce, 1974). Damaged bases excised by NER and nucleotides resulting from exonucleolytic digest of free ends are exported from the cell and further processed by an extracellular nuclease that is associated with the outer membrane (Mitchel, 1978). Following exposures >5 kGy of ionizing radiation, even large segments of ssDNA (~1 kb) have been observed in the medium which are then rapidly degraded to mono-nucleotides and potentially taken back into the cell once DNA synthesis has resumed (Vukovic-Nagy *et al.*, 1974). The export of damaged DNA, which can account for upwards of 20% of the genomic content of a cell (Bonura & Bruce, 1974), is thought to occur as a means of protecting the cell from mutagenesis through the incorporation of damaged bases (Battista, 1997).

DNA synthesis is absolutely essential for recovery in irradiated cells and is a tightly regulated process that does not resume until DNA degradation has begun to abate (Dean *et al.*, 1966). During repair, synthesis is carried by two DNA polymerases, with Pol I taking a secondary role to DNA polymerase III (Pol

III) (Slade *et al.*, 2009). While Pol I functions primarily in filling small gaps and fragment maintenance (Bonura & Smith, 1975), Pol III is involved in extended synthesis dependent strand annealing (ESDSA), which will be discussed later in detail (Section 1.5.3).

Recovery requires healthy growing conditions and depends on *de novo* protein synthesis. Treatment with chloramphenicol (a bacteriostatic antibiotic targeting the ribosome, inhibiting protein synthesis) of *D. radiodurans* cells recovering from ionizing radiation immediately following, and 30 minutes subsequent to exposure, have dramatically different effects on survival (Driedger & Grayston, 1971). In cells unable to synthesize new protein, the only type of damage repaired is direct sealing of single-strand breaks, which does not require conditions promoting growth or DNA synthesis. In addition to repair proteins, a radiation inducible inhibitor of DNA degradation (IrrI) may be involved in mediating the switch from degradation and export to synthesis and repair (Udupa *et al.*, 1994).

Due to the importance of *de novo* protein synthesis during recovery, the damage induced transcriptome has been analyzed in *D. radiodurans* following both ionizing radiation and desiccation (Tanaka *et al.*, 2004, Liu *et al.*, 2003), and in *D. gobiensis* recovering from irradiation by UV-C (Yuan *et al.*, 2012). In total, 72 genes are induced at least 3-fold relative to exponential growing cells following an acute ionizing radiation dose of 3 kGy. Of these, 33 are in common

with genes induced in cells recovering from 2 weeks held at 5% relative humidity (Tanaka *et al.*, 2004). Within this subgroup, there are proteins involved in HR (RecA, RuvB), NER (UvrA, UvrB), general DNA metabolism (GyrA, GyrB), and the largest fraction corresponds to hypothetical proteins of unknown function (PprA and 16 DNA damage response proteins designated DdrA-P). PprA, DdrA, and DdrB have all since been implicated in DNA repair in *Deinococcus* (Narumi *et al.*, 2004, Bouthier de la Tour *et al.*, 2011, Harris *et al.*, 2004), discussed later in detail (Section 1.5.5).

Cells are only able to recommence DNA replication once all the damage has been repaired, indicating that there is a cellular switch present controlling cell division. To date, only one protein (ClpPX) has been identified that may be involved in this regulation. ClpPX is an ATP-dependent protease which when rendered inactive, results in cells with long lag periods post-repair and abnormalities in chromosome segregation and cell division (Servant *et al.*, 2007).

1.4 Factors contributing to damage resistance

Damage recovery in *D. radiodurans* requires both protein and DNA synthesis and the correlation between radiation dose and repair kinetics suggests the existence of regulated checkpoints for DNA degradation, export, synthesis, and replication. None of these processes, however, are unique to *Deinococcus* and do little to explain the extent of damage from which these bacteria can recover. Efforts to identify a single determinant of damage resistance in *Deinococcus* have

been thus far unsuccessful. Instead, a number of factors have been suggested to contribute to *Deinococcus'* resilience, which can be grouped into three major categories: physical scaffolding (Section 1.4.1), ROS scavenging (Section 1.4.2), and DNA repair (Section 1.5).

1.4.1 Physical scaffolding

Past efforts to explain the radiation resistance of *D. radiodurans* have pointed towards a peculiar 'toroidal' (doughnut-shaped) arrangement of the genomic DNA observed in stationary phase cells (Levin-Zaidman *et al.*, 2003). It was proposed that this condensed form of the genomic content of the cell aided in maintaining the proximity of broken ends through mechanical scaffolding and that these breaks could then be re-sealed in a fashion similar to eukaryotic non-homologous end joining (NHEJ). The absence of any genetic evidence for NHEJ in *Deinococcus* (Daly & Minton, 1996), the reliance on recombinational repair requiring a template strand (Daly *et al.*, 1994), the enhanced radiation resistance of cells grown in media abrogating toroid formation (Daly *et al.*, 2004), and the fact that this is not a characteristic shared by all *Deinococcus* (Zimmerman & Battista, 2005), all provide evidence against any contribution of this phenomenon to radiation resistance. Nevertheless, physical effects such as the formation of DNA-membrane complexes (Burrell *et al.*, 1971) and pre-alignment of homologous chromosomes (Minton & Daly, 1995) are still considerations as contributors to the damage resistance phenotype.

1.4.2 ROS scavenging and protection of the proteome

D. radiodurans has a comprehensive array of cell cleaning enzymes and free radical scavengers to counteract the deleterious effects of ROS produced following both irradiation and desiccation. In addition to export from the cell (as discussed in Sections 1.2.3 and 1.3), damaged nucleotides are targeted for degradation by Nudix family hydrolases (Xu *et al.*, 2001) and nucleotidases (Kota *et al.*, 2010). *D. radiodurans* contains 23 different Nudix hydrolases, which is double the number found in *E. coli*. Of these, 5 are up-regulated following irradiation (Liu *et al.*, 2003). This theme of redundancy extends to the family of subtilisin-like proteases, which is also significantly expanded relative to *E. coli* (Makarova *et al.*, 2001). Proteolysis is induced in the lag phase following damage, removing modified, inactive or otherwise damaged proteins that are then resynthesized (Joshi *et al.*, 2004).

Although it has been demonstrated that *D. radiodurans* accumulates DNA damage at the same rate as non-radiation resistant bacteria, there is clear evidence that the proteome is considerably protected from oxidative damage (Daly *et al.*, 2007, Krisko & Radman, 2010). Protein carbonylation (PC) refers to the oxidation of amino acid side chains by ROS to generate reactive aldehydes and ketones, and is commonly used as a biomarker of oxidative stress (Dalle-Donne *et al.*, 2006). Unlike damage to the DNA, where strand breakages are observed at the same frequency despite disparate survival rates, the level of PC

detected in *D. radiodurans* is 20 to 30-fold lower than that in *E. coli* at the same dose of radiation (Krisko & Radman, 2010). However, a clear correlation is still observed between increasing PC and decreasing cell viability in both organisms. The observed discrepancy in oxidative damage to DNA and protein is counter to the long-held theory that ROS damage biological macromolecules indiscriminately. Radiolysis of water produces three primary reactive bi-products: H_2O_2, $HO^{\cdot}$, and O_2^{-} (Figure 1.1). While all have the propensity to inflict damage, it has been demonstrated that these ROS have differential effects on protein and DNA. O_2^{-} is an inefficient oxidizing agent because of its negative charge and does not act directly on DNA or amino acids (Imlay, 2003). Instead, it mainly targets iron-sulfur clusters but does not oxidize the coordinating residues (Flint *et al.*, 1993, Imlay, 2003). Metallo-proteins containing iron-sulfur clusters play a central role in metabolism and cellular respiration (Roche *et al.*, 2013), and their inactivation would result in termination of metabolic activity. H_2O_2 also does not damage DNA, but will readily oxidize sulfur containing residues and residues coordinating either iron or iron containing ligands (Imlay, 2003). $HO^{\cdot}$ is generated from both radiolysis of water and the Fenton reaction (Figure 1.1), and can oxidize proteins and DNA. Unlike H_2O_2 and O_2^{-}, which persist for lengthy periods of time unless scavenged, $HO^{\cdot}$ is short-lived and only reacts with molecules in its immediate proximity (Imlay, 2008).

D. radiodurans possesses an arsenal of catalases, peroxidases, and superoxide dismutases for the enzymatic scavenging of ROS (Makarova *et al.*, 2001). Although the relative activity of these enzymes are elevated in *D. radiodurans* in comparison to *E. coli*, mutants deficient in catalase and superoxide dismutase activity were found to be only marginally sensitive to ionizing radiation (Markillie *et al.*, 1999). Moreover, in an assay of seven strains of *Deinococcus*, there was no correlation found between elevated enzymatic scavenging of ROS and ionizing radiation resistance (Shashidhar *et al.*, 2010). This suggests that the primary function of these enzymes rests in scavenging ROS arising from regular cellular events, and that they are of reduced importance in responding to ROS generated from external stimuli.

Instead, the main contributor to antioxidant activity is thought to be elevated concentrations of intracellular manganese (Mn) and the resultant high Mn/Fe ratio that is common not only across the *Deinococcus* family, but also in unrelated organisms also resistant to ionizing radiation (Daly *et al.*, 2007, Daly, 2009, Daly *et al.*, 2010). *D. radiodurans* grown in TGY (D_{10} ~16 kGy) contains a concentration of Mn of approximately 0.36 nmol/mg of protein, and a Mn/Fe ratio of approximately 0.24, compared to *E. coli* (D_{10} ~0.7 kGy) and *S. oneidensis* (D_{10} ~0.07 kGy) containing Mn concentrations of 0.0197 nmol/mg and 0.0023 nmol/mg, and Mn/Fe ratios of 0.0072 and 0.0005, respectively (Daly *et al.*, 2004). Furthermore, when grown in media lacking Mn, the D_{10} of *D. radiodurans*

is reduced to <2.5 kGy (Daly *et al.*, 2004). The effects of an elevated Mn/Fe ratio are thought to be two-fold: first, Mn-complexes formed with orthophosphate and peptides act as efficient non-enzymatic scavengers of H_2O_2 and O_2^- (Daly *et al.*, 2010); and second, attenuated $HO^\cdot$ generation by the Fenton reaction. $HO^\cdot$ present due to Fenton chemistry is only produced in proximity of Fe, and therefore targets primarily Fe-metallo-proteins, while $HO^\cdot$ generated by radiolysis of H_2O is indiscriminate.

The selective reduction of ROS which specifically oxidize proteins in *Deinococcus* explains the disproportionate protection of protein over DNA that has been observed following irradiation. Lack of protection of DNA therefore necessitates an extremely coordinated and efficient mechanism for DNA repair. As the work described in this thesis pertains to a protein involved in double-strand break repair, the following section will explore what is known about this pathway in *Deinoccocus*.

1.5 Recombinational DNA repair in *D. radiodurans*

Fragmentation of the genomic DNA of *D. radiodurans* following acute ionizing radiation exposure has been observed by pulse-field gel electrophoresis (Grimsley *et al.*, 1991) and sucrose gradients (Burrell *et al.*, 1971). At the D_{10} dose of ~7,000 Gy, the average fragment size is in the range of 20-30 kb, consistent with 100-200 double-strand breaks per genome copy (Zahradka *et al.*, 2006). *Deinococcus* possess multiple copies of their genome (typically 4-10) at

all stages in their cell cycle and therefore always have a template from which to repair (Harsojo *et al.*, 1981). As strand breaks are a random event, the probability that a specific gene will be fragmented in the same location on every copy is therefore very low.

1.5.1 RecBCD pathway (Figure 1.3)

The RecBCD complex initiates homologous recombination in the majority of bacteria and has been extensively characterized in *E. coli* (Dillingham & Kowalczykowski, 2008). In the classic model, RecBCD binds to a free DNA end generated by a double-strand break and proceeds to both unwind and digest the exposed strands of ssDNA (with a preference for 3'->5' activity) (Muskavitch & Linn, 1982). Degradation continues until the enzyme reaches a specific 'chi' sequence (5'-GCTGGTGG), upon which the strand preference of DNA digestion reverses, terminating degradation of the 3'-ended strand (3'-ssDNA) and instead favouring 5'->3' exonuclease activity (Anderson & Kowalczykowski, 1997). The resultant 3'-ssDNA product is coated by SSB, preventing secondary structure formation and any further degradation (Muskavitch & Linn, 1982, Mackay & Linn, 1976). Perhaps the most important protein in recombinational repair, RecA, is then recruited to the ds/ssDNA junction by RecBCD, and polymerizes to form a helical filament (proceeding 5'->3', displacing SSB in the process) which is primed for strand invasion of homologous duplex DNA (Tsang *et al.*, 1985).

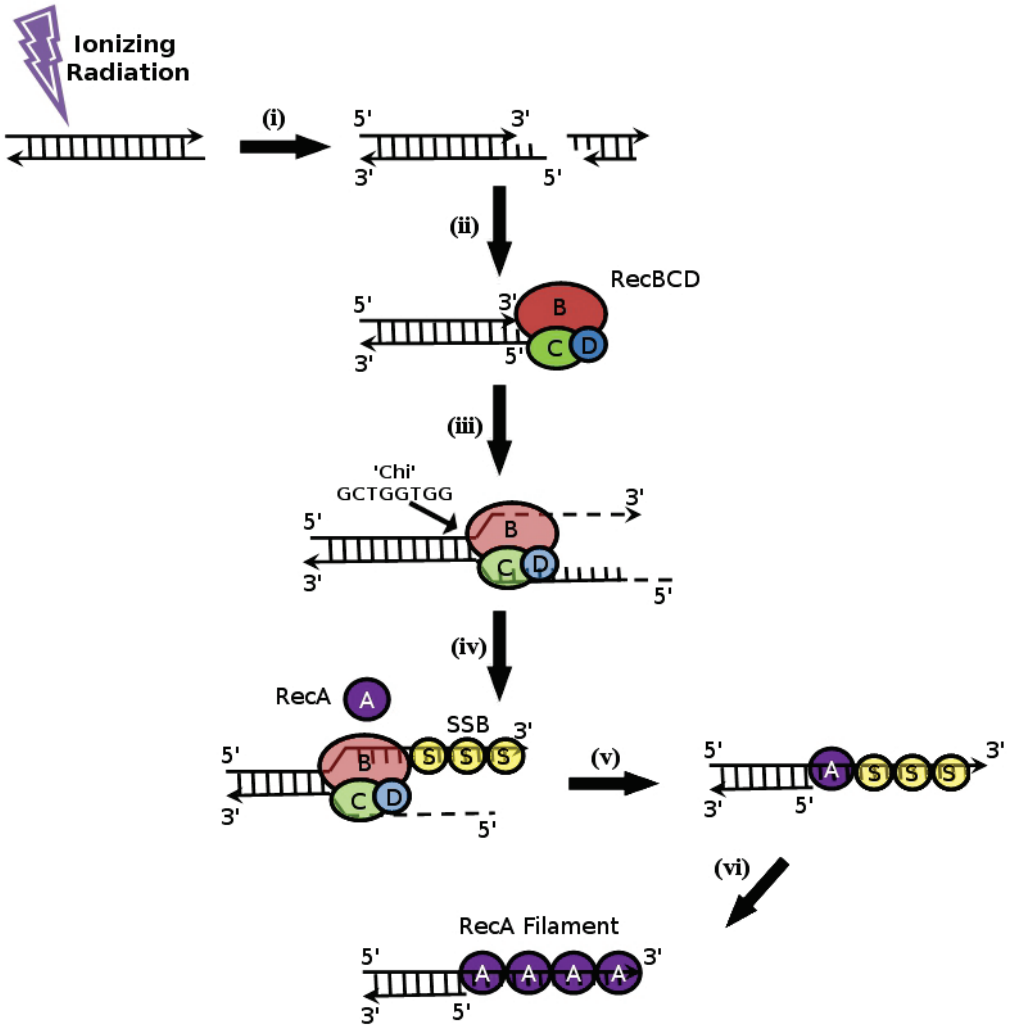

Figure 1.3 RecA loading by RecBCD. Broken ends (i) bound by RecBCD (ii) are unwound and digested 3'->5' (iii). Upon encountering the 'chi' sequence, exonuclease activity switches polarity to 5'->3', while SSB coats and protects exposed ssDNA (iv). RecA is recruited to the ss/dsDNA junction (v), and polymerizes 5'->3', displacing SSB and forming a helical filament on the 3'-ssDNA (vi).

D. radiodurans notably lacks homologues to *recB* and *recC*, and while it does encode a homologue to *recD*, deletion of this gene has been reported to have no effect on radiation resistance (Zhou *et al.*, 2007). In fact, heterologous expression of *E. coli recBC* in *D. radiodurans* results in a reduction of resistance in the wild-type strain of up to 2 log-cycles (Khairnar *et al.*, 2008), further strengthening the evidence that *D. radiodurans* initiates recombinational repair via a pathway other than RecBCD.

1.5.2 RecFOR pathway (Figure 1.4)

E. coli mutants deficient in *recBC* activity are able to initiate loading of RecA onto ssDNA by the RecFOR pathway (Lloyd & Buckman, 1985). In addition to encoding homologues to the key players in this alternative pathway of recombinational initiation (White *et al.*, 1999), heterologous expression of *E. coli sbcB* (inhibitor of the RecFOR pathway) renders *D. radiodurans* cells sensitive to irradiation (Misra *et al.*, 2006). Furthermore, deletion mutants of *recF*, *recO*, and *recR* all display similar radiosensitive phenotypes, comparable to deletion of *recA* (Bentchikou *et al.*, 2010). Taken together, these observations suggest that RecFOR is the principle pathway through which *D. radiodurans* initiates RecA mediated repair.

In *D. radiodurans*, it is thought that UvrD is the helicase responsible for unwinding of the DNA duplex in RecFOR mediated repair (rather than RecQ as in *E. coli*), allowing RecJ to digest the exposed 5’ ended strand of ssDNA (5’-ssDNA)

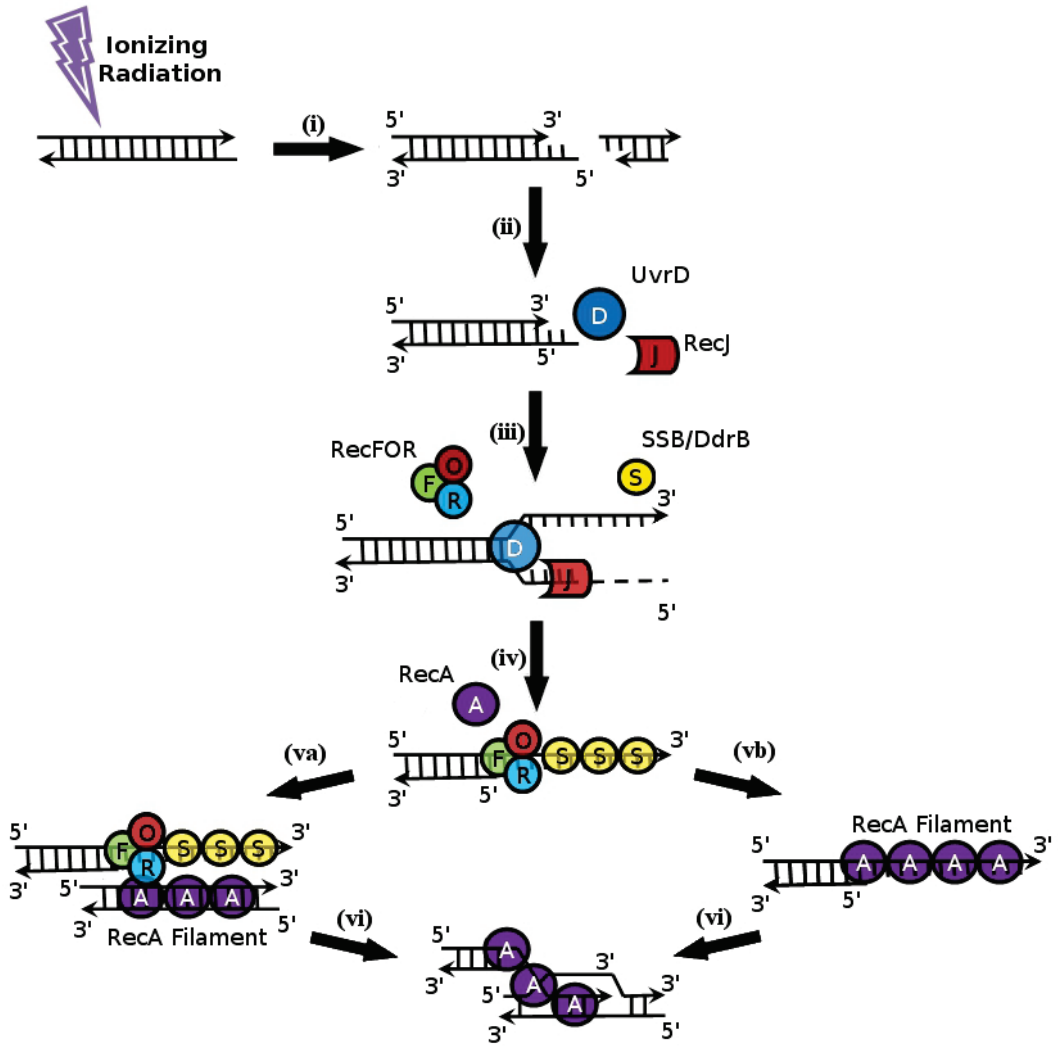

Figure 1.4 RecA loading by RecFOR. Broken ends (i) are bound by UvrD (ii), which unwinds the duplex while RecJ digests the 5' strand (iii). RecFOR is recruited to the ds/ssDNA junction while SSB coats and protects the 3'-ssDNA (iv). RecA, coating either a homologous duplex (va) or the 3'-ssDNA (vb), promotes strand exchange by homologous pairing of the ss and dsDNA (vi).

(Bentchikou *et al.*, 2010). The mechanism by which the nuclease activity of RecJ is halted remains unknown. The 3'-ssDNA is then coated with either SSB or the *Deinococcus* specific protein DdrB (Norais *et al.*, 2009), while RecFOR binds to the ds/ss-DNA junction (Timmins *et al.*, 2007). In contrast to *E. coli* RecA ($RecA_{Ec}$), *Deinococcus* RecA ($RecA_{Dr}$) promotes a reverse strand exchange reaction *in vitro*, binding dsDNA first and ssDNA second (Kim & Cox, 2002). Despite this observed difference *in vitro*, $RecA_{Dr}$ is able to fully complement a Δ*recA* strain of *E. coli* (Narumi *et al.*, 1999), so it is unclear what these observations mean for the mechanism of strand exchange *in vivo*. Whether RecA forms a helical filament on 3'-ssDNA as in *E. coli*, or coats duplex DNA prior to initiating a homology search for complementary ssDNA (Kim & Cox, 2002), the end result is RecA mediated strand-invasion by 3'-ssDNA into a homologous duplex.

1.5.3 Extended synthesis dependent strand annealing (Figures 1.5 and 1.6)

The observation that complete and efficient recovery from genome fragmentation requires massive DNA synthesis ruled out the possibility that conventional homologous recombination is the primary pathway of damage induced repair in *Deinococcus* (Zahradka *et al.*, 2006). Instead, it has been proposed that a variation of traditional recombinational repair, termed "extended synthesis dependent strand annealing", is the dominant mechanism for double-strand break repair.

In this model, a D-loop is formed by the RecA mediated strand-invasion of duplex DNA. Pol III initiates extension of the invading 3' overhang, carrying out the majority of DNA synthesis during double-strand break repair. Pol III is aided by Pol I, which can only extend but not initiate synthesis in a newly formed D-loop (Slade *et al.*, 2009). After extending the length of the invaded fragment, the ssDNA then dissociates and either invades another homologous duplex (to initiate a new round of extension), or anneals with a complementary extension generated through the same process (Zahradka *et al.*, 2006). Due to the rapidity of conversion of long ssDNA overhangs to duplex DNA, a model involving simultaneous extension along a single "bridging" fragment has been proposed (Figure 1.6) (Slade *et al.*, 2009). The final step in this process is recircularization of the newly formed duplex DNA fragments via a RecA mediated recombination event.

1.5.4 Single-stranded annealing (Figure 1.5)

In addition to ESDSA, fragment assembly has been observed in *D. radiodurans* preceding RecA dependent processes (Daly & Minton, 1996). This repair takes places both in wild-type and Δ*recA* strains and proceeds in the absence of major DNA synthesis (Slade *et al.*, 2009). Approximately one-third of double-strand breaks generated following an ionizing radiation dose of 10 kGy are repaired prior to RecA mediated repair, generating larger fragments which may serve as better substrates for ESDSA (Daly & Minton, 1996). It is thought

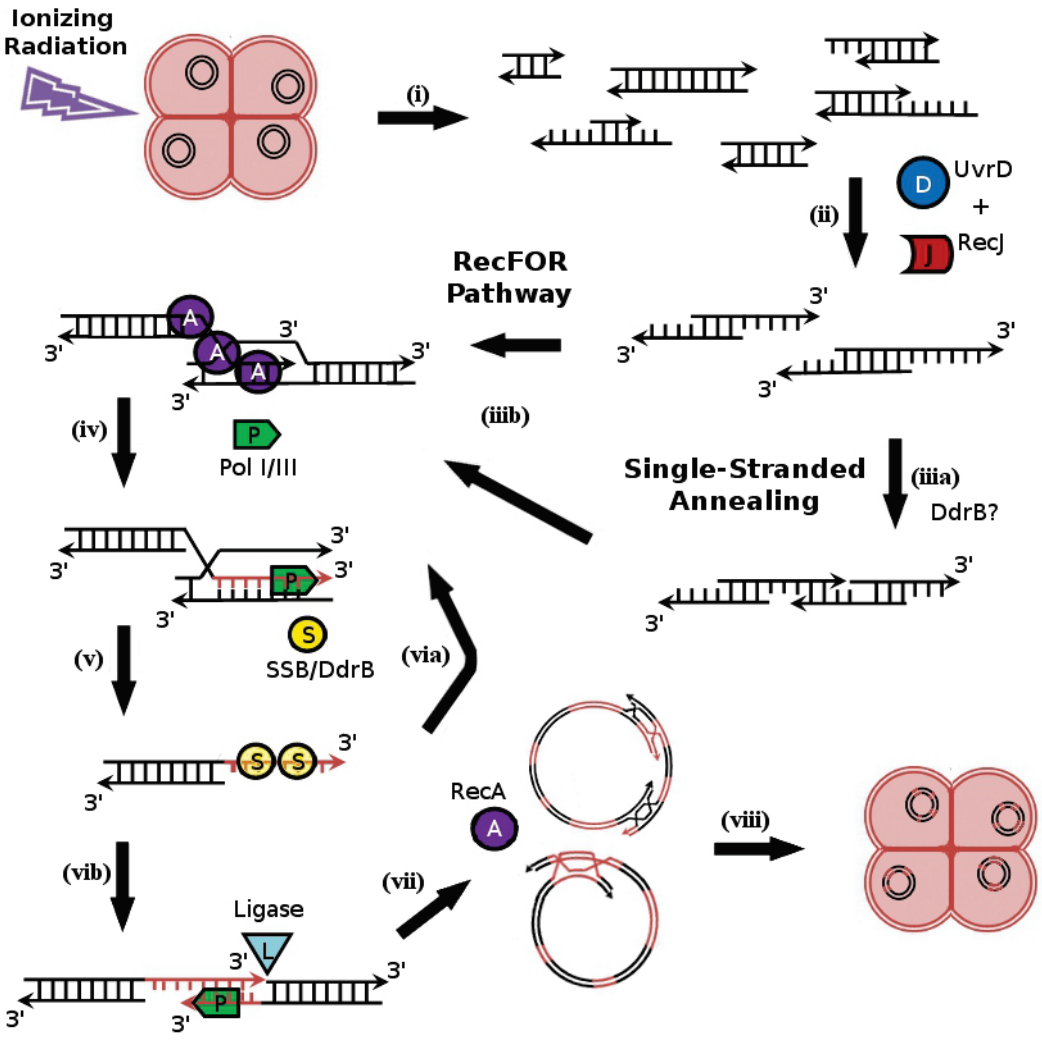

Figure 1.5 Double-strand break repair in *D. radiodurans*. Irradiation of *D. radiodurans* generates hundreds of fragments (i) which are processed by UvrD and RecJ (ii). Approximately one-third of the fragments are assembled into larger fragments by single-stranded annealing (iiia), which then participate in RecA-mediated strand-invasion (iiib). The invading 3'-ssDNA is extended by Pol I/III (iv) and then subjected to either a successive round of strand invasion (via) or anneal to a complementary fragment (vib). Any gaps in the annealed fragments are filled and nicks are sealed by ligase (vii). The reassembled fragments are then recircularized by RecA (viii).

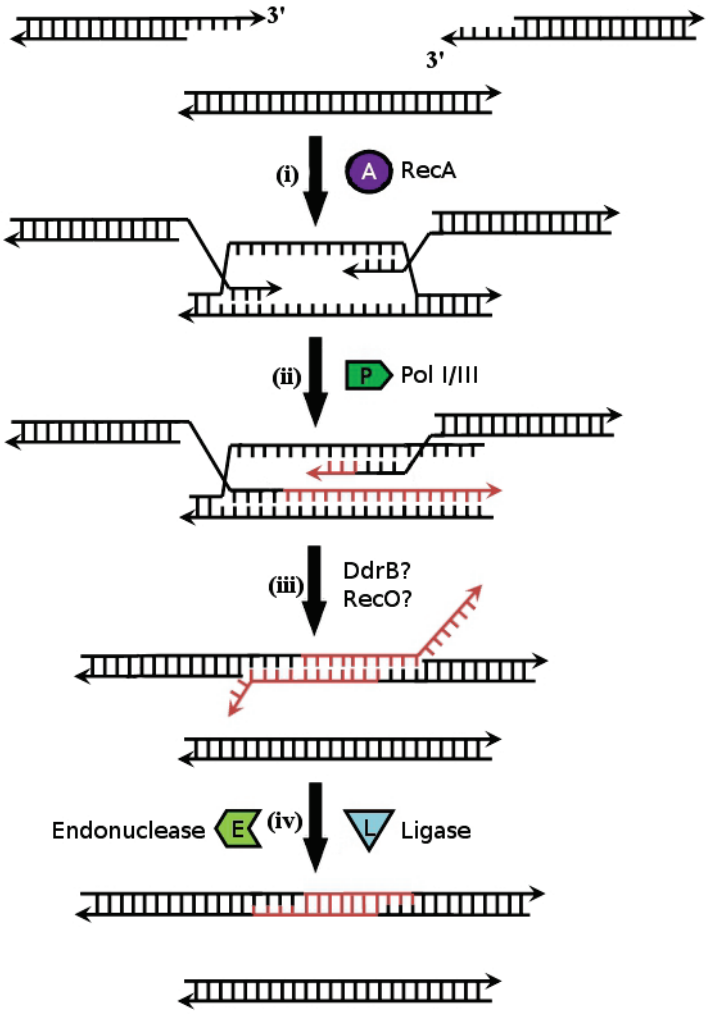

Figure 1.6 Synthesis along a bridging fragment. Two fragments missing a segment of sequence between them simultaneously invade a third fragment containing that intervening sequence (i). Both fragments are extended by Pol I/III (ii), dissociate from the bridging fragment, and anneal to each other (iii). Extraneous sequence is then trimmed by endonucleases while nicks are sealed by a ligase (iv).

that this RecA-indepedent process is mediated by an SSA pathway similar to what has been observed in *E. coli* (Daly & Minton, 1996, Kowalczykowski *et al.*, 1994). The proposed mechanism is as follows: 3'-ssDNA generated by UvrD and RecJ are annealed to a complementary fragment from a different genomic copy that has been processed in the same manner; overlapping fragments are then degraded; and any gaps are filled in by DNA polymerase (Daly & Minton, 1996). The subject of the research described in this thesis, DdrB, has been proposed to mediate this process and will therefore be discussed in detail throughout.

1.5.5 Novel proteins involved in repair

As ESDSA and SSA have recently been proposed in *Deinococcus* repair only a small number of key players have been confirmed (RecA, Pol I, Pol III, RecFOR, UvrD) (Slade *et al.*, 2009). The coordination and execution of such a complex process undoubtedly includes additional components that have not yet been identified. Among those in consideration, three of the novel proteins identified by transcriptional analysis of *D. radiodurans* recovering from irradiation have been suggested to play roles. PprA, DdrA, and DdrB are all found uniquely in *Deinococcus*, induced following irradiation, and homologues are present in all of the genomes that have been sequenced from the genus thus far. Deletion mutants of all three genes are sensitive to ionizing radiation, while combinations of double deletion mutants of *recA*, *pprA*, *ddrA*, and *ddrB* led to the classification of three separate epistasis groups (Tanaka *et al.*, 2004). Both

ddrA and *ddrB* were found to be epistatic to *recA* and to one another, while *recA* and *pprA* are believed to act within the same pathway. A different interpretation based on data presented in this thesis is that *ddrA* and *ddrB* may perform redundant functions, explaining why the deletion of both would render *D. radiodurans* more sensitive than either mutant alone.

1.6 Research outline

When work on this project began, it had been demonstrated that *ddrB* was induced 40-fold in response to ionizing radiation, that the deletion mutant was sensitized to radiation damage, and that it had a homologue in *D. geothermalis* (the only other genome sequence available at the time) (Tanaka *et al.*, 2004, Makarova *et al.*, 2007). The protein itself had never been cloned or purified, and its function was unknown. The goal of this project was to gain an understanding of the protein through its structural and biochemical characterization, and attempt to determine its involvement in damage recovery in *Deinococcus*. In Chapter 2, we report the crystal structure of DdrB from *D. geothermalis* and the previously uncharacterized ability to bind ssDNA. This structure represents a novel fold for ssDNA binding and also elucidates the oligomeric state of DdrB in solution. Building upon the knowledge that DdrB is a ssDNA binding protein (Norais *et al.*, 2009, and this work), Chapter 3 describes the crystallization of a DdrB from *D. radiodurans* in complex with ssDNA. Co-crystallization of protein and DNA can be a challenging undertaking and the

methods described in this chapter may provide assistance to others that encounter difficulties in this process. The analysis of the DdrB/ssDNA co-crystal structure featured in Chapter 4 is enhanced by evidence presented in the literature that DdrB is able to promote annealing of complementary strands of ssDNA (Xu *et al.*, 2010). We also report the *in vitro* biochemical characterization of a number of DdrB mutants based on the crystal structure, predict an extended DdrB/ssDNA interface, and propose a mechanism for DdrB's annealing activity. In Chapter 5, we report a second crystal structure of the DdrB/ssDNA that confirms the predictions we had made in Chapter 4. The structure captures a snapshot of DdrB mediating the annealing of a ssDNA/dsDNA intermediate, providing insight into the mechanism of protein mediated DNA annealing, which may be shared by other single-stranded annealing proteins such as eukaryotic Rad52. The final chapter comprises a summary of the research contained in this thesis, a discussion of its implications, and a description of unresolved questions to be answered and future work to be performed.

CHAPTER 2 – THE STRUCTURE OF DDRB FROM *DEINOCOCCUS*: A NEW FOLD FOR SINGLE-STRANDED DNA BINDING PROTEINS

Sugiman-Marangos, S., Junop, M.S. (2010). The structure of DdrB from *Deinococcus*: a new fold for single-stranded DNA binding proteins. *Nucleic Acids Research* **38**: 3432-3440
Reproduced with permission from Oxford University Press (#3180780566089)

2.1 Author's Preface

Research presented in Chapter 2 was published in the peer-reviewed journal *Nucleic Acids Research* and is presented in published form (formatted to complement the rest of the thesis). This article described the structure of DdrB for the first time, presenting a novel fold for single-stranded DNA binding function. S.N. Sugiman-Marangos performed all of the experimental work described and wrote the manuscript with M.S. Junop.

Figure 2.0 Cover Image. The method by which the bacterial family *Deinococcus* is able to recover rapidly from extensive radiation damage is still poorly understood. Shown is the structure of the *Deinococcus* specific single-stranded DNA binding protein DdrB, which possesses a novel fold and has been demonstrated to play an important role in extreme damage recovery.

2.2 Abstract

Deinococcus spp. are renowned for their amazing ability to recover rapidly from severe genomic fragmentation as a result of exposure to extreme levels of ionizing radiation or desiccation. Despite having been originally characterized over 50 years ago, the mechanism underlying this remarkable repair process is still poorly understood. Here we report the 2.8 Å structure of DdrB, a single-stranded DNA binding protein unique to *Deinococcus* spp. that is crucial for recovery following DNA damage. DdrB forms a pentameric ring capable of binding single-stranded but not double-stranded DNA. Unexpectedly, the crystal structure reveals that DdrB comprises a novel fold that is structurally and topologically distinct from all other single-stranded binding proteins characterized to date. The need for a unique single-stranded DNA binding function in response to severe damage, suggests a distinct role for DdrB which may encompass not only standard single-stranded binding protein function in protection of single-stranded DNA, but also more specialized roles in protein recruitment or DNA architecture maintenance. Possible mechanisms of DdrB action in damage recovery are discussed.

2.3 Introduction

Of the various types of damage that can occur within a cell, damage to genetic material in the form of DNA double-strand breaks (DSB) is particularly detrimental. A single unrepaired DSB is lethal to unicellular organisms such as

Escherichia coli, while incorrect repair can lead to the loss of important genetic information, potentially resulting in chromosomal re-arrangement and cancer in higher organisms (Pardo *et al.*, 2009). *Deinococcus* spp. possess remarkable resilience to DNA damage. The model organism *D. radiodurans* is able to withstand ~ 15,000 Gy of γ-radiation, which effectively shatters the genome into hundreds of fragments (~ 20-30 kb) (Zahradka *et al.*, 2006). Such a catastrophic event would be lethal several times over in the majority of terrestrial organisms, a lethal radiation dose in humans is in the range of 2-10 Gy, yet *D. radiodurans* is able to survive and accurately reassemble its genetic material in a matter of hours.

Since its discovery over 50 years ago (Anderson *et al.*, 1956), a number of mechanisms have been proposed to explain the extreme radiation resistance observed in *Deinococcus* spp. *D. radiodurans* does not prevent formation of DSBs and is observed to accumulate damage at the same rate as other, non-radiation resistant bacteria. Resistance to extreme ionizing radiation (IR) is thought to result from a combination of efficient protection of repair proteins by Mn^{2+}-dependent ROS scavengers (Zahradka *et al.*, 2006, Daly *et al.*, 2004, Daly *et al.*, 2007) and a robust repair pathway reliant on proteins unique to *Deinococcus* spp. (Zahradka *et al.*, 2006, Tanaka *et al.*, 2004, Slade *et al.*, 2009, Makarova *et al.*, 2007).

Repair in *D. radiodurans* that occurs in response to severe IR exposure takes place in a two-stage process. The first stage, termed **E**xtended **S**ynthesis **D**ependent **S**trand **A**nnealing (ESDSA), involves the formation of >20 kb long 3' single-stranded DNA (ssDNA) extensions. These unusual structures result from successive rounds of strand invasion of homologous fragments followed by Pol I- and Pol III-mediated extension (Zahradka *et al.*, 2006, Slade *et al.*, 2009). Exceptionally long stretches of ssDNA generated by this process must be protected from degradation, non-specific annealing, and self-association so that they can be efficiently converted into linear duplex DNA in the final stage of ESDSA. In the second stage of repair, long linear DNA molecules generated by ESDSA are pieced together to generate complete circular chromosomes via RecA-dependent homologous recombination.

Damage recovery is also dependent on *de novo* protein synthesis (Dean *et al.*, 1970). Microarray hybridization studies identified a small subset of *Deinococcus* spp.–specific genes that are highly up-regulated in response to extreme IR exposure and necessary for recovery (Tanaka *et al.*, 2004, Liu *et al.*, 2003). Of the proteins identified, **D**NA **D**amage **R**esponse **B** (DdrB) is perhaps the most intriguing. In *D. radiodurans*, *ddrB* (DR0070) experiences a >40-fold induction immediately following exposure to 3 kGy of γ-radiation, while a Δ*ddrB* strain experiences a 100-fold decrease in viability with respect to the wild-type strain following exposure to 10 kGy (Tanaka *et al.*, 2004). In addition to being

highly up-regulated and of obvious importance to damage recovery, DdrB is conserved within and unique to *Deinococcus* spp.

Recently, it was reported that DdrB may represent a member of a new family of bacterial single-stranded binding (SSB) protein (Norais *et al.*, 2009). SSBs are essential proteins found in organisms from all domains of life, which play an important role in DNA metabolism, replication, recombination and repair (Pestryakov & Lavrik, 2008). Each of these processes generate ssDNA, which has the tendency to form secondary structures and is susceptible to non-specific cleavage by rogue nucleases. SSBs protect and stabilize exposed ssDNA by wrapping the nucleic acid strand around a conserved flattened face of a 5-stranded β-barrel structure, known as an OB fold (Pestryakov & Lavrik, 2008). Single strand DNA makes multiple non-contiguous contacts with each monomer within a SSB tetramer (Raghunathan *et al.*, 2000). This mode of binding efficiently compacts ssDNA into a highly intertwined complex. SSBs also act as a recruiting scaffold for targeting other proteins and protein-complexes to the site of action (Pestryakov & Lavrik, 2008). Considering the importance of SSB function in protecting the hundreds of >20 kb ssDNA fragments generated during ESDSA, it is surprising that even under the stresses of massive DNA damage, *ssb* in *D. radiodurans* only experiences a slight increase in expression (~3-fold) (Liu *et al.*, 2003). Under the same conditions, *ddrB* expression is increased >40-fold, suggesting that it may substitute for SSB during damage recovery (Tanaka *et al.*,

2004). If DdrB is in fact an alternative SSB, unique to *Deinococcus* spp., it may serve to recruit a distinct set of proteins necessary for recovery from extreme IR exposure.

To date, all SSB homologues that have been characterized interact with their ssDNA substrates by means of a structurally conserved oligonucleotide-binding (OB) domain (Pestryakov & Lavrik, 2008). In this article, we report the X-ray crystal structure of DdrB from *D. geothermalis* to 2.8 Å resolution. Unexpectedly, DdrB was found to contain a novel ssDNA binding fold, which is structurally and topologically distinct from the OB-fold. DdrB, therefore represents the founding member of a new class of SSBs that lack the otherwise universal OB-domain.

2.4 Materials and methods

2.4.1 Protein expression and purification

DdrB (Dgeo_0295) from *D. geothermalis* was cloned into the pET151-D-topo vector (Invitrogen) according to the manufactures protocol and expressed in *E. coli* BL21(DE3) as an N-terminal hexa-histidine (6His) tagged protein. Cultures were grown at 37^{o}C to an OD_{600} of ~0.5 and induced with 1 mM isopropyl β-D-thiogalactopyranoside (IPTG) for 3 hours. DdrB labeled with SeMet was expressed in the methionine auxotrophic strain *E. coli* B834 using SeMet M9 media from Shanghai Medicilon Inc. (http://www.medicilonInc.com). DdrB-SeMet was expressed in the same manner as wild-type DdrB except that

the cells were induced with IPTG when the OD_{600} reached ~1.2. Cell pellets of both native and SeMet DdrB were resuspended in lysis buffer (20 mM Tris pH 8.0, 1 M NaCl, 5 mM imidazole) and lysed by sonication. Following clarification by centrifugation at 48,000 g, soluble lysate was loaded onto a 5 mL Ni-IMAC column at 1 mL/min using an AKTA FPLC. The bound protein was washed with 5 column volumes of wash buffer (105 mM imidazole) prior to elution (250 mM imidazole). Ni-IMAC column eluate was exchanged into low salt buffer (20 mM Tris pH 8.0, 150 mM KCl) prior to cleavage of the 6His tag with TEV protease. Un-cleaved fusion, cleaved 6His tag and TEV were separated from the cleaved DdrB by passing the TEV digestion mixture over the 5 mL Ni-IMAC column. Pure, untagged DdrB was collected in the flow through fraction (SI Figure 2.3).

2.4.2 Electrophoretic mobility shift assay

Nucleic acid binding experiments were performed in EMSA buffer (20 mM Tris pH 8.0, 150 mM NaCl, 10% glycerol) by mixing 150 pmol of 20b ssDNA, 20bp dsDNA or 20b ssRNA for 15 minutes with increasing amounts of DdrB (100, 250, 500, 1000 pmol). The reactions were resolved by electrophoresis on a 10% polyacrylamide native TBE gel running at 80 V for 1 hour.

2.4.3 Structure determination of DdrB

All DdrB crystals were grown at 20^{o} C using the hanging-drop vapour diffusion method. Equal volumes (1 µL) of native DdrB (24.7 mg/mL) and crystallization solution (0.1 M sodium acetate anhydrous pH 4.6, 2 M ammonium

sulfate) were mixed and dehydrated over 0.5 mL 1.5 M ammonium sulfate. SeMet DdrB (25 mg/mL) was mixed with an equal volume (3 µL) of crystallization solution (0.1 M sodium acetate anhydrous pH 5.5, 2.45 M ammonium sulfate, 0.01 M Praseodymium(III) acetate hydrate) and dehydrated against 0.5 mL 1.5 M ammonium sulfate. DdrB-SeMet crystals were transferred into cryogenic buffer (0.1 M trisodium citrate dehydrate pH 5.6, 20% isopropanol, 20% PEG 4000) prior to flash cooling in a nitrogen stream. A SAD data set was collected at a wavelength of 0.979 Å on the X26C beamline of the National Synchrotron Light Source at Brookhaven National Laboratory. The data set was processed and scaled with HKL2000 (Otwinowski & Minor, 1997) to 2.8 Å. Of the 15 expected SeMet sites, 10 were located using Phenix-AutoSol (Adams *et al.*, 2002). Phasing and density modification carried out with the Phenix software package was used to generate an experimental map. Model building and refinement of the DdrB structure was carried out through multiple iterations of Coot (Emsley & Cowtan, 2004) and Phenix-Refine until R and R_{free} values converged and geometry statistics reached suitable ranges.

Surface area calculations to determine the extent of protein-protein interaction surfaces were performed by AreaIMol (Lee & Richards, 1971, Saff & Kuijlaars, 1997). Least squares analysis to determine the structural similarity between regions of DdrB and SSB was carried out using LSQKAB (Kabsch, 1976).

2.5 Results and discussion

2.5.1 DdrB from *D. geothermalis* binds ssDNA but not dsDNA

We have performed EMSAs to assess *D. geothermalis* DdrB's ($DdrB_{Dg}$) nucleic acid binding capabilities with ss and dsDNA as well as ssRNA (Figure 2.1). $DdrB_{Dg}$ shifted a 20b ssDNA substrate, but failed to bind 20bp duplex DNA even at the highest protein concentration tested (Figure 2.1), suggesting that $DdrB_{Dg}$ is specific for its ability to interact stably with ss but not dsDNA. From this analysis it would appear that $DdrB_{Dg}$ binds ssDNA with an affinity in the low μM range (<20 μM), comparable to other characterized SSBs (Norais *et al.*, 2009, Weiner *et al.*, 1975).

Analysis of the $DdrB_{Dg}$:DNA ratios used in this study suggests that approximately 1 molecule of $DdrB_{Dg}$ is bound for every 5 nt of DNA substrate. When a 40 nt substrate was used this value increased to 10 nt per $DdrB_{Dg}$ monomer (SI Figure 2.1), similar to findings for DdrB from *D. radiodurans* ($DdrB_{Dr}$) (Norais *et al.*, 2009). $DdrB_{Dg}$ and $DdrB_{Dr}$ are 72% identical by primary amino acid sequence and therefore would be expected to display similar DNA binding characteristics. Both $DdrB_{Dg}$ and $DdrB_{Dr}$ were also found to associate weakly with ssRNA (Figure 2.1) (Norais *et al.*, 2009). At this time the biological significance, if any, of this interaction is unclear. It will be interesting, however, to determine if DdrB-RNA binding plays a role in the ability of *Deinococcus* to recover from extreme DNA damage.

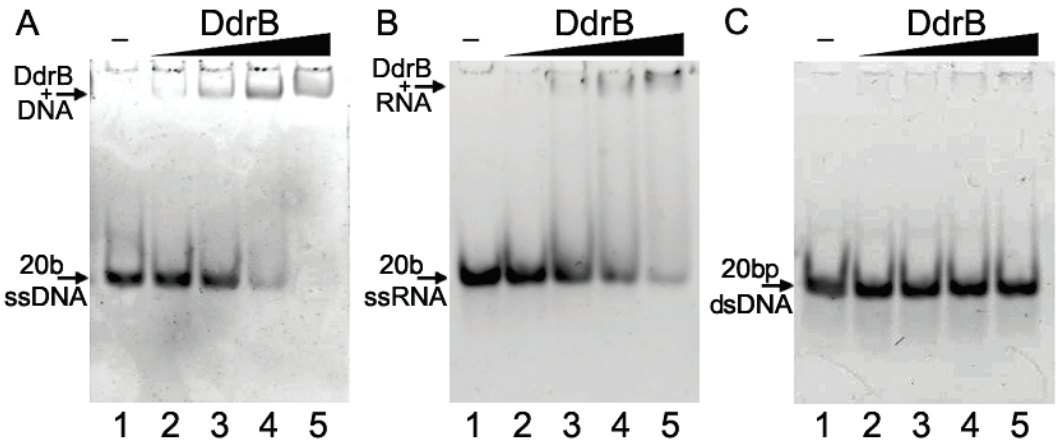

Figure 2.1 Electrophoretic mobility shift assay of ssDNA, ssRNA and dsDNA by DdrB. 150 pmol of **(A)** 20b ssDNA, **(B)** 20b ssRNA and **(C)** 20bp dsDNA substrates were incubated with 100 (lane 2), 250 (lane 3), 500 (lane 4) and 1000 (lane 5) pmol of DdrB and resolved by 10% polyacrylamide native TBE gel electrophoresis. DdrB bound ssDNA but not dsDNA.

2.5.2 The crystal structure of DdrB from *D. geothermalis*

DdrB is a single-stranded DNA binding protein that exhibits no primary sequence similarity to any other SSB characterized to date. This raises the possibility that DdrB may represent a new structural motif for ssDNA binding. By determining its crystal structure we hoped to answer the question of whether DdrB is a distantly related homologue of the standard SSB, or a structurally distinct protein that has arisen to perform a specialized function in *Deinococcus* spp. The structure of DdrB was solved by Single-wavelength Anomalous Diffraction (SAD) phasing using a 2.8 Å dataset collected from Selenomethionine (SeMet) derivatized protein. DdrB crystallized in the space group $P3_2$ and contained 5 monomers in the asymmetric unit. In our model, the main chain spans amino acid residues 1-126 in chains A and B, 1-127 in chains D and E, and 1-129 in chain C while full-length DdrB is 178 amino acid residues in length (discussed below). The final model was refined to R and R_{free} statistics of 23.5% and 28.5% respectively. A complete list of x-ray diffraction data and model refinement statistics are given in Table 2.1.

The DdrB monomer (Figure 2.2) consists of an N-terminal β-β-α motif followed by a six-stranded β-sheet (β3-β8-β7-β6-β5-β4) of which one face is solvent exposed and the other is packed against the N-terminal motif. Loop regions joining β6 to β7, and β7 to β8 are poorly ordered, leading to missing residues in both of these regions as well as little to no density for the majority of

Table 2.1 – Data collection and model refinement statistics

Data collection		**Model and refinement**	
Space group	$P3_2$	Resolution (Å)[a]	35.24 - 2.80
Cell parameters		R_{work}/R_{free} (%)	23.5/28.5
a,b,c (Å)	102.9, 102.9, 96.7	$Reflections_{observed}$	27, 742
α, β, γ (°)	90, 90, 120	$Reflections_{Rfree}$	1, 867
Molecules in ASU	5	No. atoms	
Resolution (Å)[a]	50.0 - 2.80	Protein	4, 715
Unique reflections	28, 588	Ligand/ion	0
Redundancy[a]	9.9 (9.9)	Water	34
Completeness (%)[a]	99.9 (100.0)	R.m.s.d. bond	
I/σ(I)[a]	17.4 (3.7)	Lengths (Å)	0.013
R_{merge} (%)[a]	9.6 (42.3)	Angles (°)	1.63
Wilson B Factor (Å^2)	89.8	Average B Factor (Å^2)	97.4
		PDB Accession Code	3KDV

[a] Statistics for the highest resolution shell are shown in parentheses.

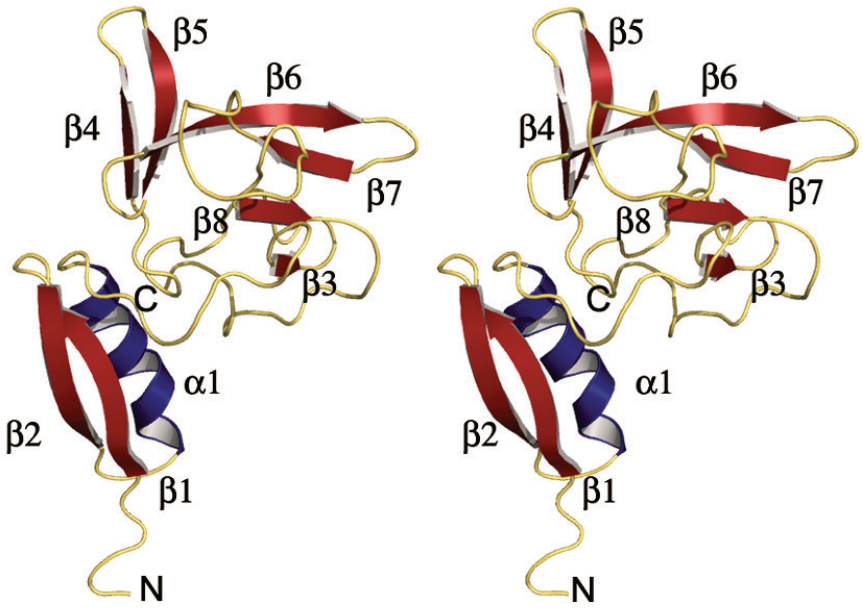

Figure 2.2 Stereo image of a DdrB (1-127) monomer. Secondary elements are colored as follows, α-helices in blue and β-strands in red.

the side chains, suggesting that these are flexible regions of the protein with high tendency towards disorder.

The five monomers in the asymmetric unit are arranged in a ring-structure with a 10 Å solvent accessible pore running through the middle (Figure 2.3). The central pore is comprised of a ten-stranded anti-parallel β-barrel that is stabilized primarily through interactions of DdrB's N-terminal β-β-α motif. Protein-protein interactions within the pentamer bury approximately 30% of the total solvent-accessible area of each monomer (1,991 $Å^2$), suggesting that the pentamer is a very stable structure. The formation of this pentameric structure was demonstrated in solution by gel-filtration experiments and is consistent with analytical ultracentrifugation studies performed with $DdrB_{Dr}$ (Norais *et al.*, 2009).

2.5.3 The C-terminal region of DdrB

Analysis of the primary amino acid sequence of DdrB using the PSIpred server (Jones, 1999, McGuffin *et al.*, 2000) predicts the C-terminal 35 residues of the protein as disordered. This is consistent with our observation that the final 51 residues of DdrB are unable to be assigned due to a lack of electron density, suggesting a high degree of mobility in this region of the protein. It does not, however, discount the potential importance. A BLAST (Altschul *et al.*, 1990) search using $DdrB_{Dg}$ as a query sequence, returned a related sequence within *D. geothermalis* (*Dgeo_2983*) that is predicted to encode an 83 amino acid protein sharing 72% similarity and 63% identity to the C-terminal region of $DdrB_{Dg}$ (SI

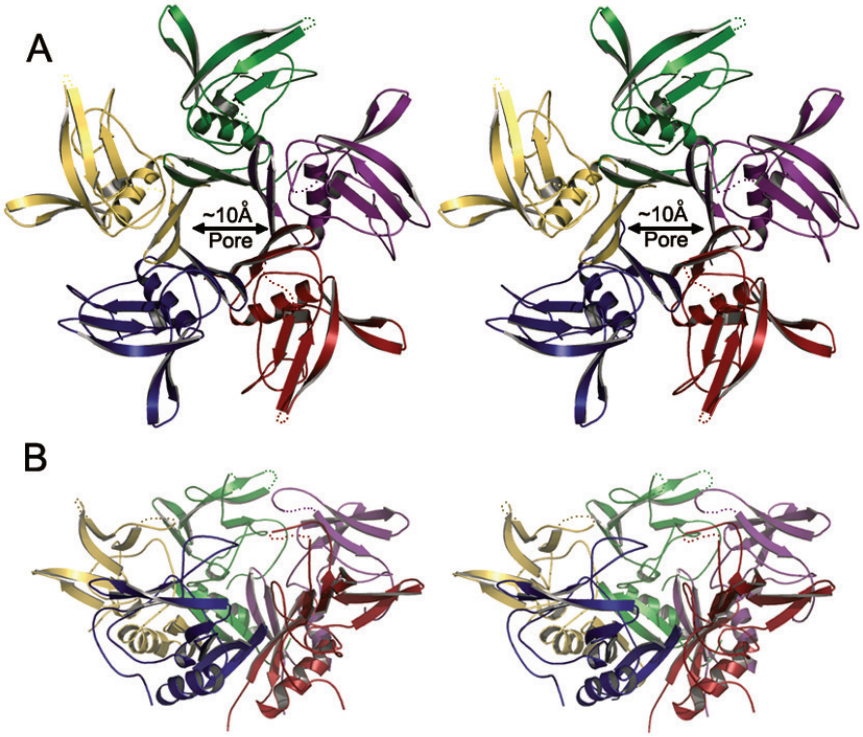

Figure 2.3 Stereo image of DdrB pentamer colored by chain (A-red, B-green, C-blue, D-yellow, E-purple). **(A)** View of 'top' face of the pentamer displaying the 10 Å central pore. **(B)** 'Side' view of the pentamer. Missing loop segments are represented by dotted lines.

Figure 2.2). Although the function of this hypothetical protein is unknown, its existence gives support to the idea that the C-terminal region of DdrB may form a functional domain.

Interestingly, the latter region (~60 residues) of SSBs is also disordered (Sancar *et al.*, 1981) and has been shown to be essential for mediating protein-protein interactions via a conserved patch of C-terminal negatively charged residues (Curth *et al.*, 1996). It is not uncommon for such clusters of charged amino acids to be involved in mediating protein-protein interactions (Zhu & Karlin, 1996). DdrB possesses several highly conserved charged residues within its last 50 amino acids, including a negative patch of residues directly at its C-terminus (SI Figure 2.2). It is, therefore, quite possible that the C-terminus of DdrB behaves in a similar way as SSB, mediating interactions with other proteins important for DNA damage recovery.

2.5.4 Structure based comparison of DdrB and OB-fold ssDNA binding proteins

To date all SSB homologues have been shown to interact with ssDNA through a conserved OB-fold (Pestryakov & Lavrik, 2008). The OB-fold is characterized by a pair of three-stranded anti-parallel β-sheets (β1-β2-β3 and β5-β4-β1) that form a five-stranded β-barrel (Theobald *et al.*, 2003). Strand β1 contributes to both sheets due to a conserved glycine residue close to its N-terminal end, and a β-bulge in the latter portion of the strand. All OB-fold proteins adopt a Greek key motif in the arrangement of the strands that

contribute to the β5-β4-β1-β2-β3-barrel (Figure 2.4 – SSB and DnaE) (Theobald *et al.*, 2003).

It was originally thought that DdrB may possess an OB-fold domain similar to those found in SSB and DNA polymerase III alpha subunit (DnaE) (Norais *et al.*, 2009). Searches performed using the structure of DdrB as query with the iCOPS (Suhrer *et al.*, 2009), DALI (Holm *et al.*, 2008), 3D-BLAST (Yang & Tung, 2006) and MATRAS (Kawabata, 2003) servers did not identify any OB-fold proteins as structural homologues. In fact, these standard homology searches did not yield any matches from the current structural databases, indicating that DdrB has a unique structure and fold not previously observed. Although the secondary-structure matching (SSM) superposition algorithm in Coot was not able to align DdrB with either *E. coli* SSB (SSB_{Ec}) (Raghunathan *et al.*, 2000) or *T. aquaticus* DnaE (Bailey *et al.*, 2006), we were able to perform a manual structural alignment in which the C_{α}-chains of four of the β-strands are in a similar spatial orientation (Figure 2.4). C_{α} carbons from DdrB $\beta4_{64-68}$, $\beta5_{71-77}$, $\beta6_{80-87}$ and $\beta7_{91-95}$ superimpose onto SSB_{Ec} $\beta4_{82-86}$, $\beta5_{97-103}$, $\beta3_{59-52}$ and $\beta2_{37-33}$ with root mean squared deviations (RMSD) of 1.02, 0.87, 1.34 and 1.93 Å respectively. Despite the very obvious and distinct structural similarities apparent between DdrB and the two OB-fold proteins, there are a number of features that clearly differentiate DdrB from the canonical OB-family. First, the β-sheet (excluding β3) adopts an up-and-down structural topology, rather than the Greek key motif

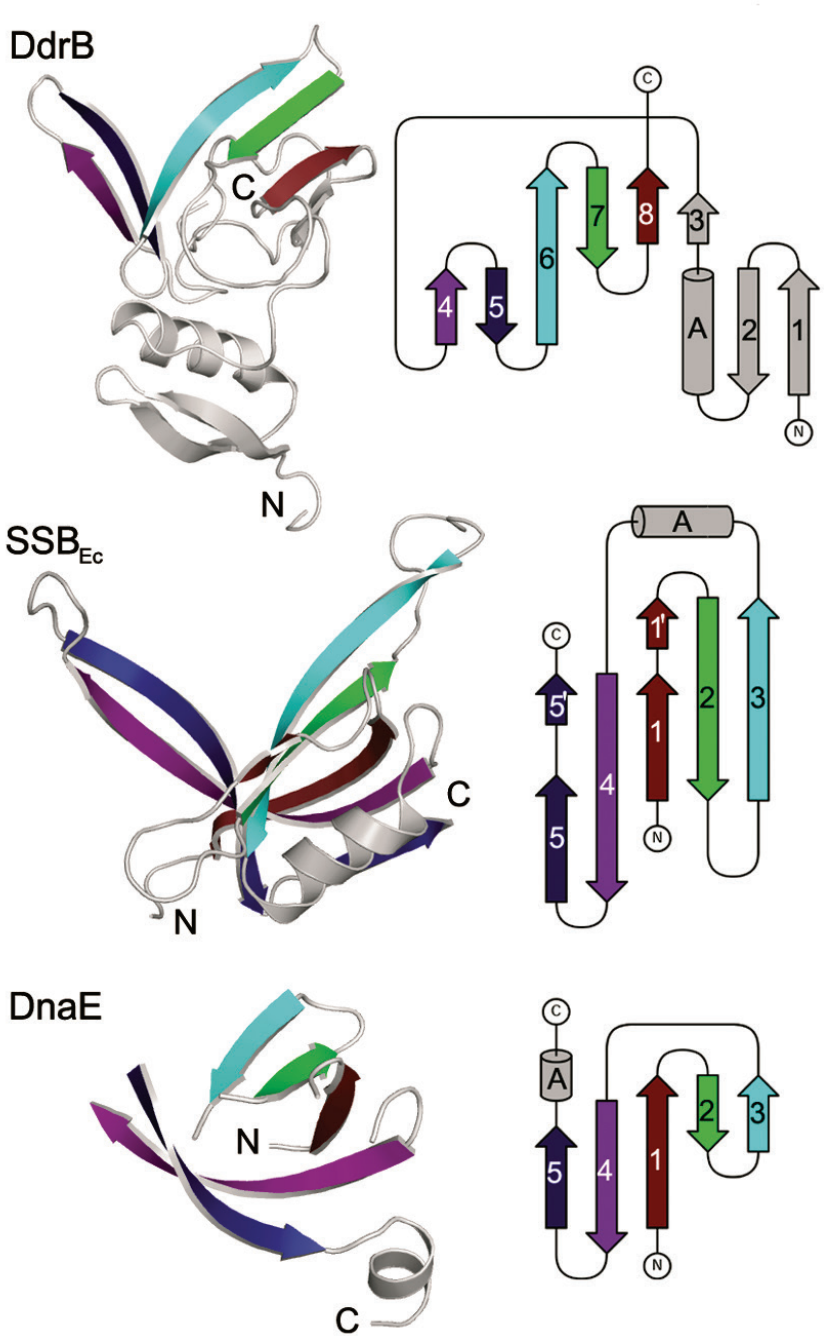

Figure 2.4 Structural comparison of DdrB (PDB: 3KDV), SSB_{Ec} (PDB: 1EYG) and DnaE (PDB: 2HPM). Structurally analogous strands are color-coded on the structures and topology diagrams; unrelated segments are colored in gray.

that is conserved within the OB-fold (Figure 2.4). Second, the strands that display structural similarity between DdrB and SSB_{Ec} do not show similar topology, connectivity or directionality. Finally, DdrB's β-sheet does not form a β-barrel and none of its strands possess the conserved glycine or β-bulge that permit the OB-fold β1 to contribute to multiple β-sheets. Taken together, it is evident that DdrB represents a new subfamily member of the OB-fold superfamily, as it possesses a unique architecture that is in all likelihood evolutionarily distinct from SSB_{Ec} and other members of the canonical OB-family.

2.5.5 Analogous ssDNA binding surfaces of DdrB and SSB_{Ec}

Alpha hemolysin, hexameric helicases such as *T7* gp4, *E. coli* RuvB and *Papillomavirus* E1, and sliding clamp proteins such as PCNA and *E. coli* β all form closed ring-structures that are able to thread DNA through their central pores. The central pore of DdrB's, however, is unlikely to bind DNA in a similar fashion. First, it has a very small (~10 Å) diameter compared to other ring-forming proteins known to associate with ssDNA, which are typically in the range of 14-40 Å (Gulbis *et al.*, 1996, Kong *et al.*, 1992, Patel & Picha, 2000, Song *et al.*, 1996). Secondly, the electrostatic surface potential of the pore carries a net negative charge (Figure 2.5), making it unfavorable for DNA association.

It would appear that despite structural differences, DdrB and SSB_{Ec} maintain similar DNA binding surfaces. In the crystal structure, SSB_{Ec} is observed

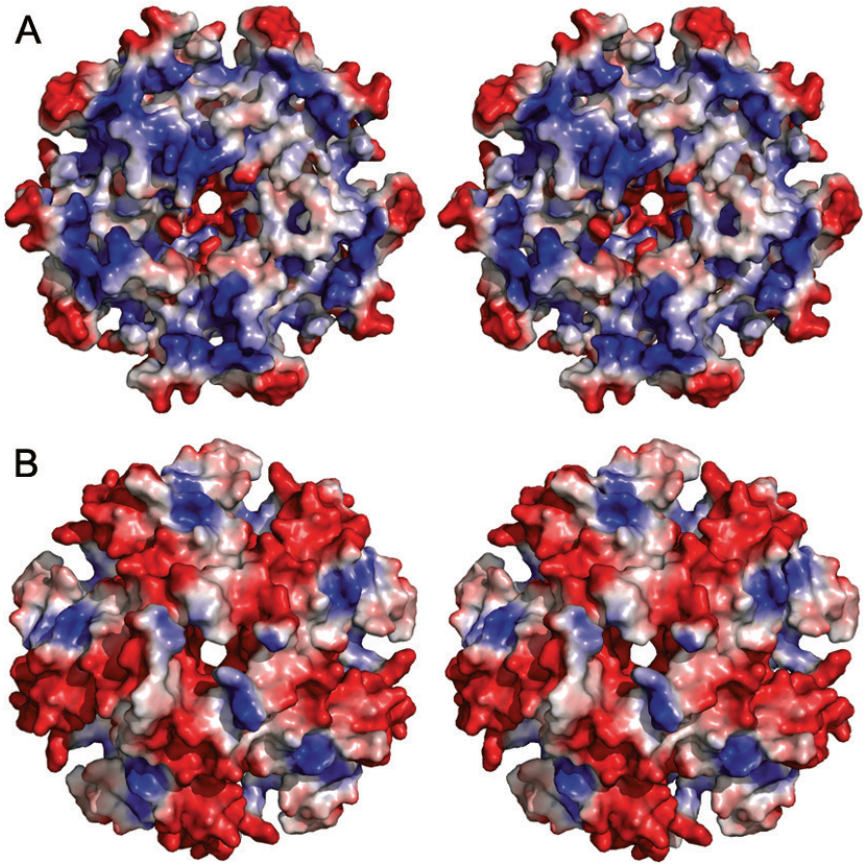

Figure 2.5 Stereo image of surface representation of the DdrB pentamer. **(A)** 'Top' face. **(B)** 'Bottom' face. Positive and negative electrostatic charge potentials are represented in blue and red, respectively.

to interact with DNA primarily via electrostatic and base-stacking interactions mediated by residues lying on the solvent exposed faces of β3, β4 and β5. Both positively charged and aromatic hydrophobic amino acids are important for this DNA interaction (Figure 2.6A) (Raghunathan *et al.*, 2000). The only positively charged surface on DdrB corresponds to the solvent exposed face of the six-stranded beta sheet (Figure 2.5) that precisely aligns to the segments of SSB_{Ec} that display structural similarity (Figure 2.4). This surface contains a number of conserved charged, aromatic and hydrophobic residues able to fulfill the necessary interactions with ssDNA (Figure 2.6B).

The quaternary structures of DdrB (pentameric ring) and SSB_{Ec} (dimer of dimers) are very different, suggesting that their overall modes of DNA association may also be distinct. SSB_{Ec} binds ssDNA in a serpentine fashion with a single DNA molecule making multiple non-contiguous contacts with each monomer in a tetramer (Figure 2.7A). This type of binding efficiently compacts ssDNA into a highly intertwined complex. The pentameric ring structure of DdrB, however, has its DNA binding surfaces positioned such that intertwining of DNA is not possible. Rather, the quaternary structure of DdrB is more consistent with a simple contiguous wrapping mode for ssDNA binding analogous to the tire on the rim of a wheel (Figure 2.7B). Without a crystal structure, it is difficult to expand further; however, even from this simple comparison, it is apparent

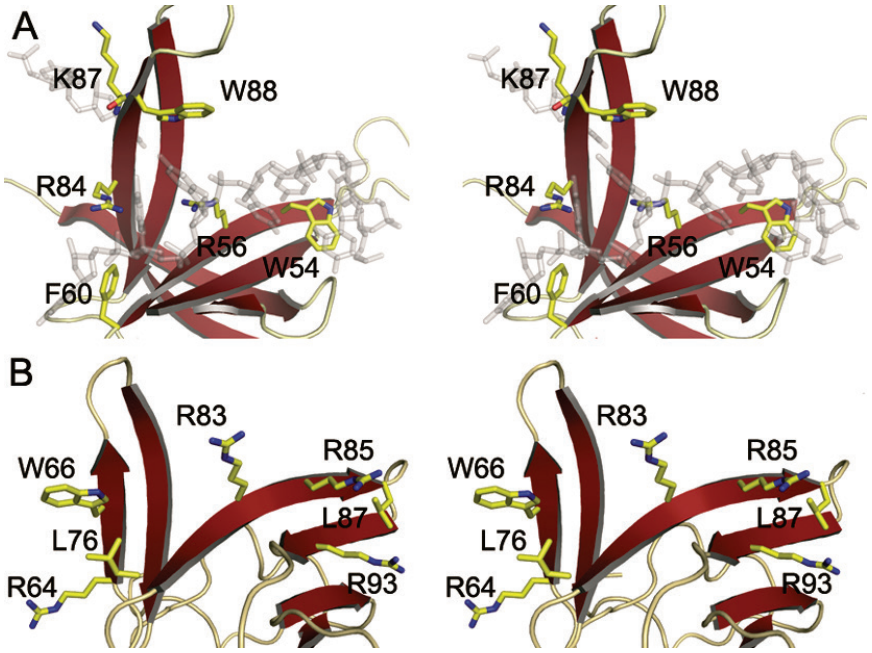

Figure 2.6 Stereo image of the conserved amino acid residues lining the solvent exposed DNA binding β-sheet surface of SSB_{Ec} **(A)** and the analogous surface of DdrB **(B)**. Bound ssDNA is represented in gray to delineate the DNA binding surface of SSB_{Ec} (PDB: 1EYG).

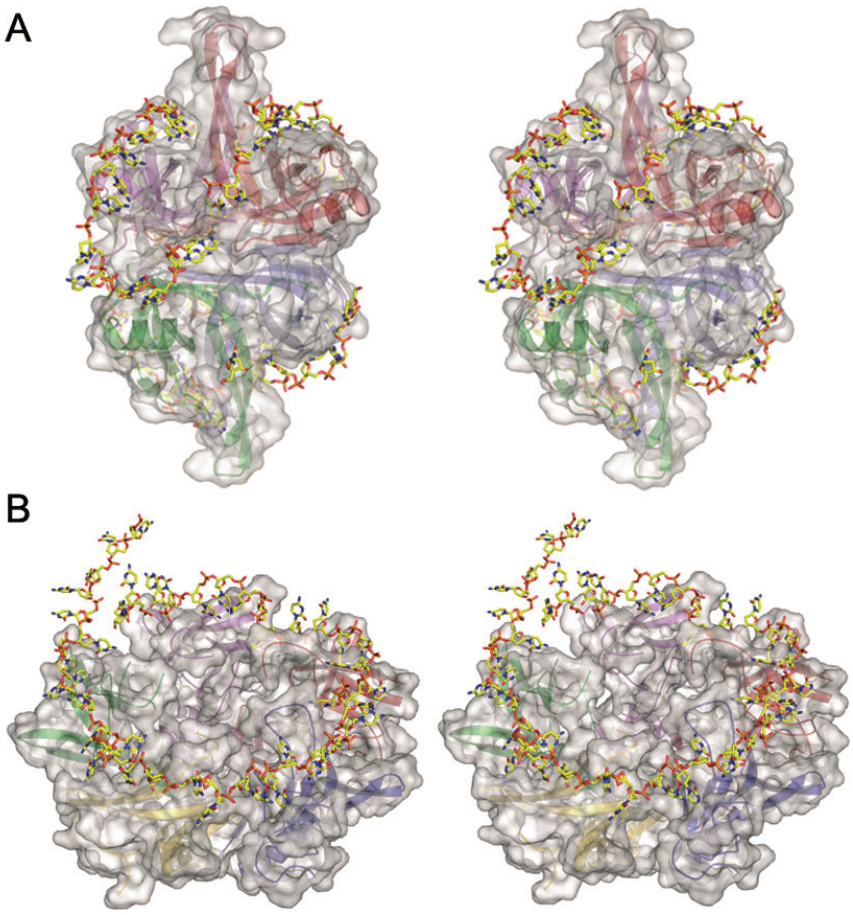

Figure 2.7 Stereo image of surface/cartoon representations of quaternary structures of SSB_{EC} (PDB: 1EYG) and DdrB (PDB: 3KDV). Surfaces are represented in gray, and bound ssDNA is represented in stick form. **(A)** SSB_{EC} tetramer colored by chain (A-green, B-blue, C-red, D-purple) bound to two 35mers of ssDNA. **(B)** DdrB pentamer colored by chain (A-red, B-green, C-blue, D-yellow, E-purple). A 40mer of ssDNA is modeled onto the positively charged surface of the DdrB pentamer.

that the mechanisms for DNA binding are very different, reflecting the unique roles these proteins play in DNA metabolism.

2.5.6 The role of an alternative, DNA damage-inducible SSB

Standard bacterial SSB is expressed continuously and plays an essential role in stabilizing and protecting exposed ssDNA throughout regular cellular processes (Pestryakov & Lavrik, 2008). During ESDSA repair following extreme DNA damage, immense spans of ssDNA totaling hundreds of kb are generated (Zahradka *et al.*, 2006), however, SSB expression is only moderately elevated (Liu *et al.*, 2003). DdrB, on the other hand, is present at almost undetectable levels under regular growth conditions, but is among the top five most highly up-regulated genes under the stresses of excessive DNA damage (Tanaka *et al.*, 2004). In addition to its role in protecting exposed ssDNA, SSB acts as a scaffolding protein able to recruit a variety of proteins during different cellular processes. As repair from extreme damage appears to involve a more diverse set of proteins and protein-complexes than simple double-strand break repair, DdrB may function as a specialized SSB reserved exclusively for use in ESDSA. The discovery of a new SSB-like protein in *Deinococcus* spp. opens the question of whether additional specialized SSB-like proteins may also exist in other organisms that have missed being identified due to sequence and structural diversity.

2.6 Funding

This work was supported by a *Natural Sciences and Engineering Research Council* of Canada grant [2008R00075 to M.S.J.] and studentship to S.N.S.M.

2.7 Acknowledgments

Structural data was collected at the National Synchrotron Light Source, Brookhaven National Laboratories, at Beamlines X26C. We would like to thank Annie Héroux, Alexei Soares, and Robert Sweet for their technical assistance. We also wish to thank Elena Gaidamakova for providing us with *D. geothermalis*.

2.8 Supplemental data

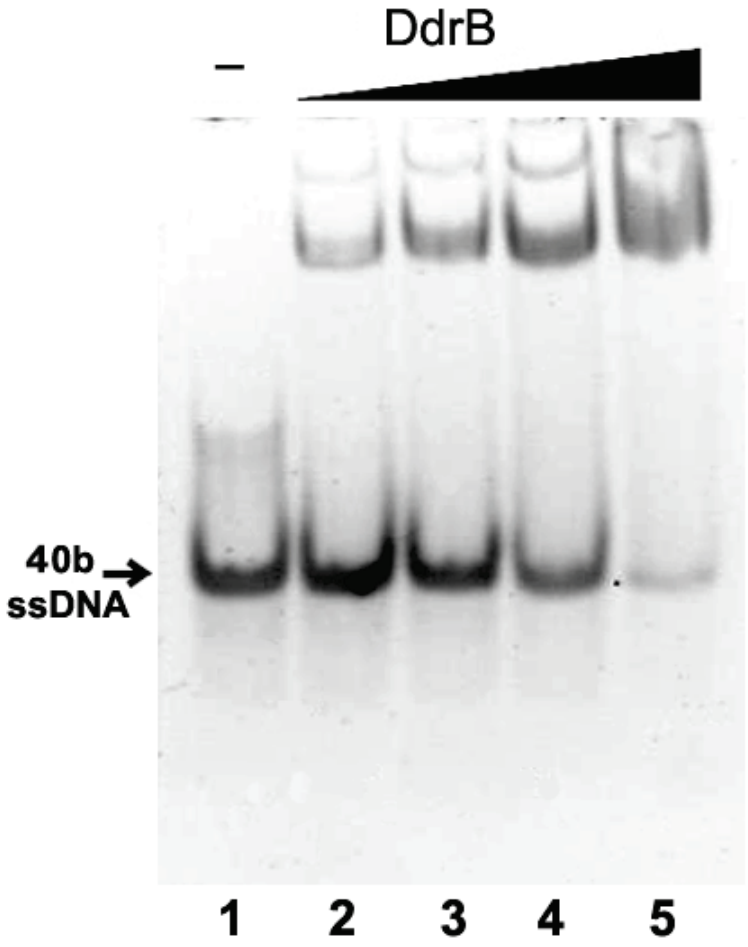

Supplementary figure 2.1 Electrophoretic mobility shift assay of ssDNA by DdrB. 150 pmol of 40b ssDNA substrate was incubated with 100 (lane 2), 250 (lane 3), 500 (lane 4) and 1000 (lane 5) pmol of DdrB and resolved by 10% polyacrylamide native TBE gel electrophoresis.

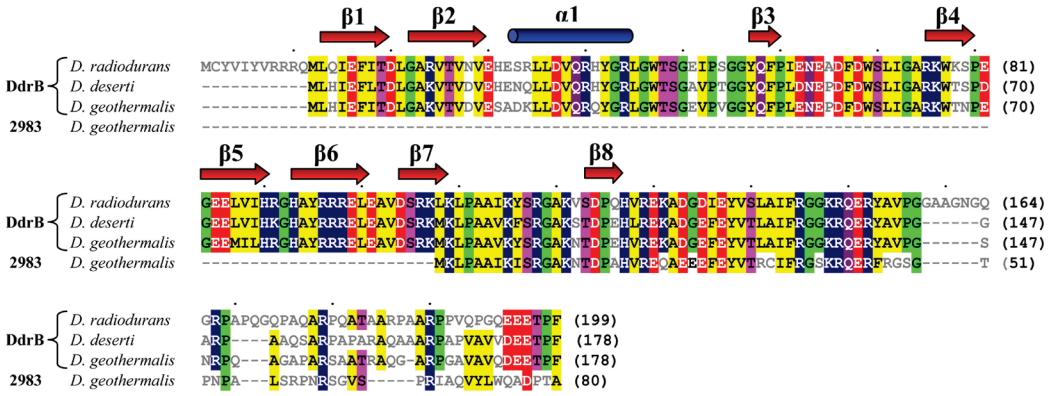

Supplementary figure 2.2 Structure based sequence alignment of DdrB homologues. DdrB homologues from *D. radiodurans, D. deserti* and *D. geothermalis* are shown aligned with another gene from *D. geothermalis* that shares significant similarity to the carboxy-terminus of DdrB. The secondary structure (strands in red, helices in blue) of DdrB is shown above the sequence for reference.

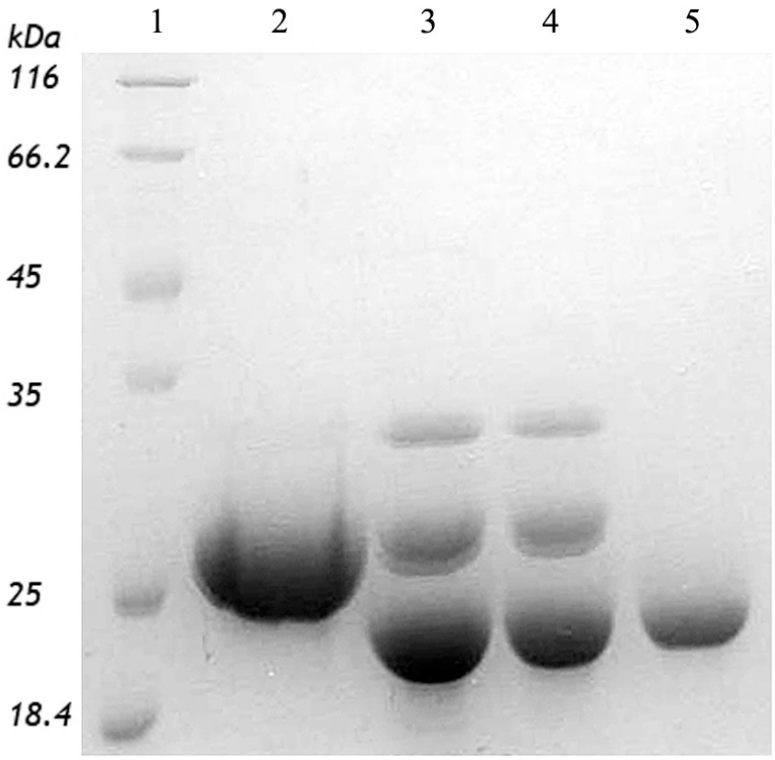

Supplementary figure 2.3 12% SDS PAGE of samples from the purification of DdrB. Individual lanes contain: (lane 1) molecular weight marker, (lane 2) 6His-Ddrb after purification by Ni-IMAC, (lanes 3-4) His-DdrB after treatment with TEV protease, (lane 5) Pure, untagged DdrB.

CHAPTER 3 – CRYSTALLIZATION OF THE DDRB-DNA COMPLEX FROM *DEINOCOCUS RADIODURANS*

Sugiman-Marangos, S., Junop, M. (2012) Crystallization of the
DdrB-DNA complex from *Deinococcus radiodurans*.
Acta Crystallographica Section F **68**: 1534-1537

3.1 Author's Preface

Research presented in Chapter 3 was published in the peer-reviewed journal *Acta Crystallographica Section F* and is presented in published form (formatted to complement the rest of the thesis). This article described the crystallization and data collection of a DdrB/ssDNA co-crystal complex, focusing on the difficulties encountered in this process. S.N. Sugiman-Marangos performed all of the experimental work described and wrote the manuscript with M.S. Junop.

3.2 Abstract

The remarkable ability of members of the *Deinococcus* family to recover from extreme DNA damage is in part due to its robust DNA repair mechanisms. Of particular interest is its ability to repair hundreds of double-strand DNA breakages through a rapid and efficient mechanism involving novel proteins that are uniquely found in *Deinococcus* spp. One such protein, DdrB, which is thought to play a role early in DSB repair, has been crystallized in complex with ssDNA and data has been collected to 2.3 Å.

3.3 Introduction

Deinococcus radiodurans is able to withstand and recover from extreme doses of ionizing radiation which shatter its chromosome into hundreds of fragments (Zahradka *et al.*, 2006). DdrB is a protein unique to the *Deinococcus* family that is thought to be implicated in recovery following extensive damage (Tanaka *et al.*, 2004). Early characterization of the protein revealed its single-stranded DNA (ssDNA) binding activity (Norais *et al.*, 2009, Sugiman-Marangos & Junop, 2010) and, as it is highly upregulated following both irradiation and desiccation (Tanaka *et al.*, 2004), it was thought that it played a role as a DNA-damage induced functional equivalent to canonical single-stranded binding protein (SSB) (Norais *et al.*, 2009). Structural characterization later revealed that DdrB in fact possesses a novel fold, distinct from the structurally conserved OB-fold present in SSB (Sugiman-Marangos & Junop, 2010). In addition to binding

ssDNA, DdrB has recently been shown to promote annealing of complementary strands of DNA *in vitro* (Xu *et al.*, 2010). Here, we report the crystallization and data collection of a DdrB/ssDNA co-crystal complex, the solution from which will provide valuable information with regards to the mechanism through which DdrB is able to carry out its biological functions. Co-crystallization of protein/DNA complexes adds an additional dimension to the already arduous task of protein crystallography, as characterization of crystals containing protein but not DNA typically only takes place after diffraction quality crystals have been optimized and X-ray data has been collected. Optimization of the pH of the protein buffer prior to screening and the use of a fluorescently labelled DNA substrate significantly reduced the number of false positives encountered in the search for a condition that maintained protein/DNA interactions during crystallography.

3.4 Materials and methods

3.4.1 Cloning and protein expression

A C-terminal truncation of DdrB from *D. radiodurans* was generated by PCR amplification of the gene, DR0070, incorporating a stop codon following residue 144. This PCR product was incorporated into the expression vector pET151-D-topo as per the manufacturer's protocol (Invitrogen), and expressed as an N-terminal 6His fusion in *E. coli BL21(DE3)*. Purification was carried out as described previously (Sugiman-Marangos & Junop, 2010). Briefly, cell pellets

were lysed by sonication in lysis buffer (20 mM Tris pH 8.0, 1 M sodium chloride, 5 mM imidazole), and clarified by centrifugation at 48, 000 g. Soluble lysate was purified by Ni-IMAC FPLC, exchanged into a low salt buffer (20 mM Tris pH 8.0, 150 mM potassium chloried) and treated with TEV protease to cleave the N-terminal 6His tag. The cleaved 6His tag and TEV protease were separated from $DdrB_{1-144}$ by a second pass over the Ni-IMAC column, and then exchanged into the final crystallization buffer (20 mM Tris pH 6.0, 100 mM potassium chloride).

3.4.2 Electrophoretic mobility shift assay

Electrophoretic mobility shift assays (EMSA) were performed in EMSA buffer (20 mM Tris pH 8.0, 150 mM sodium chloride, 10% (v/v) glycerol) by mixing 100 µM of unlabelled and Cy5 labelled 50 b ssDNA for 15 minutes with increasing amounts of $DdrB_{1-144}$ (0, 0.1, 1, 10, 20, 50 µM) in a 15 µL reaction volume. Both unlabelled and Cy5 labelled ssDNA substrates were ordered from Integrated DNA Technologies (Iowa, USA). The reactions were resolved by electrophoresis on a 10% (w/v) polyacrylamide native Tris/Borate/EDTA (TBE) gel running at 80 V for 1 hour.

3.4.3 Crystallization

Initial crystal screening was carried out over a wide range of protein/DNA concentrations and ratios using a variety of sequences and lengths of ssDNA substrates. Approximately 2000 crystallization experiments were set by hand in 24-well screw cap plates (Qiagen), performed primarily with kits specifically

formulated for crystallization of protein/nucleic acid complexes (Nucleix from Qiagen and Protein-Nucleic Acid Complex Crystal Screen from KeraFAST), although additional screens were tested as well (Classics I, JCSG I, II, III and IV from Qiagen). Crystal hits were screened by both X-ray diffraction and visually by monitoring incorporation of a fluorescent 5'-labelled Cy5 50 b poly dT ssDNA substrate.

Crystals of $DdrB_{1-144}$ in complex with ssDNA were grown at 293 K using the hanging-drop vapour diffusion method. Initial crystals were observed approximately 48 hours after the drops were set and continued to grow over the next 2-3 days. DdrB and ssDNA were pre-mixed (1.34 µL DdrB (830 µM) in protein buffer (20 mM Tris pH 6.0, 100 mM potassium chloride) and 0.12 µL 50 b poly dT (2000 µM)) and allowed to incubate at 298 K for 10 minutes before being mixed with 1.5 µL of crystallization buffer (50 mM MES pH 5.6, 300 mM potassium chloride, 10 mM magnesium chloride, 5% (v/v) PEG 8000) and dehydrated over 250 µL of 1.35 M ammonium sulfate. No additional cryoprotectant was necessary to prevent ice crystal formation during data collection.

3.4.4 Data collection

Crystals of $DdrB_{1-144}$ and ssDNA were flash cooled to 100 K in a nitrogen stream, and diffraction data was collected at a wavelength of 1.1 Å at the X29A beamline of the National Synchrotron Light Source (NSLS) at Brookhaven

National Laboratory. A total of 360 images were collected using an ADSC Quantum 315 detector at a distance of 300.0 mm for 1 second exposures with a 0.5^{o} oscillation width.

3.5 Results and discussion

Crystallization of the apo structure was performed with full length DdrB (Sugiman-Marangos *et al.*, 2010); however, the main chain of the protein could only be traced for amino acid residues 1-144. This was consistent with previous reports that the C-terminus of DdrB is likely disordered (Norais *et al.*, 2009), in addition to being lacking in functional importance during damage recovery (Bouthier de la Tour *et al.*, 2011). A C-terminal truncation mutant was therefore constructed for co-crystallization with DNA to improve crystal packing through the elimination of a large disordered segment.

A number of initial attempts to crystallize $DdrB_{1\text{-}144}$ in complex with ssDNA produced diffraction quality crystals, however, these structures failed to capture the protein-nucleic acid interaction, as determined upon analysis of the resulting electron density maps. To differentiate between protein crystals with and without DNA bound, a technique described by Georgescu *et al.* was implemented (Georgescu *et al.*, 2008). Crystal hits shown to be protein by X-ray diffraction were screened for incorporation of ssDNA by crystallization with a Cy5 labelled DNA substrate, appearing blue upon visual inspection with a light microscope. Direct interactions between the Cy5 label and DdrB were

considered to be unlikely as EMSAs performed with labeled and unlabeled substrates demonstrated no significant differences (Figure 3.1). In order to increase efficiency, broad screening could have been performed using the labelled substrate; additionally, a second DNA substrate using a different fluorophore could have been implemented to rule out direct interactions between the label and the protein, as described previously (Georgescu *et al.*, 2008).

Early crystallization trials involved both short (8-10 b) and long (48-52 b) DNA substrates based on estimates reported in the literature of the number of bases required to fully occupy a DdrB pentamer. As DdrB has not been reported to display sequence specificity in its interaction with ssDNA, we decided to perform our trials with a repetitive sequence of DNA consisting of a unique base. This was done to facilitate eventual modeling of the DNA in the electron density, as there would be no ambiguity in identifying the identity of bases. Poly dT was ultimately selected as it does not have the propensity for self-association (as is the case with dG), and it has been used successfully in the crystallization of other proteins that bind ssDNA (Chen *et al.*, 2008, Chan *et al.*, 2009).

The isoelectric point of $DdrB_{1-144}$ calculated by the ExPASy ProtParam tool (Artimo *et al.*, 2012) is 7.17. Preliminary crystallization trials had been carried out in protein buffer at a pH of 8.0. This was not originally a concern as EMSAs had been performed at this pH, and the overall negative charge of the protein

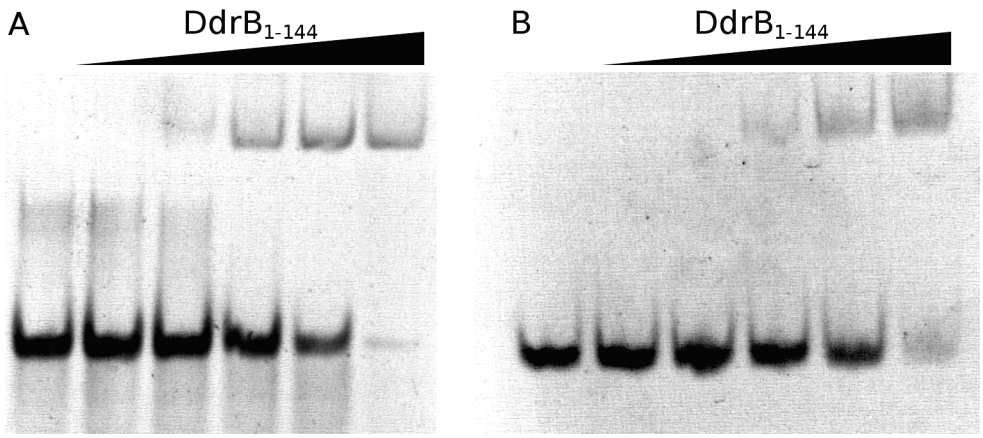

Figure 3.1 Electrophoretic mobility shift assays of 50b ssDNA substrates incubated with increasing concentrations of $DdrB_{1-144}$. 100 µM of unlabelled (A) and Cy5 labelled (B) ssDNA were incubated with 0, 0.1, 1, 10, 20, and 50 µM $DdrB_{1-144}$ and resolved by 10% polyacrylamide native TBE gel electrophoresis. No major differences are observed as a result of incorporation of a 5' Cy5 label.

did not appear to have an effect on DNA binding (Sugiman-Marangos & Junop, 2010).

In an attempt to increase the strength of the protein/DNA interaction and potentially decrease charge repulsion, and therefore overall solubility of the complex, a final buffer exchange step into 10 mM Tris pH 6.0 was appended to the original purification protocol. As pH 6.0 is outside of the range where Tris is most effective as a buffer, a more appropriate buffer, such as MES, could have been used. Re-screening at a lower pH over 500 µL of 1.5 M ammonium sulfate produced a hit from the Nucleix screen condition 5 (200 mM potassium chloride, 10 mM magnesium chloride, 50 mM MES pH 5.6, 5% (w/v) PEG 8000), yielding small crystals that were confirmed to be protein by X-ray diffraction (Figure 3.2a). Before proceeding with optimization, identical drops were set-up with Cy5 labelled ssDNA, which produced blue crystals, confirming the incorporation of the DNA into the crystal (Figure 3.2b).

Diffraction quality crystals were optimized by systematic screening of the various components of the crystallization solution, and the concentration of the ammonium sulfate in the well solution (Figure 3.2c); while the use of ssDNA substrates 1-2 bases shorter or longer than 50 b did not appear to have any measured effect on the quality or extent of diffraction observed. Modulation of the concentration of potassium chloride in the crystallization solution, and the concentration of ammonium sulfate in the well solution appeared to have the

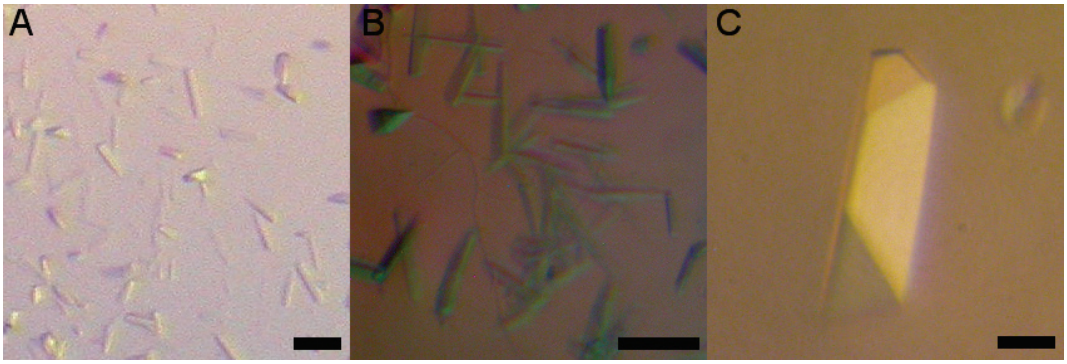

Figure 3.2 Crystals of $DdrB_{1-144}$/ssDNA complex obtained by hanging-drop vapour diffusion method. Initial screening yielded a shower of small crystals from Nucleix condition 5 (200 mM potassium chloride, 10 mM magnesium chloride, 50 mM MES pH 5.6, 5% (w/v) PEG 8000) (A), which were reproduced using the Cy5 labeled ssDNA substrate (B) . Optimization of the condition and dehydration solution yielded larger, diffraction quality crystals (C). The length of the scale bar represents approximately 100 µm.

most effect on the size and quality of the crystals grown. While dehydration over 1.5 M ammonium sulfate consistently produced showers of small crystals, dehydration over 1.3-1.35 M ammonium sulfate significantly reduced the number of nucleation events and allowed for the growth of larger crystals. Most drops contained a mixture of two morphologies of triangular prisms differentiated by the relative rate of growth of the crystal faces. The more common morphology was the one in which the length of the prism grew much more rapidly producing long, but relatively two-dimensional crystals; while the less common morphology produced a more three-dimensional crystal that was shorter in length but with a larger triangular base. Both crystal morphologies produced visible diffraction patterns; however the latter crystal morphology consistently diffracted to higher resolution.

Diffraction data was collected to approximately 2.3 Å using the X29A beamline at the NSLS. Data was processed with HKL2000 (Otwinowski & Minor, 1997) to 2.4 Å in the spacegroup $P3_2$ with unit cell parameters a=110.7, b=110.7, c=58.8 Å, $\alpha=90^{o}$, $\beta=90^{o}$, and $\gamma=120^{o}$ (Table 1). Molecular replacement was performed using the PHENIX software package (Adams *et al.*, 2010) using the structure of the DdrB pentamer from *D. geothermalis* with waters removed as a search model (PDBID 4EXW, 72% amino acid identity), yielding a top solution with a log likelihood gain of 134.55. In total, 4 other solutions were reported with LLGs of 113.91, -13.09, -28.92 and -83.46. Analysis of peaks in the resulting

F_o-F_c map revealed the presence of electron density representative of ssDNA (Figure 3.3). Model building and structure refinement are currently in progress.

3.6 Acknowledgments

This work was supported by the Natural Sciences and Engineering Research Council of Canada through grant 2008R00075. Data for this study were measured at beamline X29A of the National Synchrotron Light Source. Financial support comes principally from the Offices of Biological and Environmental Research and of Basic Energy Sciences of the US Department of Energy, and from the National Center for Research Resources (P41RR012408) and the National Institute of General Medical Sciences (P41GM103473) of the National Institutes of Health.

Table 3.1 – Data collection

Space group	$P3_2$
Unit cell parameters	
a,b,c (Å)	110.7, 110.7, 58.8
Matthews coefficient	2.61
Molecules in ASU	6
Resolution range (Å)[a]	50.0 - 2.30 (2.34 - 2.30)
Observed reflections	203,021
Unique reflections[a]	35,736 (1,844)
Redundancy[a]	5.7 (5.6)
Completeness (%)[a]	99.9 (100.0)
I/σ(I)[a]	17.4 (2.3)
R_{merge} (%)[a]	6.8 (72.6)
Wilson B Factor (Å^2)	58.3

[a] Statistics for the highest resolution shell are shown in parentheses.
R_{merge} is defined as $(\Sigma_{hkl}\Sigma_j|I_{hkl,j}-(I_{hkl})|)/\Sigma_{hkl}\Sigma_j I_{hkl,J}$

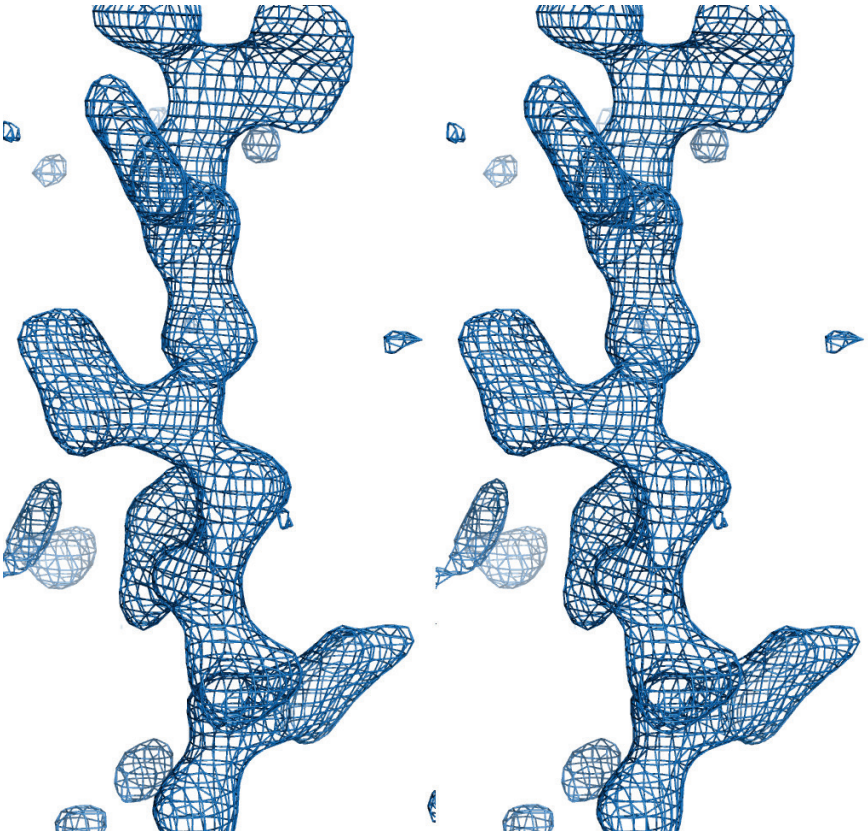

Figure 3.3 Stereo image representation of the Fo-Fc omit map (3σ) calculated following molecular replacement with Phenix, indicating the presence of bound ssDNA in the structure solution.

CHAPTER 4 – CRYSTAL STRUCTURE OF THE DDRB/SSDNA COMPLEX FROM *DEINOCOCCUS RADIODURANS* REVEALS A DNA BINDING SURFACE INVOLVING HIGHER-ORDER OLIGOMERIC STATES

Seiji N. Sugiman-Marangos, John K. Peel, Yoni M. Weiss, Rodolfo Ghirlando and Murray S. Junop (2013). Crystal structure of the DdrB/ssDNA complex from *Deinococcus radiodurans* reveals a DNA binding surface involving higher-order oligomeric states. *Nucleic Acids Research*, in press (doi: 10.1093/nar/gkt759).

4.1 Author's Preface

Research presented in Chapter 4 was published in the peer-reviewed journal *Nucleic Acids Research* and is presented in published form (formatted to complement the rest of the thesis). This article described the crystal structure of DdrB in complex with ssDNA, revealing a higher-order oligomeric assembly of DdrB pentamers. The structure, together with mutational analysis, supports a proposed model for DdrB function. S.N. Sugiman-Marangos crystallized the DdrB/ssDNA complex, and solved/refined the structure. Y.M. Weiss generated and purified DdrB mutants together with J.K. Peel, who also carried out the DNA binding experiments. R. Ghirlando performed and analyzed the analytical centrifugation experiments. S.N. Sugiman-Marangos and M.S. Junop prepared the manuscript with input from R. Ghirlando.

4.2 Abstract

The ability of *Deinococcus radiodurans* to recover from extensive DNA damage is due in part to its ability to efficiently repair its genome, even following severe fragmentation by hundreds of double strand breaks. The single-strand annealing pathway plays an important role early during the recovery process, making use of a protein, DdrB, shown to greatly stimulate ssDNA annealing. Here we report the structure of DdrB bound to ssDNA to 2.3 Å. Pentameric DdrB was found to assemble into higher-order structures that coat ssDNA. In order to gain further mechanistic insight into the protein's function, a number of point mutants were generated altering both DNA binding and higher order oligomerization. This work not only identifies higher-order DdrB associations but also suggests the presence of an extended DNA binding surface running along the 'top' surface of a DdrB pentamer and continuing down between two individual subunits of the ring structure. Together this work sheds new insight into possible mechanisms for DdrB function in which higher-order assemblies of DdrB pentamers assist in the pairing of complementary ssDNA using an extended DNA binding surface.

4.3 Introduction

Deinococcus radiodurans is renowned for its ability to recover from exposure to extreme ionizing radiation (IR), desiccation, ultraviolet radiation, and a variety of DNA damage inducing agents. Its capacity to withstand these various

forms of damage has been attributed to a combination of protection of the proteome by free-radical scavenging manganese complexes (Zahradka *et al.*, 2006, Daly *et al.*, 2004, Daly *et al.*, 2007) and an efficient DNA repair system involving several proteins found uniquely in *Deinococcus* (Zahradka *et al.*, 2006, Tanaka *et al.*, 2004, Slade *et al.*, 2009, Makarova *et al.*, 2007).

This contingent of novel proteins includes DdrB, which was identified as highly up-regulated following DNA damage by two independent experiments monitoring mRNA transcript levels in *D. radiodurans* recovering from acute IR exposure (Tanaka *et al.*, 2004, Liu *et al.*, 2003). This has recently been corroborated by mass spectrometry based proteomic analysis of *D. radiodurans* post-IR, which showed that DdrB is the second most abundant DNA repair protein during recovery (Basu & Apte, 2012). Further underlining its involvement in DNA damage recovery, *D. radiodurans* Δ*ddrB* is radiosensitive, experiencing a decrease in survival following high doses of IR and delayed recovery at low doses (Tanaka *et al.*, 2004, Bouthier de la Tour *et al.*, 2011).

Due to its abundance in the cell post-IR (Basu & Apte, 2012), its ability to bind ssDNA *in vitro* (Norais *et al.*, 2009, Sugiman-Marangos & Junop, 2010), and a disordered C-terminus, DdrB has been implicated as a stress-inducible functional equivalent to canonical single-stranded binding protein (SSB) (Norais *et al.*, 2009). It has since been demonstrated, however, that the purported SSB-like C-terminal motif is not necessary for radioresistance (Bouthier de la Tour *et*

al., 2011) and that DdrB possesses novel activities not shared by SSB, such as the ability to promote annealing of complementary oligonucleotides *in vitro* (Xu *et al.*, 2010), and suppress, rather than stimulate, RecJ exonuclease activity (Jiao *et al.*, 2012). The crystal structure of DdrB confirmed that in addition to being functionally dissimilar to canonical SSB, DdrB is structurally distinct and likely does not bind ssDNA in the same way as SSB as it lacks an OB-fold (Sugiman-Marangos & Junop, 2010).

Under extreme damaging conditions, hundreds of double strand breaks (DSB) are generated and are repaired in *D. radiodurans* by two main pathways, single-strand annealing (SSA) and extended synthesis dependent strand annealing (ESDSA) (Zahradka *et al.*, 2006, Slade *et al.* 2009). Following fragmentation of the genomic DNA, the resulting segments of dsDNA are processed by 5' exonucleases, yielding 3' overhangs. These overhangs are then either annealed directly to complementary strands yielding larger dsDNA fragments by SSA, or undergo RecA mediated strand-invasion of homologous duplexes by ESDSA (Slade *et al.*, 2009). SSA appears to function independently of RecA and is thought to play a role early during DSB repair in *Deinococcus* spp., particularly when the number of strand breakages is extensive. It has been suggested that DdrB may play an important role in SSA due to its single-strand annealing activity (Bouthier de la Tour *et al.*, 2011), similar to Rad52 in the analogous eukaryotic pathway.

Visualization by electron microscopy revealed that DdrB coats ssDNA like "beads on a string" similar to both SSB and RecA (Norais *et al.*, 2009); and, intrinsic fluorescence quenching titration demonstrated the binding stoichiometry of the complex as between 41 and 56 nucleotides per pentamer (Bouthier de la Tour *et al.*, 2011). Here we have further characterized the interaction between DdrB and ssDNA. We report the X-ray structure of DdrB in complex with ssDNA to 2.3 Å and assess the DNA binding activity of a number of point mutants generated based on this structure by fluorescence polarization. This analysis not only confirmed the ssDNA-protein interaction observed within the crystal structure, but further suggested the presence of an extension of this surface continuing along the 'top' face of the DdrB pentamer. Additionally, DdrB was found to mediate ssDNA coating through assembly of a higher-order structure involving two DdrB pentamers. These protein-protein interactions were verified in solution using analytical ultracentrifugation (AUC). Based on these results, we propose potential mechanisms for how DdrB promotes observed ssDNA annealing.

4.4 Materials and methods

4.4.1 Protein expression and purification

DdrB from *D. radiodurans* ($DdrB_{Dr}$) was synthesized and sub-cloned into pPROEX-HT by Geneart, producing the expression construct MJ4730. MJ4748 was then generated by amplifying $DdrB_{Dr}$ from MJ4730, introducing a stop codon

following residue 144. This gene product was then cloned into the expression vector pET151/D-Topo (Invitrogen) per the manufacturer's protocol. $DdrB_{1-144}$ was expressed and purified as described previously with the following amendments: (i) protein used in crystallography had the 6His tag removed by cleavage with TEV protease and was exchanged into 20 mM Tris pH 6.0, 100 mM KCl; (ii) protein used in DNA binding and AUC experiments was not treated with TEV to remove the N-terminal 6His tag. DdrB mutants were generated using the Maxime PCR PreMix (i-pfu) kit from iNtRON Biotechnology as per the manufacturer's protocol. All mutants were verified by sequence analysis.

4.4.2 Structure determination

Crystals were grown by the hanging-drop vapour diffusion method at 20.0°C. A 1.5 µL $DdrB_{Dr}$/ssDNA solution (740 µM $DdrB_{Dr}$ and 160 µM 50b poly dT (Integrated DNA Technologies) in 20 mM Tris pH 6.0, 100 mM KCl) was mixed with 1.5 µL of crystallization buffer (50 mM MES pH 5.6, 300 mM KCl, 10 mM $MgCl_2$, 5% PEG 8000) and dehydrated over 250 µL of 1.35 M $(NH_4)_2SO_4$. A description of difficulties encountered during crystallization have been published elsewhere (Sugiman-Marangos & Junop, 2012). Diffraction data was collected at the NSLS X29A beamline at Brookhaven National Laboratory (NY, USA). The dataset was processed scaled to 2.30 Å with HKL2000 (Otwinowski & Minor, 1997), and solved by molecular replacement with Phenix-AutoMR (Adams *et al.*, 2010) using the apo-structure of $DdrB_{Dg}$ (PDBID 4EXW) as a search model. ssDNA

was built into the structure manually with Coot (Emsley & Cowtan, 2004), and structure refinement was carried out through multiple iterations of manual refinement in Coot and automated refinement with Phenix-AutoMR until R and R_{free} values converged and geometry statistics reached an appropriate range (Table 4.1). Model coordinates and experimental data have been submitted to the Protein Databank (PDB) under the accession code: 4HQB.

4.4.3 Structure analysis

Analysis of protein-protein interfaces was performed using the PISA server from PDBe (Krissinel & Henrick, 2007). Assessment of protein-ssDNA interactions was carried out with the aid of NUCPLOT (Luscombe *et al.,* 1997) and BINANA 1.0.0 (Durrant & McCammon, 2011). Input files for BINANA in pdbqt format were generated with AutoDockTools (Morris *et al.*, 2009) using calculated Gasteiger charges and merged non-polar hydrogens.

4.4.4 DNA binding

Gel-shift assays were performed in 20 µL of EMSA buffer (20 mM Tris pH 8.0, 100 mM KCl, 15% (v/v) glycerol) with 10 µM of a 50b poly dT substrate and increasing concentrations of DdrB pentamer (0, 2, 10, 20, 50, 100 µM). Samples were resolved by electrophoresis on 4-20% polyacrylamide TGX precast gels (Bio-Rad) at 100 V for 90 minutes and visualized by SYBR Gold (Invitrogen) staining. For fluorescence polarization experiments, a 20b poly dT substrate with a 5' 6-

Table 4.1 – Data collection and model refinement statistics

Data collection		**Model and refinement**	
Space group	$P3_2$	Resolution (Å)[a]	40.30 - 2.30 (2.36 - 2.30)
Unit cell parameters		R_{work}/R_{free} (%)	19.0/24.6
a,b,c (Å)	110.7, 110.7, 58.8	$Reflections_{observed}$	35,711
Matthews coefficient	2.61	$Reflections_{Rfree}$	1,798
Molecules in ASU	6	No. atoms	
Resolution range (Å)[a]	50.0 - 2.30 (2.34 - 2.30)	Protein	4,703
Observed reflections	203,021	DNA	160
Unique reflections[a]	35,736 (1,844)	Water	194
Redundancy[a]	5.7 (5.6)	R.m.s.d. bond	
Completeness (%)[a]	99.9 (100.0)	Lengths (Å)	0.008
I/σ(I)[a]	17.4 (2.3)	Angles (°)	1.07
R_{merge} (%)[a]	6.8 (72.6)	Average B Factor (Å^2)	61.3
Wilson B Factor (Å^2)	52.34	Protein	61.6
		DNA	63.4
PDB Accession Code	4HQB	Water	52.0

[a] Statistics for the highest resolution shell are shown in parentheses.

FAM label (200 nM) was titrated with increasing concentrations of DdrB pentamer (0, 0.1, 0.2, 1, 2, 5, 10, 15, 20, 40 μM) in a total volume of 50 μL of binding buffer (20 mM Tris pH 8.0, 100 mM KCl). Fluorescence polarization measurements were performed in black, clear-bottom 96-well plates using a BioTek Synergy 4 Hybrid Microplate Reader (sensitivity = 0.35) using excitation and emission wavelengths of 485 and 528 nm, respectively. Fluorescence anisotropy (A) was calculated from polarization measurements (A = 2P/(3-P)). Fluorescence anisotropy binding data were modeled in terms of an A + B = AB isotherm, where A represents the 20 b dT and B the DdrB pentamer, in SEDPHAT 10.51 (Zhao & Shuck, 2012). Errors reported for the dissociation constant K_d represent 95% confidence intervals. All DNA substrates were purchased from Integrated DNA Technologies.

4.4.5 Sedimentation velocity analytical ultracentrifugation

Stock solutions of the wild-type DdrB, E51A, and R83A mutants were obtained in 100 mM KCl and 20 mM Tris pH 8.0. These were used to prepare samples for sedimentation velocity carried out at different loading concentrations, ranging from 10 μM to 0.64 mM. High concentration samples (0.04 – 0.64 mM) were loaded into 3-mm 2-channel epon centerpiece cells (100 μL), whereas low concentration samples (10 – 20 μM) were loaded into 12-mm 2-channel epon centerpiece cells (400 μL). Sedimentation velocity experiments were conducted at 20.0°C and 42 krpm on a Beckman Coulter ProteomeLab XL-I

analytical ultracentrifuge using both the absorbance (280 nm) and Rayleigh interference optical systems. Time corrected data (Zhao *et al.*, 2013) were analyzed in SEDFIT 14.3e (Shuck, 2000) in terms of a continuous *c(s)* distribution covering an *s* range of 0.0 – 35.0 S with a resolution of 350 and a confidence level (F-ratio) of 0.68 with a maximum entropy regularization. Excellent fits were obtained with r.m.s.d. values ranging from 0.002 – 0.012 fringes or 0.003 – 0.007 absorbance units. The solution density (ρ) and viscosity (η) were calculated based on the solvent composition using SEDNTERP 1.09 (Laue *et al.*, 1992, Cole *et al.*, 2008). The protein partial specific volumes *v* were calculated based on the amino acid composition using SEDNTERP 1.09 (Laue *et al.*, 1992, Cole *et al.*, 2008) and sedimentation coefficients were corrected to standard conditions $s_{20,w}$. To estimate the proportions of each of the contributing species, sedimentation velocity data were further analyzed in SEDPHAT 10.51 (Shuck, 2003) in terms of a set of non-interacting discrete species corresponding to 1, 2, 3, 4, and 5-mers of the DdrB pentamer.

4.5 Results and Discussion

4.5.1 The co-crystal structure of DdrB bound to ssDNA

The structure of $DdrB_{Dr}$ bound to ssDNA (Figure 4.1A) was solved by molecular replacement using the apo-structure of $DdrB_{Dg}$ (PDBID: 4EXW) as a search model. Molecular replacement produced a good quality electron density map for the entire asymmetric unit (one $DdrB_{Dr}$ pentamer) with very clear

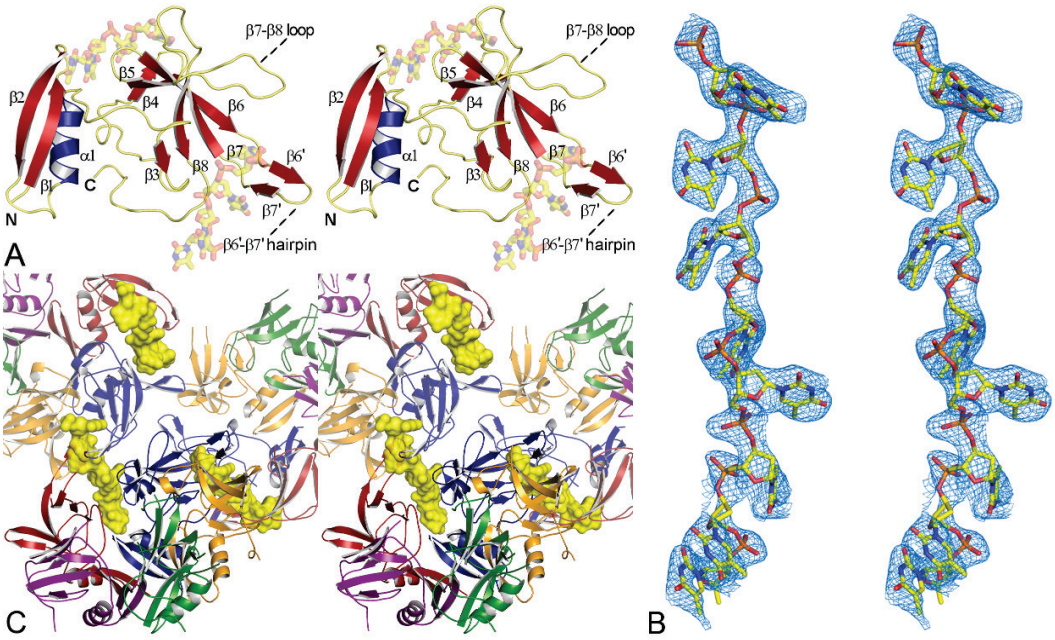

Figure 4.1 – Structure of $DdrB_{1-144}$ from *D. radiodurans* bound to ssDNA (stereo-images). (A) DdrB monomer bound to two 4-mers of ssDNA. (B) 'Kicked' 2Fo-Fc OMIT map (calculated with DNA removed), illustrating the electron density of the bound ssDNA. (C) Three DdrB pentamers. The 8b DNA molecule (yellow) bridges symmetrically related pentamers (displayed in partial transparency). This figure (and figures 4.2, 4.3, 4.6, 4.7) was prepared using PyMol (http://www.pymol.org/).

density for bound ssDNA in two clefts formed between three DdrB subunits. In total, 8 bases of dT could be modeled into the density (Figure 4.1B), which appear to form a continuous chain through the crystal when crystallographic symmetry is applied (Figure 4.1C). Although there are 5 channels formed between adjacent monomers within a single pentamer, only 2 are occupied by DNA. This may simply reflect constraints imposed by crystal packing. Alternatively, such an arrangement may be required for function in ssDNA annealing. Consistent with this possibility, the chemical environment surrounding each DNA base, observed in both occupied channels, is unique (described in detail below).

The overall structures of apo $DdrB_{Dg}$ and ssDNA bound $DdrB_{Dr}$ do not deviate to a great degree, with two notable exceptions. The regions joining β6-β7 and β7-β8 ($L_{\beta7\text{-}\beta8}$), which were unstructured in the apo model are stabilized through interactions with ssDNA and are now visible in the electron density (Supplemental Figure 4.1). Due to high B-factors, disordered side-chains, and poor connectivity in the electron density, the original structure of $DdrB_{Dg}$ deposited to the PDB was misnumbered in the latter portion of the protein. The sequence joining β6 to β7 contains a β-hairpin comprising two short β-strands spanning residues 89-91 (β6') and 94-96 (β7'), and a short loop (R92 and K93) (Figure 4.1A). The β6'-β7' hairpin is involved in direct interactions with ssDNA in the DNA-bound structure, as well as playing a key role in mediating the

oligomeric assembly observed within the crystal lattice. Similar to the apo structure, this segment is not visible in the electron density in the 2 subunits of DdrB that are void of interactions with ssDNA. Through structural superposition with $DdrB_{Dr}$, the amino acid assignment in the structure of $DdrB_{Dg}$ has been amended and the revised structure has been deposited to the PDB under PDBID: 4EXW, superseding the previous entry. A secondary structure topology diagram is presented in Supplemental Figure 4.3.

4.5.2 DNA binding residues

In the structure, eight DNA bases were bound to a single pentamer. The coordinates for this model have been deposited with two individual 4-mers of dT bound between subunits E/A (T1-T4) and A/B (T5-T8); however, when crystallographic symmetry is applied, the two 4-mers form a continuous 8-mer related by the symmetry operation [-Y, X-Y, Z+2/3]. For purposes of clarity, the binding between DdrB and ssDNA will be described for the unbroken 8-mer of ssDNA as it passes between chains A and E in the 'first' pentamer, to the groove formed between chains A and B in the 'second' pentamer (referred to as chains A' and B' hereafter). The first three bases of dT interact exclusively with residues from chains A and E, and run in the 5'->3' direction in the cleft between the two subunits from the 'bottom' face of the pentamer towards the 'top' surface (Figure 4.2A). This binding channel is flanked on one side by β3-β5 from chain A, and $L_{\beta7\text{-}\beta8}$ and the C-terminal coil from chain E on the other. Nucleotides T1 and

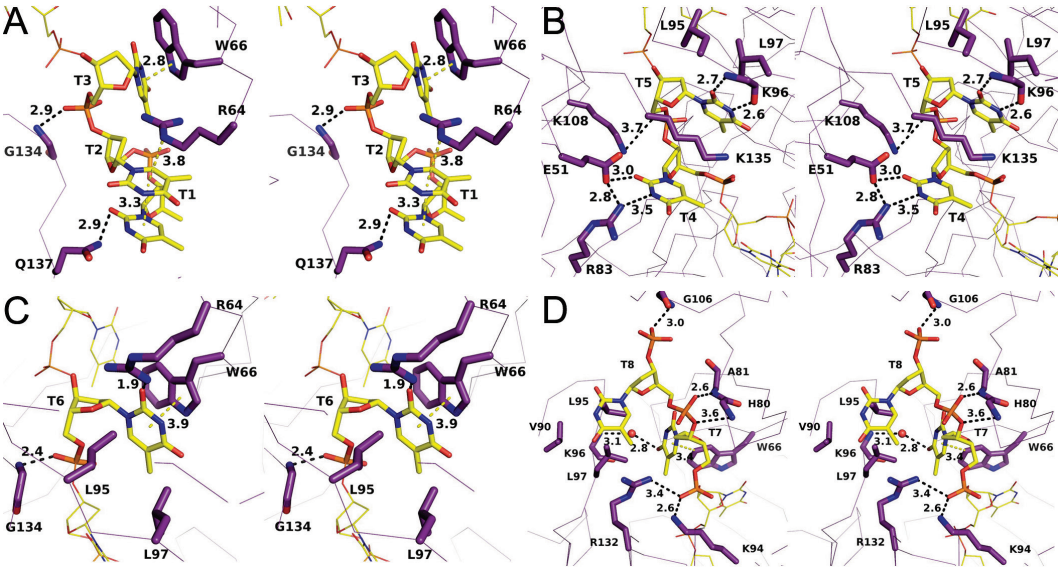

Figure 4.2 – Stereo-images of DdrB interactions with T1-T3 (A), T4-T5 (B), T6 (C), T7-T8 (D). Protein is represented in C_α form with highlighted residues and ssDNA represented in stick. Amino acid residues (yellow), DNA bases (purple) and interaction distances are labeled (Å). Polar interactions and π-interactions are denoted by black and yellow dashed-lines, respectively.

T2 base-stack and form a planar array through a cation-π interaction with $R64_A$ from β3, with T2 sandwiched between T1 and the guanidinium group of $R64_A$. The nucleobase of T1 also forms a hydrogen bond with $Q137_E$. The nucleobase of T3 forms hydrogen bonds with the guanidinium group of $R64_A$, and a π-π interaction with the indole ring of $W66_A$ from β3. T3 is further stabilized by a hydrogen-bond between the 5'-phosphate and the backbone amine of $G134_E$.

Bases T4-T6 bridge the two pentamers, interacting with a surface delineated by: β5, β6 and $L_{β7\text{-}β8}$ from chain A; the β6'-β7' hairpin and β8 from chain E; α2 and the C-terminal coil from chain A'; and β4 from chain B' (Figure 4.2B). T4 is stabilized through electrostatic interactions with $R83_A$ and $E51_{A'}$, which also form a salt bridge between them. T5 forms hydrogen bonds between its nucleobase and the backbone amino and carboxylic groups of $K96_E$, as well as significant van der Waals (vdW) contacts with the aliphatic portion of $K135_{A'}$. T5 is further stabilized through vdW interactions with the hydrophobic patch on the β6'-β7' hairpin ($L95_E$ and $L97_E$), and electrostatic interactions between $K108_A$ from $L_{β7\text{-}β8}$ and the 5'-phosphate. The nucleobase of T6 forms a hydrogen bond with the guanidinium group of $R64_{B'}$, vdW interactions with $L95_E$ and $L97_E$, and a π-π interaction with the indole ring of $W66_{B'}$. The 5'-phosphate of T6 also forms a hydrogen bond with the backbone amine of $G134_{A'}$ (Figure 4.2C).

Bases T7 and T8 emerge from the binding channel at the 'top' face of the second pentamer (Figure 4.2D). The 5'-phosphate of T7 forms hydrogen bonds

with the ε-amino group of $K94_{E}$ and the guanidinium group of $R132_{A'}$. The nucleobase of T7 forms a t-shaped π-π interaction with the indole ring of $W66_{B'}$ and is further stabilized by a solvent mediated hydrogen bond network with the backbone of $K96_{A'}$, and vdW interactions with $L95_{A'}$ and $L97_{A'}$. This hydrophobic patch on the β6'-β7' hairpin, completed by $V90_{A'}$, is also a key factor in stabilizing the nucleobase of T8. The phosphate groups of T8 are stabilized entirely by hydrogen bonding with the backbone amines of $A81_{B'}$, $H80_{B'}$ and $G106_{B'}$. Residues involved in DNA interaction are among the most highly conserved within DdrB. A multiple sequence alignment of DdrB homologues highlighting residues involved in DNA interaction is provided in Supplemental Figure 4.2.

In accordance with DdrB DNA binding studies published to date, which have used a variety of substrates interchangeably (Bouthier de la Tour *et al.*, 2011, Norais *et al.*, 2009, Xu *et al.*, 2010, Sugiman-Marangos & Junop, 2010), the interactions observed between DdrB and DNA within the crystal structure suggest a non-specific mode of binding. Overall, the interactions between DdrB and the bound ssDNA consist largely of charged interactions with the phosphate backbone, and interactions with the planar surfaces of the nucleobases. W66 in particular is involved in stabilizing three nucleobases (T3, T6, and T7) through both face-face and T-shaped π-π interactions. The limited number of hydrogen bonding interactions with the nucleobases, further points to a lack in sequence specificity within the binding channel. Consistent with this interpretation, DdrB

crystals of similar morphology could also be obtained using identical crystallization conditions with poly dA ssDNA.

4.5.3 Quaternary structure

Interaction with the continuous 8-mer is coordinated by two pentamers which form an extensive protein-protein interface (Figure 4.3A) stabilized by numerous electrostatic and hydrogen bonding interactions, and significant buried surface area (1082 $Å^2$ as calculated by the PISA server). Dimerization of DdrB pentamers is therefore required to generate the DNA binding channel occupied within the crystal structure. This interface is made up of two major contacts, insertion of the β6'-β7' hairpin from chain E into the cleft formed between chains A' and B' (Figure 4.3B), and three salt-bridges formed between chains A and A' (Figure 4.3C). Among these numerous interactions, the salt-bridge formed between residues E51 and R83 appeared to be a particularly strong interaction.

In order to verify the assembly of higher-order complexes and evaluate potential significance of this assembly in DNA binding, a mutant (E51A) targeting the pentamer self-association interface was generated. Sedimentation velocity AUC was performed with purified recombinant wild-type DdrB and the E51A mutant at 10, 20, 40, 80, and 160 μM protein concentrations utilizing both the absorbance (280 nm) and interference (655 nm) optical detection systems. *C(s)* profiles for wild-type DdrB were consistent with the assembly of pentamers,

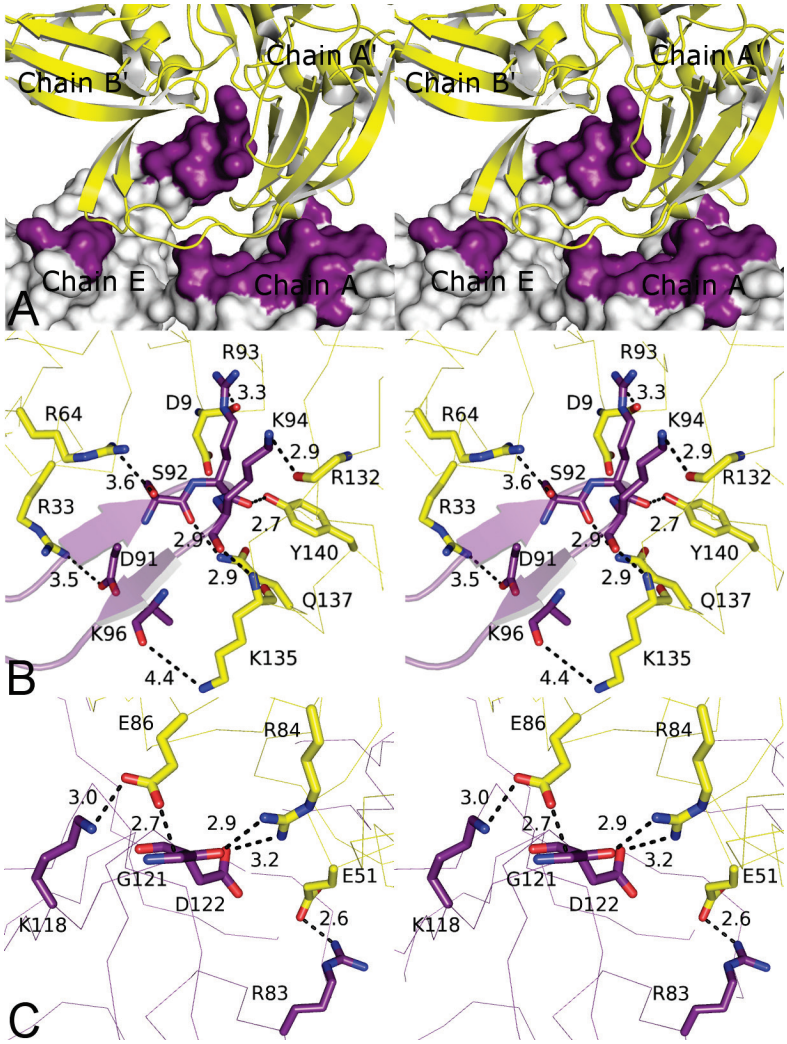

Figure 4.3 – DdrB quaternary interactions (stereo-images). (A) The pentamer-pentamer interface. Pentamer '1' (purple) interfaces with pentamer '2' (yellow) through contact surfaces distributed across 4 chains. (B) Close-up of the major interactions formed between the β6'-β7' hairpin of chain E (purple), inserted into the cleft formed between chains A' and B' (yellow). (C) Closeup of the major interactions formed between chains A (purple) and A' (yellow). Distances denoted with dashes represent polar interactions (electrostatics + H-bonds).

decamers, penta-decamers, and didecamers (Figure 4.4). While the major species in all concentrations assayed was the pentamer, contributing 39±4% to the total signal, based on an assessment of the relative signal contributions, higher-order assemblies of DdrB made up the remaining 61% of the distribution in solution. The E51A mutant, however, displayed *c(s)* profiles representative of primarily a pentameric assembly, with this species accounting for 88±2% of the total signal (Figure 4.4). To corroborate this finding, an additional mutant (R83A) was similarly analyzed. Like E51A, R83A greatly reduced higher-order assembly, resulting in 92±3% contribution from the single pentameric species (Figure 4.4). As both E51A and R83A mutants are deficient in their ability to assemble into larger complexes, the interface observed in the crystal packing appears to reflect a quaternary assembly that is relevant in solution. Importantly, this analysis clearly demonstrates that DNA binding is not required for formation of higher-order DdrB pentamer complexes.

Despite DNA having no obvious effect on the ability of DdrB pentamers to oligomerize, disruption of higher-order assemblies would be expected to disrupt DNA binding since this surface/channel is formed precisely at the pentamer-pentamer interface. In order to investigate this possibility, DNA binding of the E51A mutant was assessed using a 50 base DNA substrate. As predicted from the crystal structure, wild-type DdrB was able to form a series of higher-order protein-DNA complexes (eg. pentamer, decamer, penta-decamer) when resolved

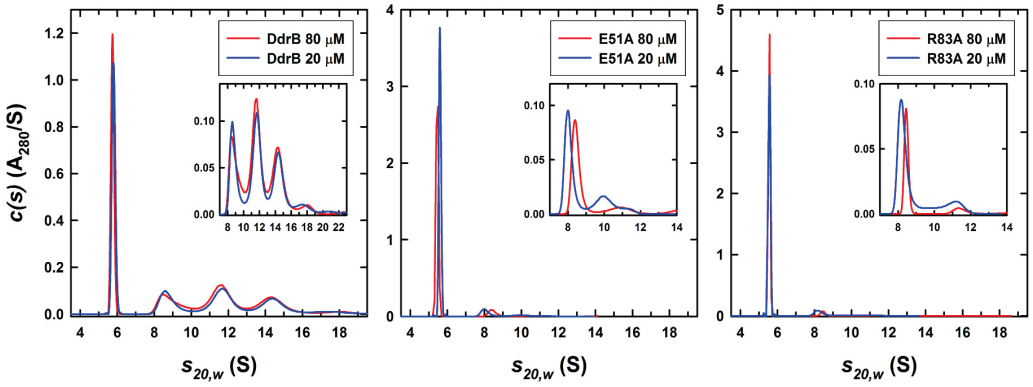

Figure 4.4 – Sedimentation velocity analytical ultracentrifugation. Absorbance *c(s)* profiles for wild-type, E51A, and R83A DdrB at loading concentrations of 20 and 80 μM. Similar profiles were obtained using the interference optical detection system. In addition similar profiles were observed for wild-type DdrB at 0.32 and 0.64 mM. A sedimentation coefficient of 5.76 S was obtained for the wild-type DdrB pentamer in a linear extrapolation of the sedimentation coefficient to zero concentration. The best-fit molar mass for this species was 118 ± 6 kDa, consistent with a DdrB pentamer. Values obtained for the E51A pentamer were 5.64 S and 116 ± 6 kDa, values for the R83A pentamer were 5.57 S and 111 ± 5 kDa. Insets expand the *c(s)* profiles to highlight contributions from the decamer (~9.1 S), penta-decamer (~11.8 S), didecamer (~14.6 S) and higher species.

on a native polyacrylamide gel (Figure 4.5). Interestingly, while the initial binding event (single DNA-pentamer complex) was unaffected by disruption of higher-order oligomerization, E51A was unable to generate more than a single nucleoprotein complex (Figure 4.5). The fact that disrupting oligomerization had no apparent effect on DNA binding affinity suggests that pentamer multimerization may not be required for DNA binding. The presence of a single species with the E51A mutant is still somewhat surprising. If a single DdrB pentamer were still able to bind DNA at the surface observed within the crystal structure, it would only require 4 bases and therefore with a 50 base oligomer one would have expected multiple individual pentamer binding events and subsequent shifts to have been observed. A more direct interpretation of this result is that although disruption of pentamer oligomerization disrupts the observed DNA binding surface/channel the single pentamer retains DNA binding function. This would imply the existence of an additional, unidentified DNA binding surface and would help to reconcile the crystal structure with earlier findings that suggested the size of DNA required to fully saturate DdrB is 40-50 bases (Bouthier de la Tour *et al.*, 2011).

4.5.4 An extended ssDNA binding surface

It was proposed previously that DdrB might interact with ssDNA through a surface formed along one continuous (top) face of the pentamer (Sugiman-Marangos & Junop, 2010) (Figure 4.6A). This was suggested based on the

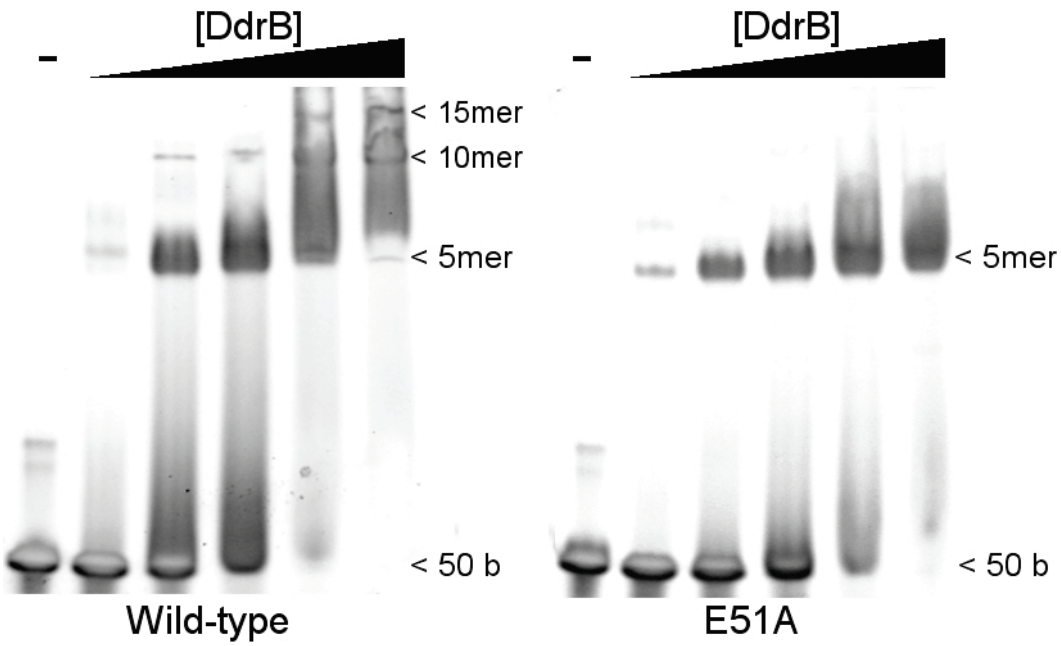

Figure 4.5 – Electrophoretic mobility shift assay of 50b ssDNA by wild-type and E51A DdrB. DNA (10 μM) was incubated with increasing concentrations of DdrB pentamer (0, 2, 10, 20, 50, 100 μM) and resolved on a 4-20% native polyacrylamide gel. Shifts corresponding to DNA-pentamer, DNA-decamer, and DNA-pentadecamer nucleoprotein complexes are visible with wild-type DdrB. While the E51A mutant readily forms the DNA-pentamer complex, no distinct shifts corresponding to higher-order assemblies are visible in the gel.

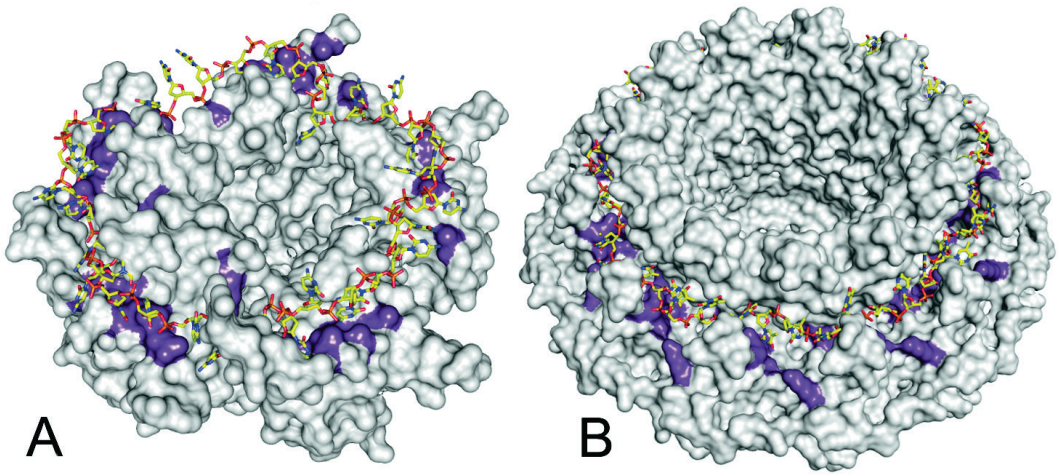

Figure 4.6 – Comparison of models of Rad52 and DdrB ssDNA interactions. (A) Model of ssDNA binding utilizing the 'top' face of the DdrB pentamer (Sugiman-Marangos & Junop, 2010). Residues with predicted DNA binding properties are colored in purple with ssDNA overlayed for reference. (B) The structure of undecameric Rad52 (PDBID – 1KN0) with predicted DNA binding interface highlighted in purple. ssDNA is overlaid on the structure of Rad52 (as reported by Singleton *et al*.) (Singleton *et al.*, 2002).

chemical nature of side chains along this surface, and the structural 'analogy' to the ssDNA binding surface of SSB. Interestingly, Rad52 has also been predicted to bind ssDNA along a similar surface formed by a ring assembly (Kagawa *et al.*, 2002, Singleton *et al.*, 2002) (Figure 4.6B). In DdrB, several residues predicted to be involved in ssDNA binding, which lie along the 'top' face of the extended β-sheet region (W66, R64, R83), do play key roles in binding ssDNA within the crystal structure. The convex shape of the β-sheets allows the ends to curve inward, forming channels between adjacent monomers. In the crystal structure, the bound ssDNA passes through this channel from one pentamer to another, rather than continuing along the surface of the β-sheet. The possibility therefore exists that DdrB possesses an extended DNA binding surface, continuing from the channel and running along the entire 'top' surface (Figure 4.6A). Evidence for such a scenario was recently reported for uracil-DNA glycosylase that demonstrated an extended DNA binding surface, not observed within the crystal structure (Roberts *et al.*, 2012). Authors suggested that due to constraints imposed on protein-DNA complexes during crystallization, many similar cases might exist in which the DNA binding interface observed within a crystal structure only partially reflects the true biological surface.

In order to explore this possibility, alanine substitutions were generated both at residues forming interactions with ssDNA in the crystal structure (R64, W66, R83, K94, K108, R132, K135) and residues that may mediate binding along

the 'top' surface (R85, K102). A fluorescence polarization based assay was used to determine an estimate of the K_d for the interaction between a 20b poly dT ssDNA substrate and wild-type DdrB pentamer and was found to be 3.6±0.6 μM (Figure 4.7A).

The ssDNA binding abilities of the DdrB mutants were assessed by the same fluorescence polarization experiment at a pentamer concentration of 3 μM and the anisotropy measurements were standardized to the wild-type protein. Under these conditions also using a 20b poly dT ssDNA substrate, all 9 mutants were found to be deficient in their ability to bind ssDNA ranging from ~20-50% of the binding capability of the wild-type protein (Figure 4.7B). This level of reduced binding is in agreement with what one would expect considering the large number of residues (15 amino acids total) involved in the interface. Mutant E51A was also analyzed in this assay and, as expected from EMSA analysis (Figure 4.5), found to retain full DNA binding activity. Residues R85 and K102 were void of any interactions with ssDNA in the crystal structure, yet substitution of these residues rendered the protein equally deficient in binding as mutation of key residues identified by analysis of the DNA-bound structure. These residues are absolutely conserved amongst all DdrB homologues despite any obvious involvement in structural integrity (Supplemental Figure 4.2). Together, these findings strongly support the idea that R85 and K102 contribute to an extended ssDNA binding surface delineated by the solvent exposed β-sheet

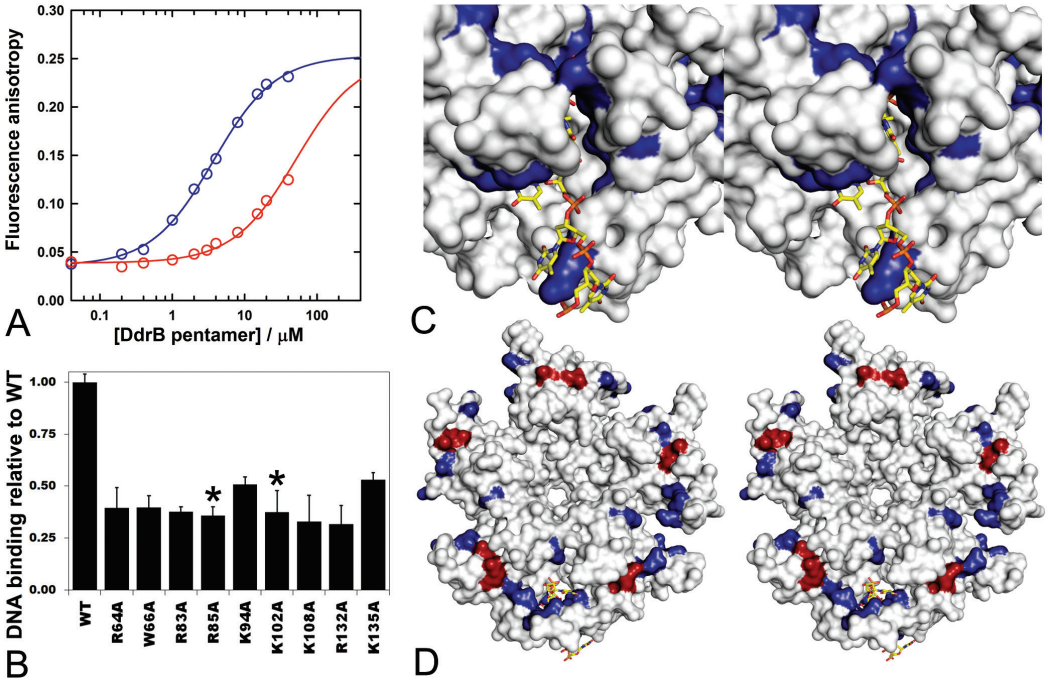

Figure 4.7 – DdrB-ssDNA interactions. (A) Titration of 20 b FAM labeled dT with increasing concentrations of wild-type (blue) and W66A (red) DdrB analyzed by fluorescence anisotropy. The fluorescence anisotropy of the labeled ssDNA substrate increases as its rotational movement decreases upon protein binding. Best-fits to a reversible A (DNA) + B (DdrB pentamer) = AB model, shown as solid lines, return K_d values of 3.6±0.6 μM for the wild-type DdrB and 51±9 μM for the W66A mutant. In the case of the latter, the saturating anisotropy was fixed at the value obtained for the wild-type DdrB. (B) DNA binding of DdrB mutants relative to wild-type DdrB at 3 μM pentamer concentration (error bars represent standard deviation of n=3 trials). Residues highlighted with a (*) were not observed to interact with ssDNA in the co-crystal structure. (C) Stereo-image of the ssDNA binding surface of DdrB from the crystal-structure. Surfaces colored in blue represent residues that were subjected to amino acid substitution and displayed decreased binding relative to wild-type. (D) Stereo-image of the `top` face of the DdrB pentamer. Colored surfaces represent residues subjected to amino acid substitution, which displayed decreased binding relative to wild-type. Residues colored in blue were observed to form interaction with ssDNA in the crystal structure, while those in red (R85, K102) showed no interaction with ssDNA. The colored (blue and red) surface defines a possible extended ssDNA binding mode in addition to the one observed within the structure.

running along the top surface of the DdrB pentamer which is distinct from the occupied channel surface within the crystal structure (Figure 4.7C, D).

4.5.6 Potential mechanisms for DdrB in DNA repair

To date, it has been suggested that DdrB may play a role as both an alternative to SSB in protection of exposed ssDNA (Norais *et al.*, 2009), and also in promoting annealing of complementary ssDNA strands during the process of SSA (Bouthier de la Tour *et al.*, 2011, Xu *et al.*, 2010). The crystal structure of DdrB bound to ssDNA illustrates a mode of binding that involves dimerization of two pentamer units. This higher-order structure was further demonstrated to extend to penta-decamers and didecamers in solution (Figure 4.4). Furthermore, DNA binding studies of wild-type DdrB and a mutant that lacks the ability to form higher-order complexes (E51A) demonstrated that oligomerization facilitates assembly of extended nucleoprotein complexes (Figure 4.5). Taken together these findings suggest DdrB assembles extended structures able to completely coat ssDNA. By involving direct protein-protein interaction of pentameric units, the cell assures that ssDNA is fully protected, occluding interaction with other proteins and preventing self-association of large stretches of ssDNA. This idea is further supported by the large abundance of DdrB during recovery (Basu & Apte, 2012), and also EM studies, which demonstrated that DdrB is able to fully coat circular ssDNA in a manner similar to SSB (Norais *et al.*, 2009).

The limited amount of ssDNA (8 bases) covered by a single DdrB decamer complex, although sufficient to function in coating DNA, is difficult to reconcile with its observed ability to stimulate ssDNA annealing. In addition, binding studies have suggested a much longer DNA length as necessary to fully saturate DdrB (Bouthier de la Tour *et al.*, 2011). An extended DNA binding interface, where ssDNA continues along the top surface of the pentamer involving longer segments of ssDNA, would explain observations from prior binding studies and provide a mechanism for coordinating DdrB's annealing activity. In this arrangement, DdrB could facilitate annealing by optimally positioning individual strands of ssDNA fed through different pores of a single DdrB pentamer (Figure 4.8A). Given that a pentamer of DdrB has 5 of these channels through which it can interact with ssDNA, the actual biological mechanism may be more complicated than the simple model that has been presented. In this scenario, it is not obvious what the role of the extended 'top' DNA binding surface would serve and, furthermore, how DdrB would stimulate accurate annealing of DNA. A similar, but more likely possibility is that DdrB may be acting in a manner similar to what has been proposed for Rad52 (Singleton *et al.*, 2002), in that ssDNA may bind to the top face of the pentamer in such a way that the nucleobases are presented outward, allowing a second strand (also associated with DdrB) to sample the exposed bases for complementarity (Figure 4.8B). In either scenario, the annealing reaction would be driven by the

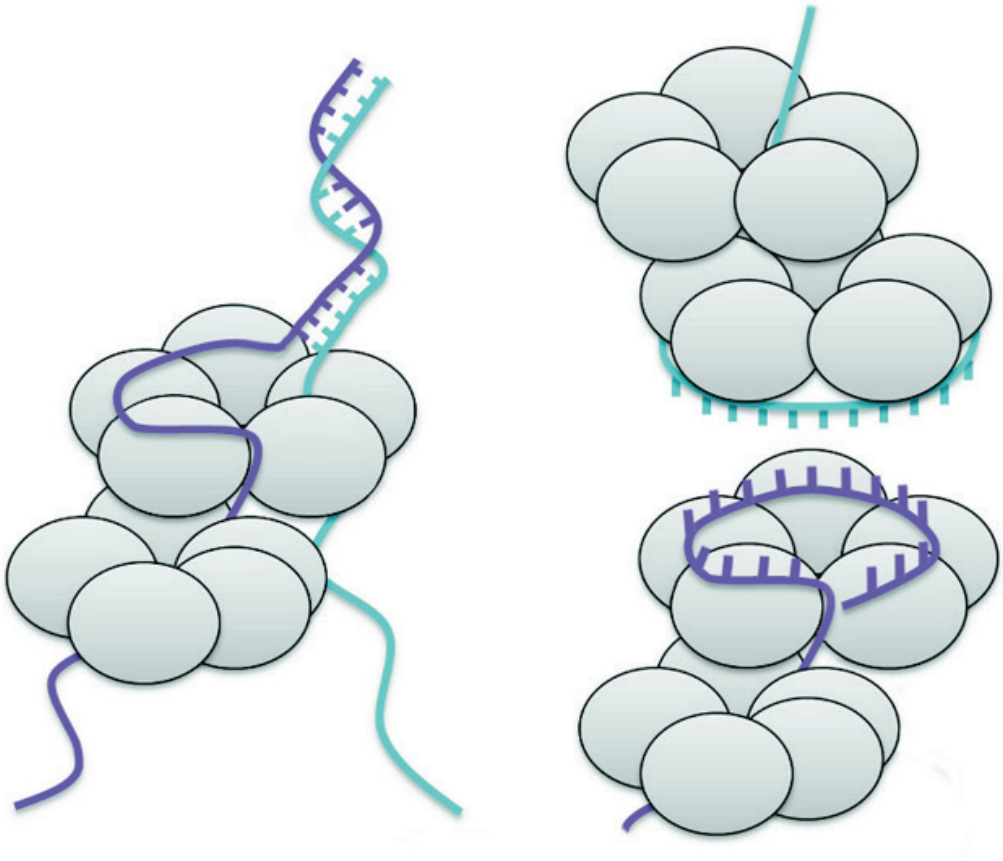

Figure 4.8 – Two models of possible mechanisms for DdrB mediated ssDNA annealing. (A) Two strands of ssDNA thread through different pores on a single DdrB pentamer. One strand is shown interacting with an extended face spanning multiple monomers within the pentamer. Annealing of strands is proposed to be facilitated by the forced juxtaposition of strands at a distinct location on the pentamer. (B) A strand of ssDNA is bound to the 'top' face of the DdrB pentamer with bases projecting outwards. A second strand, similarly bound to DdrB senses for complementarity with the outwardly pointed bases.

thermodynamically favorable formation of duplex DNA. During the preparation of this manuscript a report was published describing the EM reconstruction of HSV-1 annealing protein ICP8 in complex with ssDNA (Tolun *et al.*, 2013). The structure suggested a mechanism for ssDNA annealing involving formation of two stacked nonameric ring assemblies with DNA positioned at the interface, reminiscent to what we have proposed for DdrB in Figure 4.8B.

4.5.6 Functional similarities between Rad52, DdrB and DdrA.

Rad52 is well known for its ability to stimulate ssDNA annealing. DdrA is another protein unique to *Deinococcus* that, unlike DdrB, displays distant sequence similarity to Rad52, and has been suggested to serve a similar function in *D. radiodurans* (Gutsche *et al.*, 2008); however, its role in ssDNA annealing has never been reported. Previous experiments have demonstrated that *ddrB* and *ddrA* form separate, *recA*-independent epistatis groups, as the double-deletion mutant is more radio-sensitive than either of the single-deletion mutants alone (Tanaka *et al.*, 2004). If DdrB serves a role in *D. radiodurans* that is similar to Rad52 in eukaryotes, and DdrA is related by sequence to Rad52, it begs the question of whether DdrA and DdrB are functionally equivalent. If DdrB and DdrA are in fact functional homologues, it stands to reason that deleting one or the other may not have a significant effect on the ability to recover from extensive strand-breakages except in the most extreme cases, and that deletion of both would result in an even more severe phenotype, as was observed

(Tanaka *et al.*, 2004). Given that both DdrA and DdrB display either functional or sequence similarity to Rad52, the possibility exists that in addition to playing similar roles in alternative pathways, they may be able to complement one another. While the electron microscopy structure of DdrA illustrates a ring forming assembly similar to both DdrB and Rad52 (Gutsche *et al.*, 2008); additional structural information, in the form of a high-resolution crystal structure, would be helpful in evaluating this possibility.

4.6 Funding

This work was supported by the Natural Sciences and Engineering Research Council of Canada through grant (2008R00075 to M.S.J.), studentship (S.N.S.M. and Y.M.W.). Data for this study were measured at beamline X29A of the National Synchrotron Light Source. Financial support comes principally from the Offices of Biological and Environmental Research and of Basic Energy Sciences of the US Department of Energy, and from the National Center for Research Resources (P41RR012408) and the National Institute of General Medical Sciences (P41GM103473) of the National Institutes of Health. This work was also supported in part by the Intramural Research Program of the National Institutes Health, the National Institute of Diabetes and Digestive and Kidney Diseases, NIDDK (R.G.).

4.7 Supplemental Data

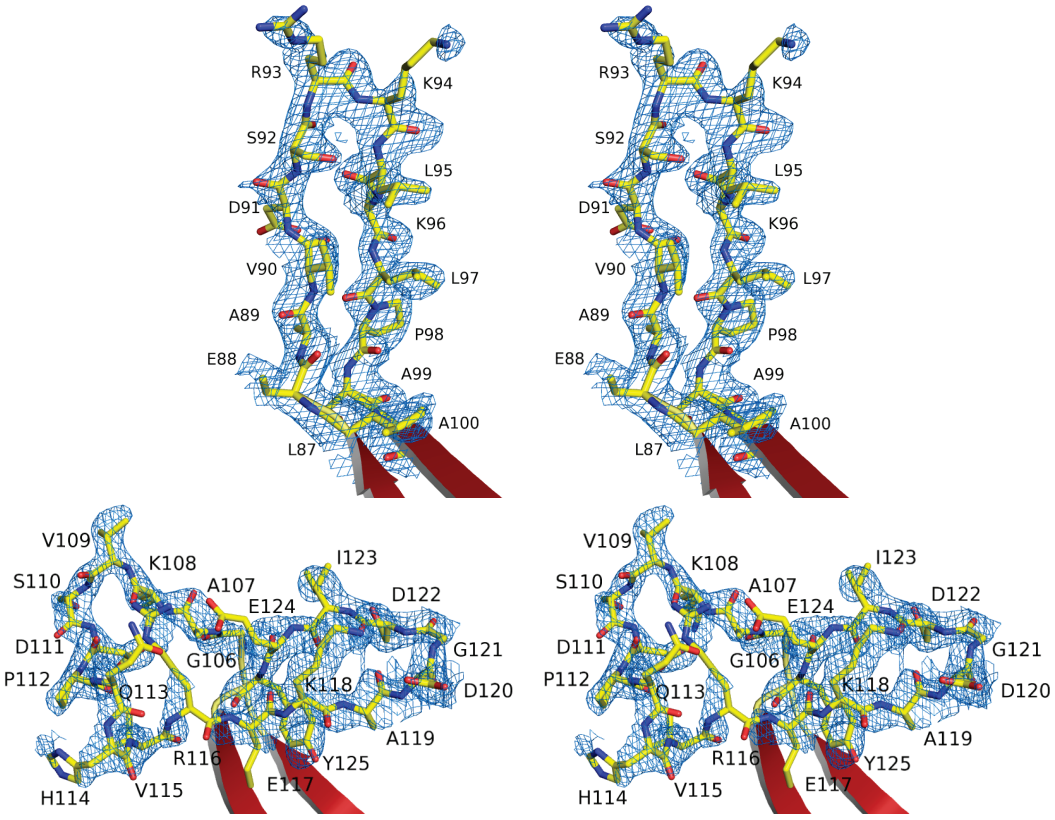

Supplemental Figure 4.1 – Stereo-images of the electron density of the β6'-β7' hairpin and $L_{β7\text{-}β8}$. Simulated annealing OMIT map (2mFo-dFc) of residues making up the hairpin joining strands β6 and β7 (top), and the loop joining β7 and β8 (bottom). Density is contoured to 1.0 σ in PyMol.

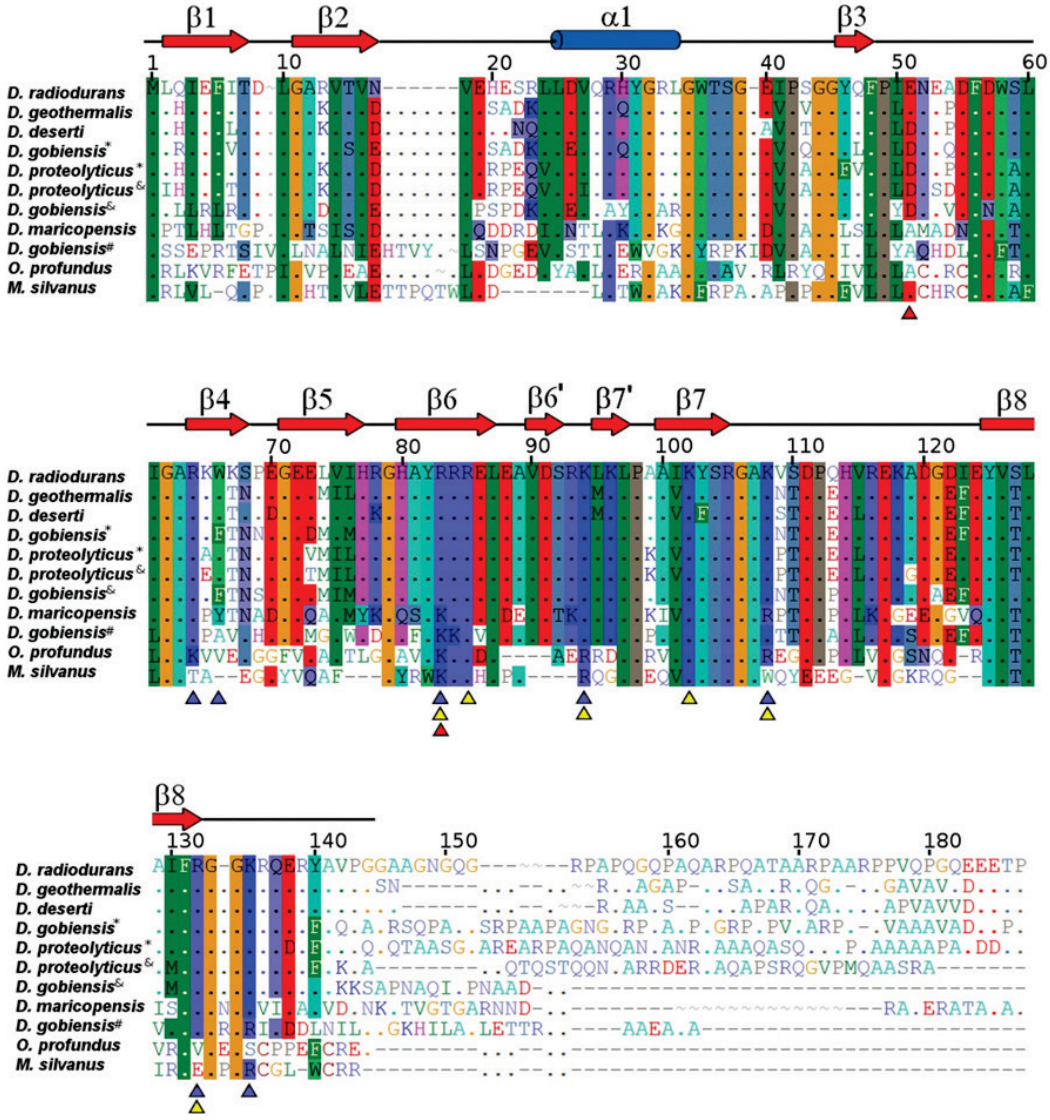

Supplemental Figure 4.2 – DdrB multiple sequence alignment. 11 homologues of DdrB were aligned using the BLAST server (http://blast.ncbi.nlm.nih.gov/). Species with more than one copy of DdrB are denoted with *(DGo_CA0350, Deipr_1603), &(Deipr_2350, DGo_PC0273) or #(DGo_PB0067). Highly conserved residues are highlighted and coloured by amino acid. Triangles indicate residues involved in: (i) decamer association, E51, R83 (red); (ii) ssDNA interaction, R64, W66, R83, K94, K108, R132, K135 (blue); and (iii) a predicted alternate ssDNA binding surface, R83, R85, K102, K108, R132 (yellow). It should be noted that some residues are likely to participate in both proposed modes of ssDNA interaction and are therefore labelled with more than one triangle.

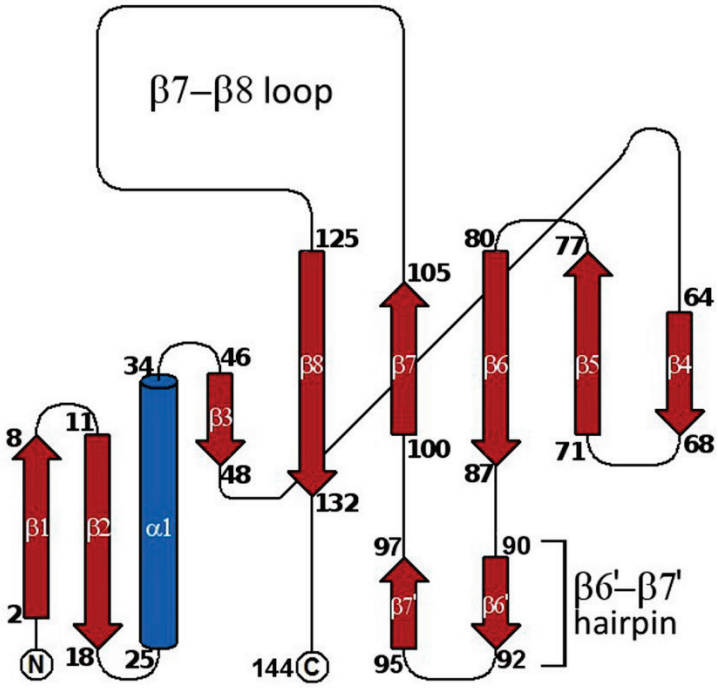

Supplemental Figure 4.3 – DdrB secondary structure topology. Secondary structure elements are labeled and coloured (red – β-strand, blue – α-helix). Diagram was generated with TopDraw.

CHAPTER 5 – CRYSTAL STRUCTURE OF DDRB/SSDNA: NEW INSIGHT INTO THE MECHANISM OF SINGLE-STRANDED ANNEALING

5.1 Author's preface

The work described in this chapter has not yet been published. The presented structure reveals an extended mode of ssDNA binding to the DdrB pentamer that confirms the predictions made in Chapter 4. In addition, the packing arrangement observed within the crystal suggests a mechanism for single-stranded annealing. This chapter will begin with a short introduction describing new information presented in the literature with regards to DdrB function. S.N. Sugiman-Marangos performed the experimental work described in this chapter with the aid of Y.M. Weiss, who helped set crystallization trials.

5.2 Introduction

DdrB has recently been demonstrated to protect oligonucleotides from the exonuclease activity of RecJ (Jiao *et al.*, 2012), supporting a role in protection of ssDNA generated during repair. This is in addition to the observations that DdrB is able to stimulate annealing of oligonucleotides, even in the presence of SSB (Xu *et al.*, 2010), and that DdrB is involved in transformation, as the deletion strain ΔddrB is approximately 100-fold less efficient than wild-type *D. radiodurans* in establishing transformed plasmid DNA (Bouthier de la Tour *et al.*, 2011). It was further shown that DdrB is not required for transformation of chromosomal DNA, while RecA demonstrates inverse trends (required in transformation of chromosomal DNA, but not plasmid DNA). This is similar to what has been observed in *B. subtilis*, which possess independent pathways for transformation of chromosomal and plasmid DNA mediated by RecA and RecO, respectively (Kidane *et al.*, 2009). *D. radiodurans* RecO has approximately 10-fold less annealing activity than *E. coli* RecO, requiring a 10:1 excess to induce pairing of complementary oligonucleotides *in vitro* (Makharashvili *et al.*, 2004). Furthermore, while deletion of *recO* reduces the frequency of plasmid transformation in *D. radiodurans*, the effect is still 10-fold less than in the Δ*ddrB* strain (Bouthier de la Tour *et al.*, 2011). Taken together, these data suggest that the annealing activity of DdrB substitutes for RecO in plasmid transformation in

D. radiodurans in addition to its role in DNA repair, making a mechanistic understanding of DdrB mediated DNA annealing even more significant.

Despite being a function conserved across all domains of life, the mechanism of protein mediated annealing of complementary ssDNA has yet to be fully characterized. Rad52 is the best studied among this group of functional analogues, playing a key role in double-strand break repair in both yeast and higher eukaryotes (Feng *et al.*, 2011). The crystal structure of the annealing domain of human Rad52 has been determined (Kagawa *et al.*, 2002, Singleton *et al.*, 2002), and a systematic analysis of single-amino acid substitutions *in vitro* have delineated a ssDNA interaction interface; however, structural data for this complex is not yet available. Mutational analysis presented in Chapter 4 defined an extended DNA binding interface on DdrB which closely resembles the proposed surface on Rad52. The structure presented in this chapter illustrates the extended DNA binding surface which traces along the 'top' face of the DdrB pentamer that we had predicted and offers insight into the mechanism of protein mediated single-stranded annealing.

5.3 Materials and methods

5.3.1 Protein expression and purification

The expression construct (pET151-D-Topo) harbouring the C-terminal truncation of DdrB from *D. radiodurans* (residues 1-144) which had been crystallized in Chapter 3 was transformed into the expression line *E. coli*

BL21(DE3) and grown in LB media to an OD_{600} of approximately 0.5. Expression was induced with 1 mM IPTG and cells were incubated for an additional 3 hours at 37°C. Cell pellets were harvested by centrifugation (10 min at 48,000 g), re-suspended in lysis buffer (20 mM Tris pH 8.0, 1 M NaCl, 5 mM imidazole), and lysed by sonication (3x1 min rounds). Soluble lysate was flown over a 5 mL Ni-IMAC column using a AKTA-FPLC, washed with a dilute imidazole solution (100 mM imidazole), and eluted (350 mM imidazole). The eluted fraction was immediately exchanged into low salt buffer (20 mM Tris pH 8.0, 150 mM KCl) and incubated overnight with TEV protease to cleave the N-terminal 6His tag. Untagged $DdrB_{1-144}$ was isolated by another pass over a 5 mL Ni-IMAC column, before a final buffer exchange into crystallization buffer (20 mM Tris pH 8.0, 150 mM KCl).

5.3.2 Crystallization and data collection

Two DNA substrates mimicking potential ss/dsDNA intermediates were designed yielding either an "overlapping" or "splitting" DNA substrate (Figure 5.1). Substrates were annealed by mixing equal volumes of AS1 and AS2 or AS2 and AS3 at DNA concentrations of 1 mM, heating to 95°C in a thermocycler, and then reducing the temperature to 25°C at a rate of 1°C/min. The protein/DNA solution was prepared by mixing purified $DdrB_{1-144}$ in crystallization buffer (20 mM Tris pH 8.0, 150 mM KCl) with either "overlapping" or "splitting" substrate to final concentrations of 462 µM (protein) and 400 µM (DNA), respectively.

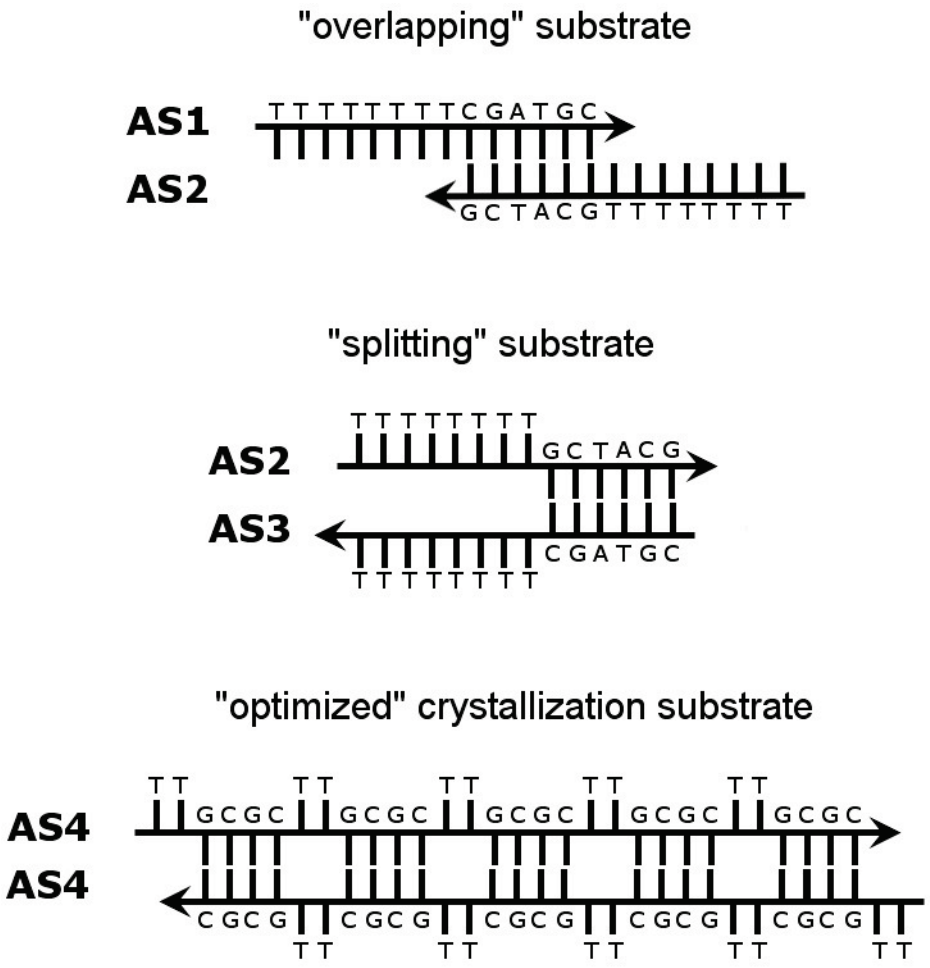

Figure 5.1 – ss/dsDNA hybrid substrates. Two hybrid substrates ("overlapping" and "splitting") were designed to capture a snapshot of DdrB in the process of mediating single-stranded annealing based on the crystal structure of the DNA/DdrB complex featured in Chapter 4. These substrates contained long, non-complementary poly dT tails and a short sequence capable of hybridizing. Data collected from crystals grown with these initial substrates was used to design an "optimized annealing" substrate (AS4), which consisted of a repeating pattern of 'TTGCGC'. This substrate is able to hybridize with itself with two mismatched bases out of every six.

Crystal screening was carried out by adding 1 µL of the protein/DNA solution to 1 µL of crystallization condition from the KeraFAST DNA/protein co-crystallization kit, and dehydrating the drops over 250 µL of 1.5 M ammonium sulfate at 20^{o}C (hanging-drop).

Initial hits nucleated in KeraFAST conditions 5 (6% PEG 4000, 0.1 M sodium acetate pH 4.6, 0.05 M $MgCl_2$), 35 (11% PEG 4000, 0.1 M sodium acetate pH 4.6, 0.1 M NaCl), and 45 (6% PEG 2000, 0.1 M HEPES pH 7.5, 0.05 M $CaCl_2$). The three hits all produced showers of small crystals that were verified to be protein/DNA complexes by X-ray screening and incorporation of a Cy5 labelled DNA substrate (as described in Chapter 3). As the conditions contained common components, 4 grid screens were prepared (4 x 48 conditions) exploring various gradients of PEG, pH, and salt. Screening of the protein/DNA complex across these conditions with varying concentrations of dehydrating solution (1.0-1.4 M ammonium sulfate) produced drops with fewer nucleants. A dataset was collected on beamline X25 at the NSLS (BNL) from a crystal of the $DdrB_{1-144}$ complex with "overlapping" substrate to a resolution of ~2.85 Å. Molecular replacement was performed using the structure of $DdrB_{1-144}$ from *D. radiodurans* (PDBID 4HQB) as a search model. Initial modelling of the data (see Appendix Table A.1 for data processing and refinement statistics) revealed that more suitable DNA substrates could be designed to better fit the observed protein/DNA interaction taking place in the crystal (discussed in Section 5.4.1).

Crystals of $DdrB_{1-144}$ and DNA substrate AS4 (5'-TTGCGCTTGCGCTTGCGCTTGCGCTTGCGC, Figure 5.1) were grown by mixing 1 µL of $DdrB_{1-144}$/AS4 (480 µM protein, 143 µM DNA) with 1 µL of crystallization condition (6% PEG 2000, 0.1 M HEPES pH 6.5, 0.05 M $CaCl_2$), and 0.2 µL of Hampton Additive Screen condition 48 (0.01 M L-Glutathione reduced, 0.01 M L-Glutathione oxidized), and dehydrating over 1.2 M ammonium sulfate at 20°C. Crystals grown with the Hampton Additive condition 48 had a different morphology and internal symmetry ($P4_22_12$) than those grown in the same condition but without additive ($P3_22_1$). Also, in addition to diffracting to higher resolution (2.2 Å), these crystals also produced data that was easier to process as the long axis present in the previous crystal form (c = 259 Å) was absent. No additional cryoprotectant was required for data collection.

5.3.3 Data processing and structure solution

The diffraction data was integrated with mosflm (Leslie & Powell, 2007), and then scaled, merged, and converted to structure factors with CCP4 (Winn *et al.*, 2011, French & Wilson, 1978). Structure solution was performed with AutoMR from the Phenix software package (Adams *et al.*, 2010) using the $DdrB_{1-144}$ monomer from *D. radiodurans* (PDBID 4HQB) as a search model. The best molecular replacement solution was generated using a search model with manually truncated loops regions, which was then rebuilt-in-place into a simulated annealing OMIT map using Phenix-AutoBuild. Missing loop regions

(87-101, and 105-125) and DNA bases were placed manually and refined in iterative cycles using Coot (Emsley & Cowtan, 2004) and Phenix-Refine until R and R_{free} values converged and geometry statistics reached suitable ranges (Table 5.1).

5.4 Results

5.4.1 DdrB binds ssDNA along its 'top' face

Molecular replacement generated a top solution with an LLG of 2175, containing 5 monomers of DdrB in the ASU, similar to the 2 previous structures of DdrB solved. The majority of the main chain could be traced; however, density for the loop regions joining β4 to β5 ($L_{\beta4\text{-}\beta5}$) and the β6'-β7' hairpin ($H_{\beta6'\text{-}\beta7'}$) could not be completely traced in all chains. Electron density for bound DNA was immediately visible in the map, and the nucleic acid chain could be traced along the continuous surface formed by the exposed faces of the β-sheets of each DdrB monomer (Figures 5.2 and 5.3). In total, 30 bases of DNA were modeled, with 6 interacting with each subunit of the ring in a repeating pattern of 2 bases turned in towards the surface of the pentamer (dT, dT), and 4 bases facing outwards (dG, dC, dG, dC) (Figure 5.2). Binding of DNA along the 'top' surface also resulted in a significant change in the tertiary structure of the loop joining β7 to β8 ($L_{\beta7\text{-}\beta8}$), allowing for additional hydrogen bonding interactions in the main chain of the protein. A new secondary structure element, comprising residues 117-120, has been designated β8' and is annotated in Figure 5.2.

Table 5.1 – Data collection and model refinement statistics

Data collection	
Space group	$P4_22_12$
Unit cell parameters	
a,b,c (Å)	131.8, 131.8, 102.3
Matthews coefficient	2.74
Molecules in ASU	6
Resolution range (Å)[a]	80.79 - 2.20 (2.32 - 2.20)
Observed reflections	545,096
Unique reflections[a]	46,259 (6,641)
Redundancy[a]	11.8 (10.1)
Completeness (%)[a]	100.0 (99.9)
I/σ(I)[a]	15.0 (2.9)
R_{meas} (%)[a]	12.1 (85.7)
R_{pim} (%)[a]	3.5 (26.4)
Wilson B Factor (Å^2)	33.2

Model and refinement	
Resolution (Å) [a]	65.88 – 2.20 (2.24 – 2.20)
R_{work}/R_{free} (%)	18.78/23.33
$Reflections_{observed}$	46,201
$Reflections_{Rfree}$	2,356
No. atoms	
Protein	5,140
DNA	612
Water	556
R.m.s.d. bond	
Lengths (Å)	0.007
Angles (°)	1.209
Average B Factor (Å^2)	28.90

[a] Statistics for the highest resolution shell are shown in parentheses.

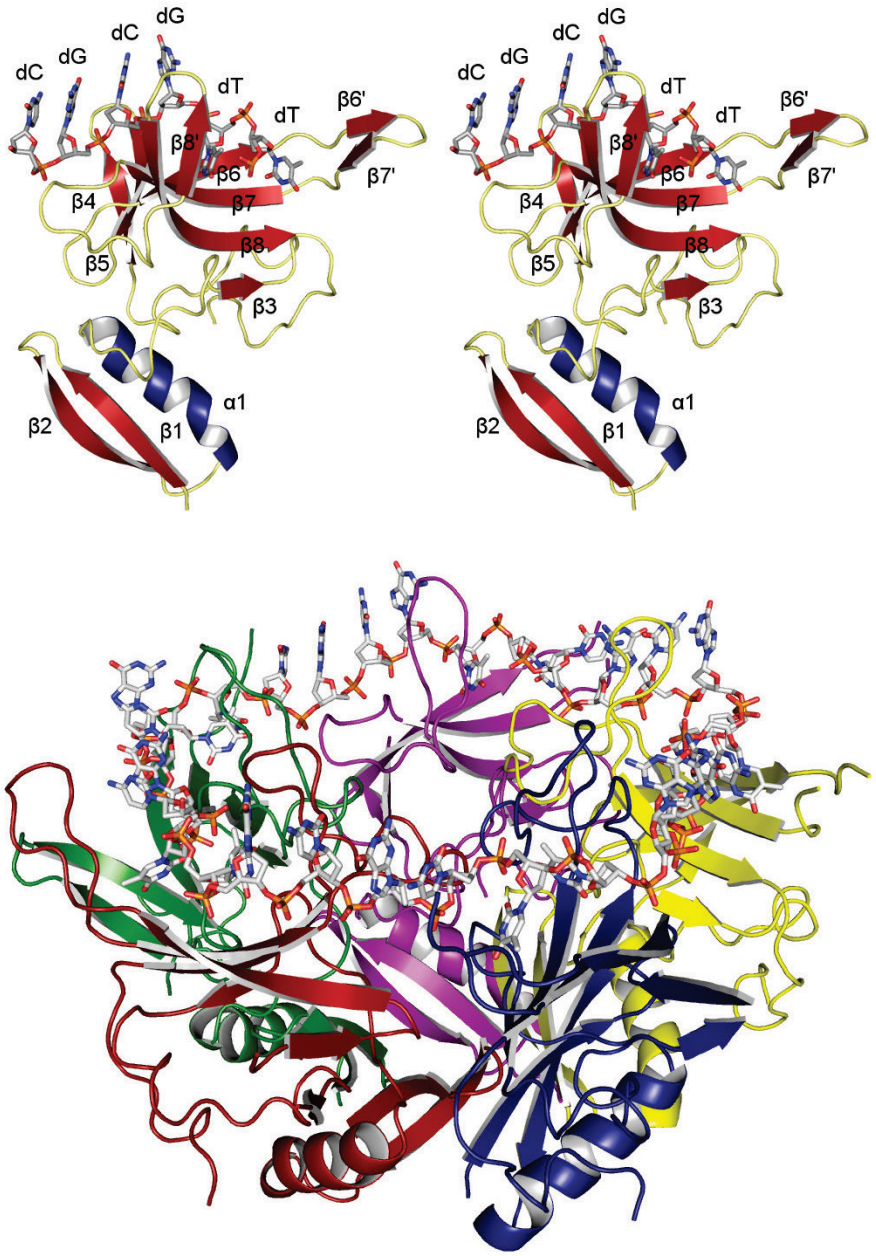

Figure 5.2 – Crystal structure of DdrB in complex with a 30 b DNA substrate (AS4). Top – Stereo-image of a monomer of DdrB (α-helix in blue, β-strand in red) interacting with the 6 bases of ssDNA (5'-TTGCGC). Bottom – DdrB pentamer with DNA bound to the 'top' surface in a repeating pattern of 2 bases turned in and 4 bases turned outward. Each subunit is coloured separately.

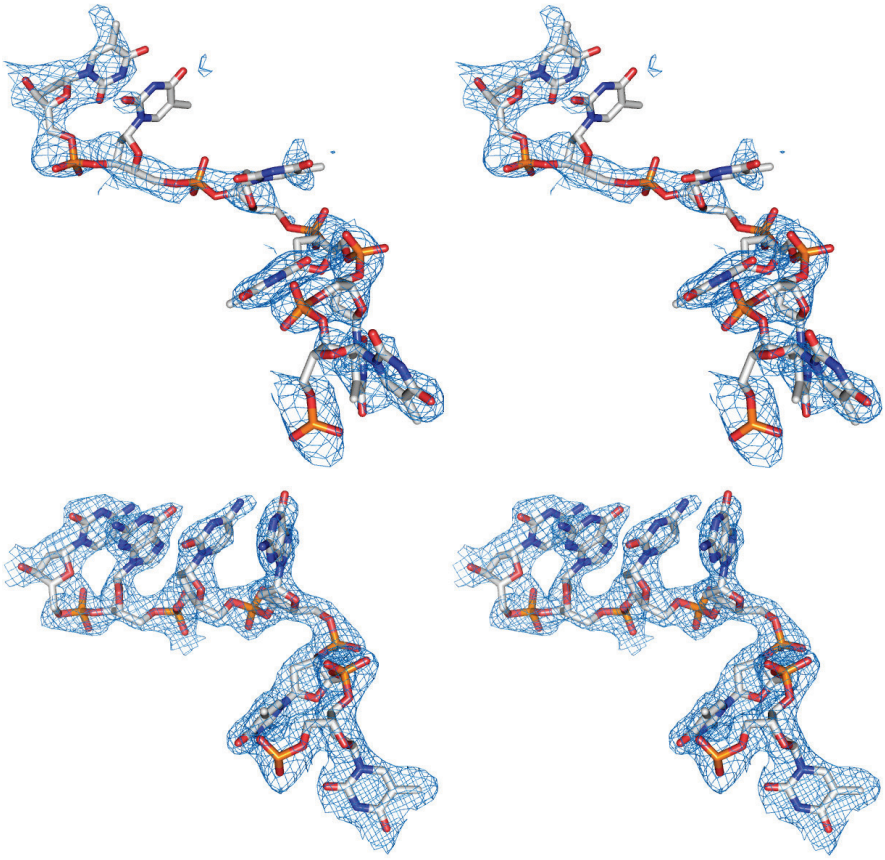

Figure 5.3 – Representative electron density of bound DNA (stereo-images). Electron density (contoured at 1 σ) and modeled bases from crystals grown with "overlapping"-AS1/AS2 (top – 2.85 Å) and AS4 (bottom – 2.2 Å) DNA substrates. A clear difference is visible in the quality of electron density and the occupancy of the nucleobases from the maps calculated with the two substrates.

The model built from the initial crystallization with the "overlapping" and "splitting" substrates had DNA bound in the same configuration as the presented structure. Due to the nature of the initial substrates, however, there was no discrete pattern of binding. This resulted in strong signal in the electron density for the common elements of the individual bases (phosphate and ribose moieties), but weak density for the nucleobases due to averaging across unit cells containing different positioning of individual nucleobases (Figure 5.3). Substrate AS4 was designed with a repeating pattern of 5'-TTGCGC such that the 2 dT residues would turn in towards the protein while the subsequent residues would face outwards, available for base pairing. The GCGC motif is able to self-anneal (Figure 5.1), yielding a ss/dsDNA hybrid with 2 unpaired bases out of 6, locking the substrate into a uniform mode of binding and producing distinct unambiguous density for each individual nucleobase (Figure 5.3).

5.4.2 DNA binding residues

Interactions between DdrB and the DNA substrate will only be described for 6 of the 30 nucleotides, as each DNA bound subunit is approximately equivalent (RMSD of 0.158-0.203 Å). The first base (dT1), is oriented towards the surface of DdrB forming primarily vdW interactions with the N-terminal end of β6 (L87, E88) and the C-terminal end of β7 (L97, P98, A99, A100) (Figure 5.4-top). In particular, L87 and L97 form significant interactions with the planar faces of the nucleobase, sandwiching it from either side. The only prominent

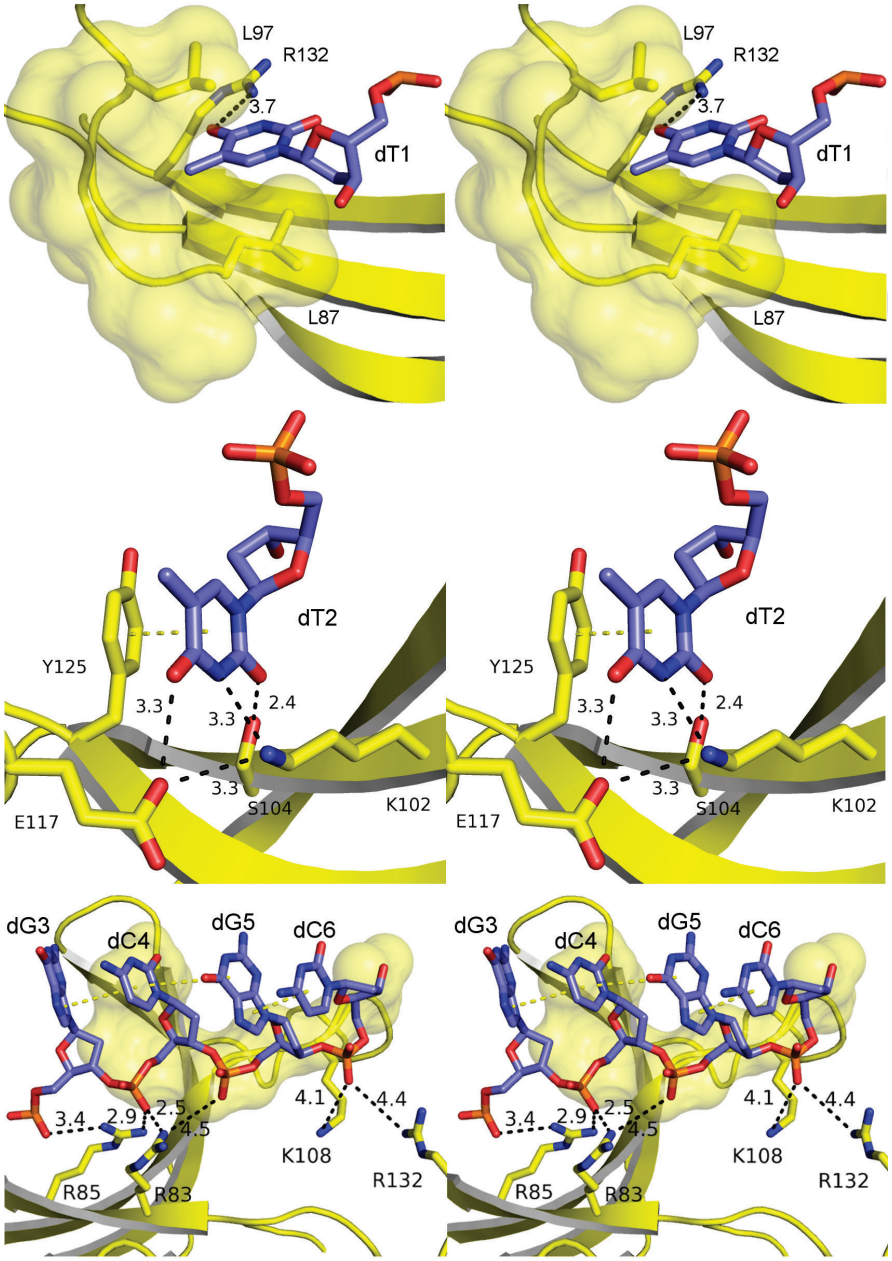

Figure 5.4 – DNA binding residues (stereo-images). Key contributors to DdrB/DNA interactions are labeled and annotated with interaction distances for dT1 (top), dT2 (middle), and dG3-dC6 (bottom). Residues participating primarily in vdWs interactions are represented in space-filling. Electrostatic and hydrogen-bonding interactions are denoted by dashed black lines, while dashed yellow lines represent π-π stacking interactions.

electrostatic interaction is between the guanidinium group of R132 and the nucleobase. Nucleotide dT2 similarly faces in towards the surface of DdrB, forming a π-π interaction with the phenol group of Y125 (Figure 5.4-middle). The nucleobase of dT2 is further stabilized through polar interactions with residues E117 and K102 (which also form a salt-bridge) and a hydrogen bond with S104.

Bases dG3, dC4, dG5, and dC6 all face outwards, while the negatively charged phosphate backbone forms stabilizing electrostatic interactions with residues R83, R85, K108, and R132' (from the adjacent subunit) (Figure 5.4-bottom). The sugar-moieties of the backbone lend further stability through vdW interactions with residues from $L_{\beta7\text{-}\beta8}$ (G106, A107, K108, V109, I123, and Y125). While the 4 bases do align face-to-face, the distance separating them is greater than the ideal base-stacking distance found in a double-helix (3.4 Å), likely due to the DNA being stretched across the surface of the complex.

Of the 6 bases, dT1 and dT2 appear to be the most stabilized due to their inward orientation, while dG3-dC6 are held in place mainly through relatively weak interactions with the sugar-phosphate backbone. This is evidenced by the distance of the electrostatic interactions, the overall number of interactions taking place, as well as the percentage of accessible surface area of each base that is buried through its interaction with DdrB (Table 5.2).

5.4.3 Quaternary structure

Similar to the structure of DdrB/ssDNA presented in Chapter 4, the

Table 5.2 Surface area buried in DdrB/ssDNA interface as calculated by PDBePISA

Base	Accessible surface area (Å^2)	Buried surface area (Å^2)	%
dT1	276.44	191.70	69.3
dT2	285.50	208.63	73.1
dG3	313.01	90.97	29.1
dC4	229.33	108.71	47.4
dG5	253.65	73.27	28.9
dC6	246.02	64.47	26.02

packing arrangement in the crystal lattice contains information about quaternary structure that may be relevant to DdrB's ssDNA annealing function. The pentamer generated by the symmetry operation [Y, X, -Z] is related by a 2-fold rotation axis, sitting face-to-face with the original (Figure 5.5). Analysis of the resulting interface using the PDBe PISA server demonstrates that only minimal protein-protein contacts are formed between the two pentamers, burying at most 340 $Å^2$ of total surface area in the decamer. This interface is mediated through two patches in $L_{\beta7\text{-}\beta8}$: residues A107 and V109; and residues R116, D120, G121, D122, and E124 (Figure 5.6).

On their own, the observed protein-protein contacts are not sufficient to stabilize the decamer. The face-to-face packing arrangment sandwiches bound DNA between the DdrB pentamers, resulting in significant contact between the two strands which accounts for the majority of the surface area buried in the interface (~1,150 $Å^2$). As the symmetrically related strands of ssDNA run in opposite directions, they are therefore in the correct polarity to form base-pairing interactions between bases that are presented away from the protein (Figure 5.1). The dG and dC bases in the model are indeed within the correct distance and in the proper orientation to form 3 hydrogen-bonds with each of the corresponding bases presented by the other DdrB pentamer (Figure 5.6).

5.5 Discussion

5.5.1 Comparison of ssDNA bound structures of DdrB

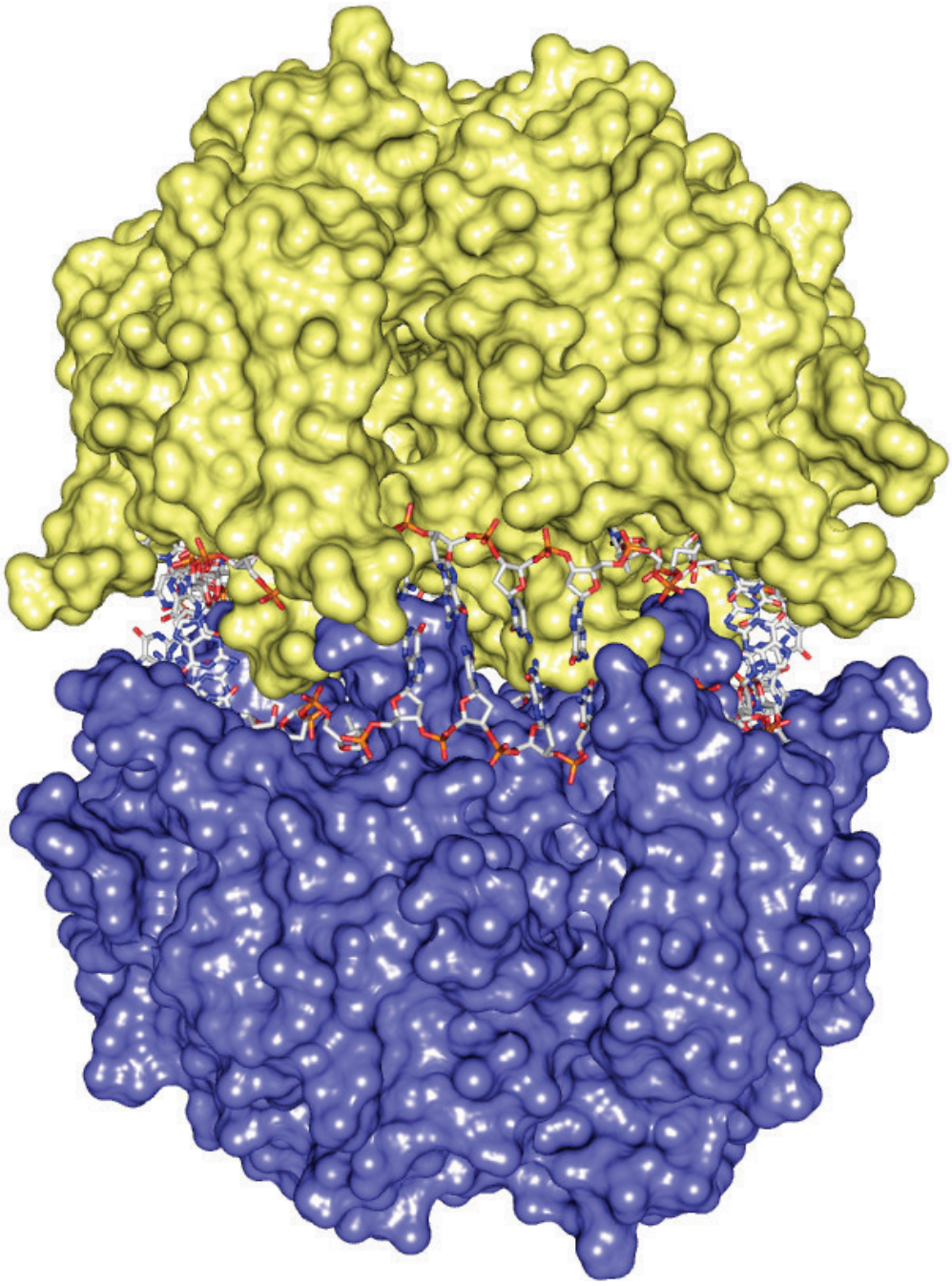

Figure 5.5 – Quaternary interface. Symmetrically related DdrB pentamers (yellow and blue) related by a 2-fold rotation axis align face-to-face in the crystal structure. DNA strands bound to the 'top' surfaces are brought together within this interface in the correct distance and orientation for base pairing.

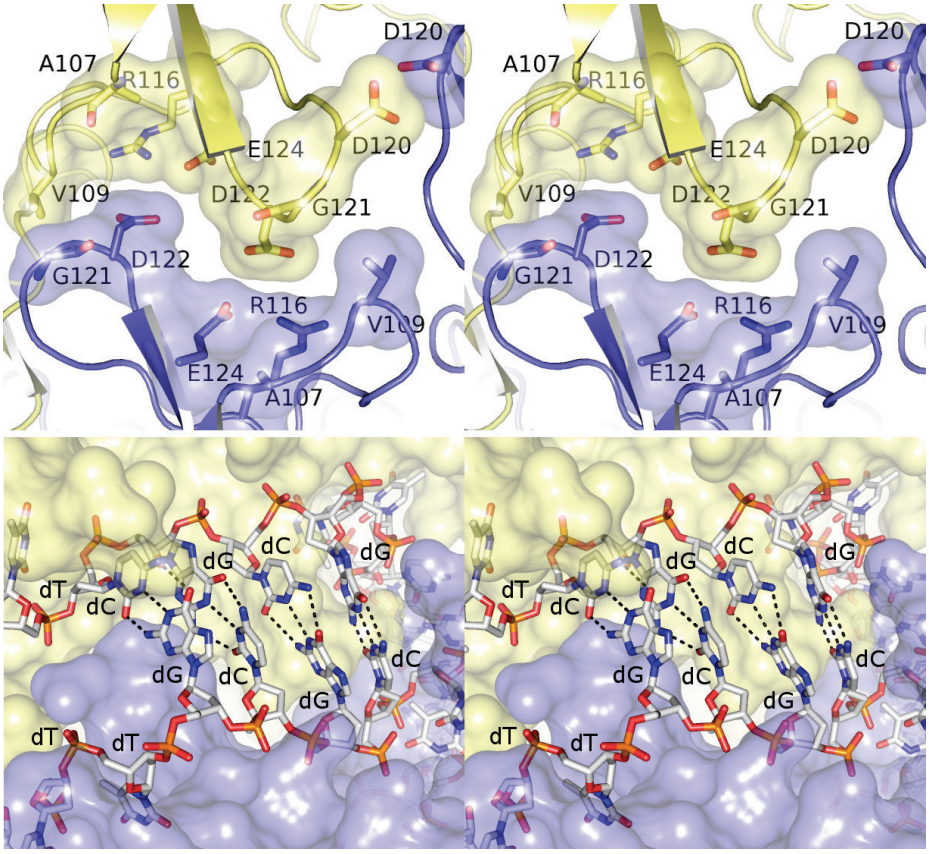

Figure 5.6 – Pentamer-pentamer interface (stereo-images). Formation of the higher order nucleoprotein assembly involving 2 DdrB pentamers is stabilized through protein-protein (top) and DNA-DNA (bottom) interactions. While interfacing amino acid residues only bury ~340 Å^2 of accessible surface area, nucleic acid interactions account for ~1,150 Å^2 in buried surface area in addition to forming 60 hydrogen-bonds through Watson-Crick base-pairing. Taken together, these observations indicate that the assembly is likely only stable in the presence of ssDNA. The protein-protein interface consists for the most part of vdW interactions, except for one long range electrostatic interaction between R116 and D122. Hydrogen bonding interactions between DNA bases are represented with black dashes.

There are two structures of DdrB currently available: the apo structure from *D. geothermalis* ($DdrB_{apo}$) (PDBID 4EXW) and a DNA-bound structure from *D. radiodurans* ($DdrB_{Db1}$) (PDBID 4HQB). A detailed comparison of $DdrB_{apo}$ and $DdrB_{Db1}$ was described in Section 4.5.2. Similar to the apo structure, the structure presented in this chapter, $DdrB_{Db2}$, is poorly ordered in $L_{\beta4\text{-}\beta5}$ and $H_{\beta6'\text{-}\beta7'}$. The C_α-carbons of the 5 subunits superimpose with low deviation (RMSD of 0.158-0.203 Å), indicating that the monomers in the ASU are equivalent. This is in contrast to $DdrB_{Db1}$, where DNA is bound asymmetrically to chains A, B, and E (RMSD = 1.28 Å). The C_α-backbones of chain A from $DdrB_{Db1}$ and $DdrB_{Db2}$ align with an RMSD of 1.73 Å, while exclusion of residues 86-97 ($H_{\beta6'\text{-}\beta7'}$) and 106-124 ($L_{\beta7\text{-}\beta8}$), both of which undergo major movements (Figure 5.7), results in a decrease of the RMSD to 0.71 Å.

This difference in tertiary structure can be attributed to two principle features. First, $H_{\beta6'\text{-}\beta7'}$ and $L_{\beta7\text{-}\beta8}$ form a 'C'-shaped clamp which is more 'open' in $DdrB_{Db2}$ (Figure 5.7-inset), ostensibly to accommodate DNA interactions with the 'top' face of the pentamer. Second, both $H_{\beta6'\text{-}\beta7'}$ and $L_{\beta7\text{-}\beta8}$ are intrinsic to the higher-order oligomeric assembly observed in $DdrB_{Db1}$ (Figure 4.3), which is not formed in $DdrB_{Db2}$. In line with the obvious importance of these elements, a mutant containing two amino acid substitutions (A107V, A163V) was unable to complement a radiosensitive Δ*ddrB* strain (P. Servant, personal communication, 2013). As A163 is located in the C-terminal region of the protein, which has

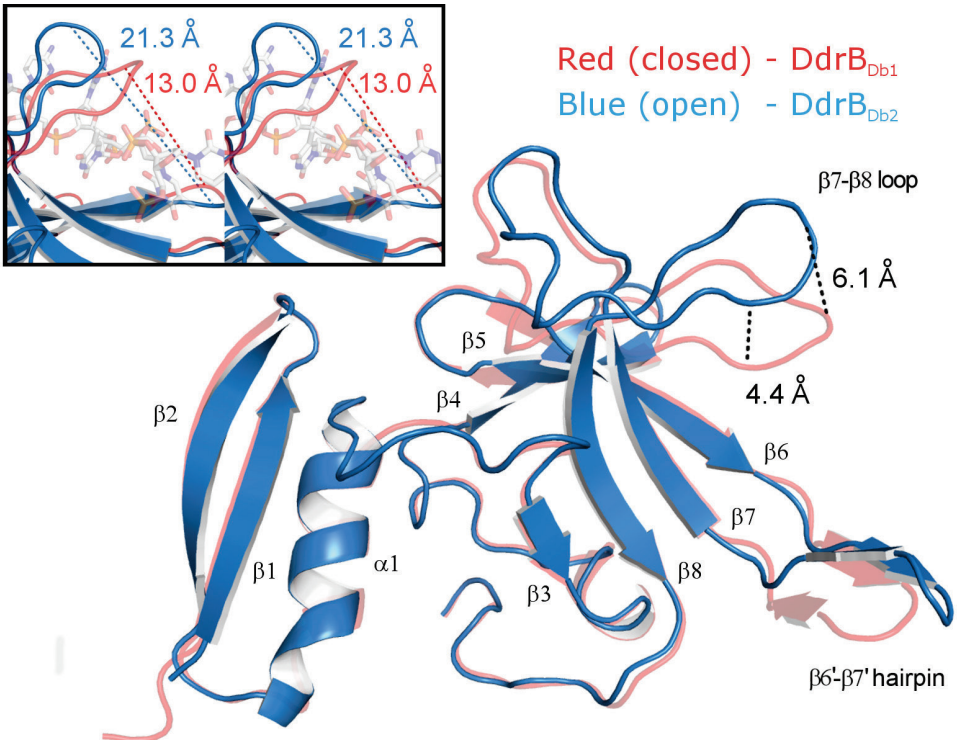

Figure 5.7 – Structural alignment of DdrB-DNA co-crystal structures. DdrB$_{Db1}$ (red) and DdrB$_{Db2}$ (blue) superimpose with an RMSD of 1.73 Å, of which the majority of the deviation can be attributed to movements in H$_{β6'-β7'}$ and L$_{β7-β8}$. In DdrB$_{Db1}$, both of these elements are involved in higher-order oligomerization, and DNA binding through the channel formed between DdrB monomers. In DdrB$_{Db2}$, the clamp formed between H$_{β6'-β7'}$ and L$_{β7-β8}$ is in a more 'open' conformation to allow DNA to bind to the 'top' surface of the pentamer (stereo-image inset).

already been demonstrated to lack functional importance in radioresistance (Bouthier de la Tour *et al.*, 2011), this phenotype is likely attributed entirely to A107V. While A107 plays no obvious role in protein-DNA or protein-protein interactions, its position at the C-terminal base of $L_{\beta7\text{-}\beta8}$ and the resulting loss of flexibility due to steric hindrance introduced by an Ala->Val substitution may reduce annealing capability and be sufficient to explain the observed radiosensitivity *in vivo*.

Based on the mutational analysis performed in Chapter 4, an extended DNA binding surface was predicted involving both the channel formed between DdrB monomers and the 'top' face of the pentamer. Consistent with this model, the trajectories of bound DNA in $DdrB_{Db1}$ and $DdrB_{Db2}$ partially overlap one another (Figure 5.8), and the two models have a number of DNA-binding residues in common (Table 5.3). Specifically, residues R83, L97, K108, and R132 are found at the junction of the two stands of ssDNA (Figure 5.8) and therefore likely play a role in transitioning DNA from the channel to the 'top' surface. As electron density maps are calculated from millions of unit cells, it was unsurprising that DNA would not be observed along the 'top' face in $DdrB_{Db1}$ or in the channel between monomers in $DdrB_{Db2}$. In the case of $DdrB_{Db1}$, the DNA substrate comprised 50 bases and ran in parallel strands through the crystal. Any situation where the length of DNA was insufficient to bridge across two DdrB decamers, the remaining portion of DNA could instead traverse across the

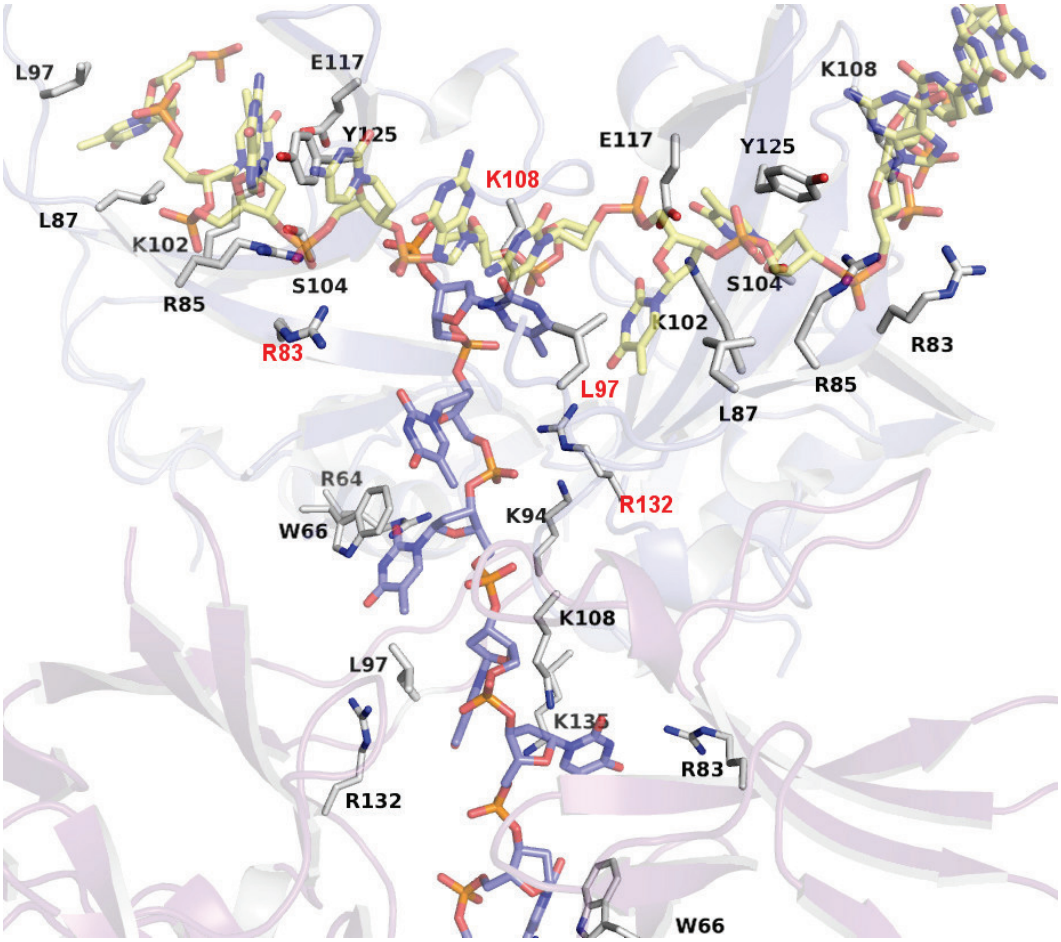

Figure 5.8 – DNA-bound structures of DdrB illustrate a continuous DNA-binding surface. Residues R83, L97, K108, and R132 (labelled in red) are involved in interactions with bound DNA in both structures, and therefore are likely to play roles in guiding DNA from the channel formed between DdrB monomers blue DNA) to the 'top' surface of the pentamer (yellow DNA).

Table 5.3 List of DNA binding residues in $DdrB_{Db1}$ and $DdrB_{Db2}$

Residue	$DdrB_{Db1}$ (Chapter 4)	$DdrB_{Db2}$ (Chapter 5)
E51	+	
R64	+	
W66	+	
R83	+	+
R85		+
L87		+
V90	+	
K94	+	
L95	+	
K96	+	
L97	+	+
K102		+
S104		+
K108	+	+
E117		+
Y125		+
R132	+	+
K135	+	
Q137	+	

'top' surface. However, due to the heterogeneity of binding within the overall crystal, evidence for such an interaction would be averaged out and not appear in the electron density. Likewise, in the case of $DdrB_{Db2}$, the length of DNA substrate (30 bases = 6 bases per monomer) and the lack of asymmetry in the pentameric assembly would result in low occupancy for any DNA bound in the channel between monomers.

5.5.2 A mechanism for DdrB mediated annealing

The repetitive mode of DNA binding (2 bases buried, 4 bases presented to the solvent), together with the observed quaternary structure that sandwiches DNA strands between DdrB pentamers (Figure 5.5), offers an attractive mechanism for protein mediated annealing. Under this proposed model, a search for homology begins with the interaction of two DdrB-DNA nucleoprotein complexes oriented 'face-to-face', which then sample the exposed bases for degree of complementarity (Figure 5.9A). Significant base-pairing interactions between the exposed bases transiently stabilize the decamer, permitting the buried bases to flip-out and sample the opposing strand (Figure 5.9B). In the event that the bases do not match (Figure 5.9C), the nucleoprotein complexes either continue their search (Figure 5.9A) or, eventually, dissociate from one another (Figure 5.9D). If Watson-Crick base-pairing takes place between the flipped-out bases (Figure 5.9E), loss of the associated DNA-protein interactions in addition to the torsional strain introduced via distortion of a DNA

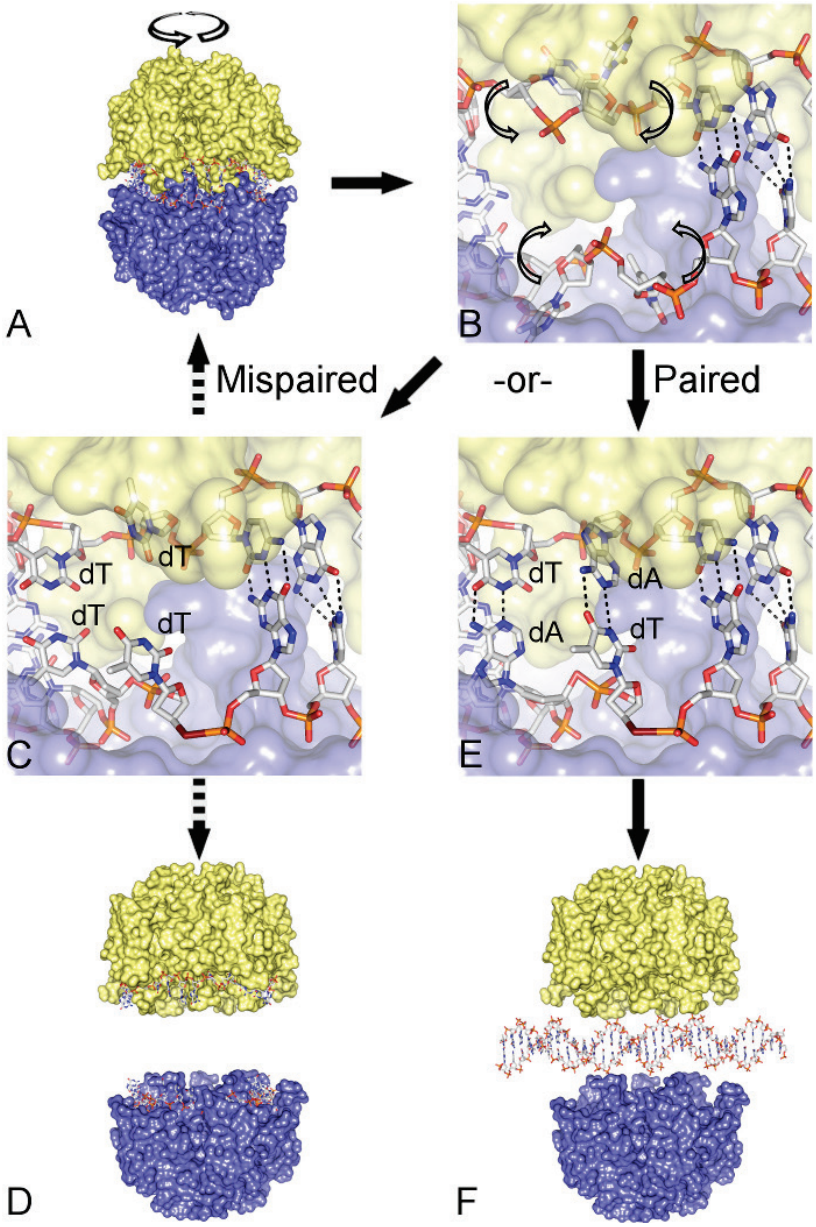

Figure 5.9 – A mechanism for DdrB mediated single-stranded annealing. (A) DNA-bound DdrB pentamers aligned face-to-face sample for degree of complementarity. (B) Hydrogen-bonding interactions between the exposed bases stalls movement, allowing buried residues to flip-out. (C) In the event of mismatched pairing, homology search continues, and eventually, (D) the higher-order complex will dissociate with ssDNA still bound to DdrB pentamers. (E) Successful base pairing leads to (F) dissociation of the nucleoprotein complex due to loss of stabilizing protein-ssDNA interactions and torsional strain induced by double-helix formation.

double-helix, would lead to dissociation of the DdrB-DNA assembly (Figure 5.9F). Dissociation of the complex upon formation of dsDNA is consistent with the observations that DdrB displays no apparent affinity for dsDNA (Figure 2.1), and that protein-protein interactions are not sufficient to stabilize a face-to-face decamer interface in the absence of DNA.

Based on available data, the length and fidelity of complementary sequence required for SSA in *Deinococcus* is still unknown. SSA in yeast, mediated by Rad52, has been estimated to have a minimum length requirement of ~30 bases, although the efficiency increases with increasing lengths of homologous sequence, plateauing between 200-400 bases (Sugawara *et al.*, 2000). The minimal length of 30 bases is consistent with the length of DNA known to associate with a single Rad52 heptamer (Parsons *et al.*, 2000). A preference for substrate lengths several times the binding capacity of a single DdrB pentamer would aid in maintaining sequence fidelity during repair, and is in accordance with observations that DdrB self-associates to form higher-order nucleoprotein complexes (Figure 4.5). The tolerance of DdrB-mediated DNA annealing for mismatches is also currently uncharacterized and is another aspect of DdrB function that remains to be explored.

5.5.3 A common mechanism for single-stranded annealing proteins

Rad52 has two major roles in homologous recombination: recruitment of Rad51 to RPA coated ssDNA and annealing of complementary ssDNA (Mortensen

et al., 2009, Sugiyama *et al.*, 2006). Its annealing activity is thought to be mediated by an N-terminal DNA-binding domain (Figure 4.6B) (Singleton *et al.*, 2002, Shi *et al.*, 2009), which bears close resemblance to the structure of DdrB presented in this chapter (Figure 5.2). Furthermore, optimal annealing has been shown to take place under conditions in which both strands of ssDNA are in complex with Rad52 at a stoichiometry of 1 heptamer per 30 nucleotides (Rothernberg *et al.*, 2008, Grimme *et al.*, 2010). These observations are consistent with the proposed mechanism for DdrB-mediated annealing, and it is therefore possible that this mechanism is functionally conserved despite the absence of sequence homology. The idea that evolutionarily distinct single-stranded annealing proteins share a common functional mechanism has been proposed previously (Passy *et al.*, 1999, Erler *et al.*, 2009). Similar to DdrB and Rad52, single-stranded annealing proteins Redβ, ERF, RecT, and Sak all assemble into ring-structures in solution, and have the propensity to form higher-order nucleoprotein filaments (Passy *et al.*, 1999, Poteete *et al.*, 1983, Thresher *et al.*, 1995, Ploquin *et al.*, 2008). Most recently, an EM structure of the annealing protein ICP8 from herpes simplex virus 1 was published in complex with ssDNA (Tolun *et al.*, 2013), in which two 9-membered rings of ICP8 were found stacked on top of each other. Docking of the crystal structure into the EM map, and calculation of the surface charge of the resulting complex, led the authors to posit that bound ssDNA was located at the interface of the two ICP8 rings. Taken

together, these findings build a strong case for a common mechanism of single-stranded annealing mediated by two ring forming oligomers as illustrated by the presented crystal structure of DdrB.

CHAPTER 6 – SUMMARY, GENERAL DISCUSSION, FUTURE DIRECTIONS, AND CONCLUDING REMARKS

6.1 Summary

When the work presented in this thesis began, DdrB was still classified as a hypothetical protein and had not been assigned biochemical or biological function. As DdrB lacked sequence homologues in the available databases, structural characterization was an important first step in identifying its function in damage recovery in *D. radiodurans*. DdrB's affinity for ssDNA was identified independently by Norais *et al.* (Norais *et al.*, 2009) leading to the misclassification of DdrB as a distant homologue of SSB. In the absence of structural information, a primary sequence alignment was presented between DdrB and SSB despite the lack of significant sequence conservation. Our latter attempts to reconcile the primary sequence alignment presented by Norais *et al*. and the crystal structures of DdrB and DnaE (SSB-fold) were unsuccessful, leading us to conclude that the proteins were in fact not evolutionarily related. Instead, the structure of DdrB from *D. geothermalis* presented in this work represents a novel fold for single-stranded DNA binding. This structure also illustrated the quaternary assembly of DdrB for the first time, confirming the *in vitro* characterization of the pentamer that had been suggested previously (Norais *et al.*, 2009). Examination of the residues mediating SSB's interaction with DNA led to the proposal of a model for DNA binding involving residues R64, W66, R83, R85, L87, and R93. The observation that DdrB promotes annealing of ssDNA, and evidence that it mediates fragment reassembly independent of RecA

(Xu *et al.*, 2010), assigned novel functions and roles in repair, increasing the impact of further structural characterization. The first co-crystal structure of $DdrB_{Dr}$/ssDNA revealed an unexpected mode of binding, wherein bound DNA threaded through channels formed between adjacent monomers, bridging individual DdrB pentamers to form higher-order complexes. Despite deviating from our hypothesized model, several of the residues that we had predicted to play roles in DNA binding were still implicated. As protein crystallization necessitates the formation of contacts, the relevance of the observed higher order assembly was investigated by sedimentation velocity AUC. Single amino acid substitution of two key salt bridge forming residues (E51 and R83) was sufficient to reduce the incidence of higher-order decamer oligomerization from ~60% in the wild-type to <12% in both the E51A and R83A mutants. Characterization of the E51A mutant's DNA binding function further revealed that it is deficient in the ability to form higher-order nucleoprotein complexes as was observed with wild-type DdrB, providing a potential biological role for the oligomeric state observed in the crystal structure. Mutational analysis also revealed several residues contributing to the DdrB/ssDNA interaction that were not represented in the structure, suggesting an extended mode of binding involving the 'top' face of the pentamer, similar to our initial prediction. A second structure of the $DdrB_{Dr}$/ssDNA complex was solved using a partially hybridized ss/dsDNA intermediate (AS4), which not only confirmed the predicted

extended DNA binding surface, but also provided insight into the mechanism by which DdrB mediates annealing. In this structure, incorporating an optimized 30 b ssDNa substrate, DNA was observed along the continuous surface formed by adjacent subunits of DdrB within the pentameric ring. Remarkably, this binding mode matches very closely with what was predicted in Chapters 2 and 4 of this thesis. Application of crystallographic symmetry generated a second pentamer, related by a 180 degree rotation, which sandwiches bound DNA between two DdrB oligomers. This assembly brings strands of ssDNA within the correct distance and alignment to allow for base stacking interaction. The observed hydrogen bonding between opposing strands of ssDNA provided an illustration of the mechanism by which DdrB mediates annealing of ssDNA during repair. This model for protein-mediated annealing is in agreement with data describing the structure and function of other single-stranded annealing proteins from virus to human, suggesting that these proteins may possess a conserved common mechanism despite their evolutionary diversity.

6.2 General discussion

6.2.1 SSB

SSB plays an essential role in DNA metabolism, protecting free ssDNA from degradation, self-association, and premature and inaccurate annealing. SSB does not carry out enzymatic function of its own, but instead, primes DNA for action by other entities through both the removal of secondary structure,

and recruitment of other repair proteins via a conserved negatively charged C-terminal motif (Shereda *et al.*, 2008). Canonical SSB consists of a single OB-fold domain which is tethered to the protein interaction motif (located at the C-terminus) by an extended flexible linker region (Shereda *et al.*, 2008). Functional SSB assembles into a tetramer. *D. radiodurans* SSB (SSB_{Dr}) differs from other bacterial SSB in that rather than consisting of a single ssDNA binding domain, the OB-fold motif has undergone a gene duplication event, resulting in an ORF containing tandem repeats (Eggington *et al.*, 2004). The overall biological quaternary structure remains the same, however, consisting of 4 OB-folds made up from a dimer of SSBs, rather than a tetramer. As the N-terminal and C-terminal OB-folds of SSB_{Dr} are not identical, it has been suggested that the two domains within each subunit have diverged to perform specialized functions in radiation resistance within *Deinococcus* (Bernstein *et al.*, 2004). While the C-terminal domain retains all the conserved DNA binding residues present in SSB_{Ec}, the N-terminal OB-fold appears to be lacking a number of these important residues. The N-terminal domain was also observed to take part in a major crystal contact, burying ~1,300 A^2 of surface area, leading the author's to suggest that its role may be mediating higher order oligomerization, allowing for a tighter coating of ssDNA than in other bacterial SSBs (Bernstein *et al.*, 2004). Interestingly, this is very similar to the model of DdrB mediated protection of ssDNA that we presented in Chapter 4.

Initial characterization of DdrB by Norais *et al*. suggested that DdrB was a homologue of SSB (Norais *et al.*, 2009), which was later demonstrated to be incorrect based on structural data that we presented in Chapter 2. This has since been supported by functional experiments, which have assigned roles that further separate DdrB from canonical SSB (Bouthier de la Tour *et al.*, 2011, Xu *et al.*, 2010). Nevertheless, DdrB and SSB remain intrinsically connected, as they act upon similar substrates and are the two most abundant DNA repair proteins following acute ionizing radiation (Basu & Apte, 2012). DdrB and SSB have also been demonstrated to directly interact *in vitro* (Xu *et al.*, 2010). The question of why *Deinococcus* has two highly abundant proteins that coat and protect ssDNA has yet to be answered, and the interplay between the two proteins is still poorly understood. Biochemical analysis of SSB_{Dr} and DdrB suggest binding stoichiometries of 45-56 nucleotides and 41-54 nucleotides per functional oligomeric unit, respectively (Bernstein *et al.*, 2004, Bouthier de la Tour *et al.*, 2011). Furthermore, the structures of both proteins in complex with ssDNA have also been solved, and in each case there are 30-35 nucleotides traceable in the electron density. The fact that DdrB and SSB form an interaction and also bind approximately the same length of ssDNA makes possible a situation where the two proteins can substitute for one another, such that ssDNA generated during processing of damaged DNA is coated by a combination of SSB and DdrB, rather than one or the other. The only data available on this interaction is from Xu *et*

al. (Xu *et al.*, 2010), which presents a conflicting scenario. In one experiment, DdrB is shown to promote annealing of complementary strands of ssDNA, even when the DNA is pre-incubated with SSB (which prevents annealing under normal conditions). In a second experiment, however, DdrB is unable to displace pre-loaded SSB from a strand of ssDNA tethered to a sepharose resin. Despite these seemingly incongruent observations, this type of relationship has also been described in yeast with the eukaryotic homologue of SSB, RPA, and the annealing protein Rad52 (Wu *et al.*, 2006). In order to more thoroughly explore this interaction, additional experiments need to be performed.

6.2.2 DdrA

Like DdrB, DdrA was originally identified due to its abundance in the cell following both acute ionizing radiation and desiccation (Tanaka *et al.*, 2004). Initial biochemical characterization of the protein revealed an affinity for the 3' ends of ssDNA, and an oligomeric state consisting of an 8-10 subunit assembly (Harris *et al.*, 2004). It was also reported that DdrA is distantly related by primary sequence to eukaryotic Rad52 (e-value of ~0.05) (Iyer *et al.*, 2002), although annealing activity *in vitro* has yet to be observed (Harris *et al.*, 2004). More recently, the EM structure of a truncated form of DdrA (1-160) from *D. deserti* was reported (Gutsche *et al.*, 2008), providing further evidence of homology with the Rad52 superfamily, and as a result, possible functional similarity as well. The 23 Å resolution model illustrates a ring-structure with 7-

fold symmetry, into which the crystal structure of the N-terminal domain of Rad52 (residues 25-178) was docked. The 7-membered ring further oligomerizes in the EM reconstruction, forming a trimer of heptamers, which the authors believe could be either an artifact due to the truncated nature of the protein, or possibly related to the protein's function.

Deletion analysis of *recA*, *ddrA*, and *ddrB* have placed the three genes into separate epistasis groups, as double deletion mutants were found to increase the DNA damage sensitive phenotype of each of the individual mutants (Tanaka *et al.*, 2004). While the function of RecA is known, and DdrB's role is gradually becoming more clear, DdrA's function is still relatively uncharacterized. Attempts to catalyze DNA annealing reactions with purified DdrA have so far been unsuccessful (Harris *et al.*, 2004). This could be because DdrA truly lacks this function (despite sequence/structure similarity to Rad52), or appropriate annealing conditions have not been optimized to observe this function *in vitro* (chemical environment, protein partners, etc.). DdrA has also been reported to inhibit the 3'->5' exonuclease activity of Exo I, presumably as a result of its strong affinity for exposed 3'-ssDNA (Harris *et al.*, 2004).

If DdrA's role in repair is to bind and protect 3' ends, it is logical that loss of this function would have deleterious effects on both RecA dependent (ESDSA) and independent (SSA) double-strand break repair processes. This is further supported by data demonstrating amplified sensitivity of the Δ*ddrA* strain

recovering in a nutrient poor environment (Harris *et al.*, 2004). As discussed in Section 1.3, Pol I is thought to participate in ssDNA end protection, which would partially compensate for an increase in DNA degradation in a strain lacking DdrA. In the absence of optimal growth conditions, however, DNA synthesis is limited and the detrimental effects of excessive degradation would therefore be much more severe. An alternative interpretation of the increased damage sensitivity of the ΔddrA/ΔddrB double deletion mutant is that DdrA and DdrB possess overlapping functions, as discussed in Section 4.5.7. If DdrA is in fact able to promote annealing of ssDNA like DdrB, then deletion of one could be compensated by activity of the other. The crystallization and X-ray diffraction of truncated DdrA (1-157) from *D. radiodurans* has been reported recently (Yamada *et al.*, 2010), however, the coordinates have yet to be released. When the crystal structure does become available, it will answer many of the questions surrounding DdrA's role and function in repair, and its relationship to Rad52 and DdrB.

6.2.3 PprA

Of the 5 proteins of unknown function that are highly expressed in response to DNA damage in *D. radiodurans*, PprA is among the 3 that were found to affect radiation sensitivity when deleted (the other two being DdrA and DdrB). The radiation inducible activator PprI controls the expression of both *recA* and *pprA* (Hua *et al.*, 2003), which form an epistatic group as evidenced by radiation

survival (Tanaka *et al.*, 2004) and repair kinetics (Devigne *et al.*, 2013) of a Δ*recA*/Δ*pprA* double deletion mutant. On its own, PprA binds dsDNA with a slight preference for free ends (Narumi *et al.*, 2004), and forms large oligomeric complexes of indeterminate size when expressed recombinantly in *E. coli* (Murakami *et al.*, 2006). EM micrographs of purified PprA demonstrate formation of long filaments *in vitro* (Figure 6.1), which may explain the report that PprA stimulates ligase catalyzed DNA end-joining (Narumi *et al.*, 2004). While PprA participates exclusively in RecA dependent repair processes, preliminary data from a pull-down experiment using 6His-DdrB and lysate from irradiated *D. radiodurans* cells suggests that PprA and DdrB form a stable interaction (discussed in Section 6.3.3). While evidence indicates that DdrB is involved in fragment reassembly via the SSA pathway, it does not exclude the possibility that DdrB also participates in DNA annealing during ESDSA. The fact that PprA and DdrB may form an interaction is therefore an important prospect that requires further investigation.

6.2.4 Single-stranded annealing in *Deinococcus*

As discussed in detail in Section 5.5.3, DdrB and Rad52 share many structural and functional features which suggest that they mediate annealing of complementary ssDNA in a similar fashion. The recombinase arbitrating HR in yeast is Rad51, which is recruited to RPA coated ssDNA by Rad52 (Mortensen *et al.*, 2009). In addition to its role as a 'mediator' of HR, Rad52 is involved in

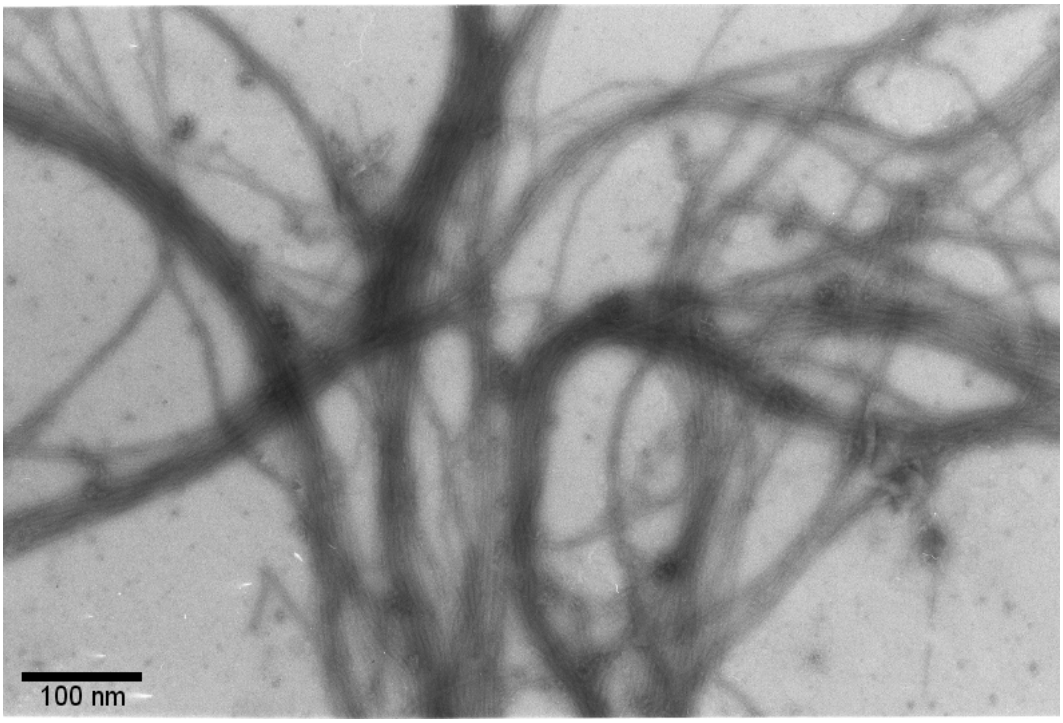

Figure 6.1 – EM micrograph of purified PprA. Images of PprA (70 µg/mL in 150 mM KCl) viewed at 25,000X magnification revealed the formation of large networks of protein filaments.

Rad51-independent SSA and a process termed 'second-strand capture', which both involve annealing of complementary strands of ssDNA (Sugiyama *et al.*, 2006). This is analogous to HR in *D. radiodurans* in which the principle recombinase, RecA, is recruited to SSB coated DNA by RecFOR (Bentchikou *et al.*, 2010). While *Deinococcus* RecO retains single-stranded annealing capabilities (Makharashvili *et al.*, 2004), unlike Rad52, it is thought to only be active in recombinase-dependent (RecA) repair processes (Bentchikou *et al.*, 2010). In *E. coli*, RecA-independent SSA is carried out by the exonuclease RecE and the annealing protein RecT (Kusano *et al.*, 1994), of which homologues are notably lacking in *D. radiodurans* (Cox & Battista, 2005). The rapid repair of approximately one-third of the double-strand breaks generated following damage in a RecA-independent manner (Daly & Minton, 1996), and the observation that DdrB is recruited to the nucleoid during this time-scale (Bouthier de la Tour *et al.*, 2011) is in concordance with the idea that DdrB is the principle promoter of SSA in *Deinococcus*. Whether DdrB is also involved in annealing ssDNA generated during ESDSA is still uncertain. Experiments monitoring genome reassembly in a Δ*ddrB* strain subjected to sub-lethal doses of ionizing radiation would suggest that DdrB only plays a role early in SSA-mediated repair (Bouthier de la Tour *et al.*, 2011). Following an initial lag phase, DNA synthesis and fragment assembly appears to proceed at rates which approximate those observed in the wild-type strain. Annealing of ssDNA

generated by RecA dependent processes could instead be carried out by RecO. However, the low *in vitro* annealing activity of RecO (Makharashvili *et al.*, 2004), and the fact that DdrB appears to substitute for RecO in plasmid transformation in *Deinococcus* (Bouthier de la Tour *et al.*, 2011) still leaves open the possibility that DdrB may function alongside RecO, and possibly DdrA, in a supportive role during ESDSA.

6.3 Future directions

Structural characterization of DdrB on its own and in complex with ssDNA has yielded significant functional and mechanistic insight, and has also set the stage for future work. Many aspects pertaining to both DdrB's annealing mechanism and its biological function remain available for analysis, and will be discussed in the penultimate section of this thesis.

6.3.1 Mechanism of release upon DNA hybridization

The crystal structure presented in Chapter 5 illustrates a reasonable mechanism for accurate protein-mediated annealing; however, many aspects have yet to be supported by experimental data. The degree of tolerance for mismatches during DNA annealing is an important feature controlling the fidelity of repair by SSA and is related to the mechanism for dissociation of the DdrB-DNA nucleoprotein assembly. A simple gel-shift assay probing various ssDNA substrates with different numbers of mismatches could be effective in addressing these questions. Based on the structure featured in Chapter 5

($DdrB_{Db2}$), the partially annealed DNA substrate used in crystallization (AS4-5'-TTGCGCTTGCGCTTGCGCTTGCGCTTGCGC) should remain bound to DdrB and would be therefore represented by a single super-shifted band corresponding to 10 monomers of DdrB and 60 bases of ssDNA when resolved by electrophoresis. The same substrate mixed together in the absence of DdrB should still anneal spontaneously at room temperature despite the mismatched bases, and would therefore migrate slower than the 30 b ssDNA substrate. A series of substrates with increasing complementarity to AS4 (1, 2, 3, 4, and 5 'AA' repeats in place of 'TT') could then be used to analyze fidelity of ssDNA annealing in the same electrophoresis experiment. Depending on the degree of ssDNA complementarity, when mixed with AS4 pre-incubated with DdrB and resolved by electrophoresis, these substrates would resolve as a band corresponding to either 30 bp of dsDNA, or as a super-shifted band corresponding to a complex with DdrB. If the complex formed in the crystal structure remains stable in solution, but dissociates upon replacement of the mismatched bases with ones capable of forming Watson-Crick base pairs, this would provide support for the mechanism of release proposed in Chapter 5. The degree of mismatch tolerance would also be directly correlated to the relative stability of the nucleoprotein complex with the various substrates tested.

A second assay using similar substrates with fluorescent labels could be used to assess the kinetics of DdrB-mediated annealing by Förster Resonance

Energy Transfer (FRET). A pair of perfectly complimentary oligos would be labeled at opposite ends (substrate 1 - 3' fluorophore, substrate 2 - 5' quencher). Separate experiments would be performed using unlabeled substrates bearing increasing complementarity to substrate 1. In each case, substrate 2 would be mixed with an excess of 'cold' competitor and then added to substrate 1 either on its own or with DdrB. The degree to which DdrB promotes accurate pairing of the perfectly complementary strand versus the partially complementary strand (in excess) would then be assessed in real time by monitoring quenching of the fluorescent signal from substrate 1. Two key trends would be expected in this experiment based on the current model of DdrB mediated annealing. First, hybridization of perfectly complementary oligos should occur more rapidly in the presence of DdrB, and second, the rate and extent of quenching would be expected to increase as the complementarity of the 'cold' competitor decreases in trials using DdrB.

6.3.2 Structural studies

Many aspects of DdrB function that remain to be explored may still be best approached using structural characterization. Current structures of DdrB in complex with DNA delineate a continuous binding surface, however, an additional crystal structure capturing ssDNA bound simultaneously to the channel between adjacent monomers and the 'top' surface of the complex would provide further mechanistic detail. Given the crystal contacts observed in

the current structures, such an assembly would necessitate a novel packing arrangement, requiring re-screening with a specifically designed DNA substrate. A longer self-complementing substrate capable of bridging and saturating two DdrB pentamers (~60 bases) may be an appropriate starting point.

In the current model, DdrB coats ssDNA, forming higher order complexes involving extensive protein-protein interaction interfaces, and annealing is initiated upon interaction of two of these DdrB nucleoprotein filaments. Whether multiple pentamers within this complex simultaneously align face-to-face, or homology search occurs through a single face-to-face assembly that must first disassociate before allowing a second set of pentamers to assemble remains to be answered. Another possibility is that a single face-to-face assembly mediates annealing but then threads DNA through the complex, zippering the strands together. The dynamics of this system are likely too complex to be elucidated by X-ray crystallography; however, a combination of EM and atomic force microscopy (AFM) may be well suited to address this question.

EM images of DdrB in complex with a 7,250 b ssDNA substrate have been published (Norais *et al.*, 2009); however, the resolution makes it difficult to distinguish any features. Complexes of DdrB with a smaller DNA substrate would provide a more homogeneous sample, allowing for higher resolution representations afforded through particle averaging. As EM does not require

formation of a crystalline state, sample preparation is much more straightforward than X-ray crystallography; therefore EM may be the best approach for further structural analysis of DdrB's oligomeric state in the presence of ssDNA. While EM provides a powerful tool for resolving large rigid complexes, the flexibility inherent in long spans of ssDNA make EM less useful for analyzing nucleoprotein complexes involving greater lengths of DNA (such as those that would be used in studying DdrB mediated single-stranded annealing).

Since its invention in 1986, AFM has been used extensively in the analysis of protein-protein and protein-nucleic acid complexes (Yang *et al.*, 2003). In particular, ssDNA (M13) and ssDNA-protein complexes (SSB, gp32, yRPA) have been visualized to high resolution using AFM (Hamon *et al.*, 2007). If DdrB could be similarly visualized, the question of whether annealing is mediated by single or multiple face-to-face DdrB interactions could be addressed by incubating DdrB-coated M13 with a short oligo substrate bearing partial complementarity to M13.

6.3.3 Interaction partners

To gain further understanding of DdrB's biological role, identification of interacting proteins is an important next step. So far, only two potential interaction partners have been identified in the literature: SSB (discussed in Section 6.2.1) (Xu *et al.*, 2010), and DR1245 (Norais *et al.*, 2013). DR1245 was identified using a TAP-tag pulldown methodology from cells recovering from

ionizing radiation exposure, and was the only protein identified as interacting with DdrB under these conditions. Being a protein of unknown function, the authors solved the crystal structure and submitted it to the Dali protein structure database searching server. DR1245 was revealed to be structurally homologous to a group of type III secretion system (T3SS) chaperones, and also a member of the YbjN family (unknown function). Despite confirming DdrB and DR1245's interaction *in vitro* with purified proteins, deletion of DR1245 had no effect on the radiosensitivity of *D. radiodurans*, suggesting that its interaction with DdrB is unrelated to DdrB's function in DNA repair (Norais *et al.*, 2013). It is possible that DR1245 may instead be involved in DdrB's role in plasmid transformation. Natural plasmid transformation in bacteria requires that DNA crosses the plasma membrane. Because the DNA uptake machinery only transports ssDNA, the other strand is degraded into nucleotides extracellulary (Chen & Dubnau, 2004). In *B. subtilis*, RecO is observed to accumulate at a single pole, ostensibly at the location where DNA is being translocated, and is responsible for annealing imported strands of ssDNA to establish transformed plasmid (Kidane *et al.*, 2009). As DNA translocation makes use of machinery that is reminiscent of the type IV pilus (T4P) assembly (termed 'competence pseudopilus') (Chen & Dubnau, 2004), it is possible that DR1245 is somehow involved in mediating recruitment of DdrB to the site of DNA uptake.

Preliminary data from a pulldown experiment using purified 6His-tagged DdrB and irradiated *D. radiodurans* cell lysate produced a short list of potential interacting proteins that require further investigation. Included in this list are: DRA0346 (PprA), DR1262 (implicated in UV-resistance), DRA0069 (a β-CASP nuclease family protein putatively involved in RNA metabolism), DR2281 (a hypothetical protein displaying sequence homology to ribonuclease III), and DR2263 (Dps, a DNA-binding and iron scavenging protein). Interestingly, neither SSB nor DR1245 were identified as hits in this assay, likewise, DR1245 was the only protein identified by Norais *et al*. (Norais *et al.*, 2013). As we have yet to pursue any of these potential binding partners, valuable information could be gained from interaction studies performed with purified protein. PprA was the highest scoring hit obtained from this assay, and also the most intriguing due to its involvement in double-strand break repair in *Deinococcus*, making it a good first target to explore. Direct investigation of this putative interaction using standard techniques such as gel filtration or native-PAGE may prove difficult due to the complex oligomeric state of purified PprA (Narumi *et al.*, 2004, Murakami *et al.*, 2006); however, other techniques such as far-Western blotting and ammonium sulfate co-precipitation could instead be implemented.

6.3.4 *In vivo*

To date, mutants affecting DdrB function *in vitro* have never been confirmed to have an effect on DNA repair or radioresistance. Data reflecting

biological effects consistent with mutational analysis presented in Chapter 4, would provide strong support for the mechanisms of DdrB function that have been presented in this thesis. *In vivo* characterization of DdrB has been spearheaded by the group of Dr. Pascale Servant, who has generously provided us with *D. radiodurans* strain GY12835 (Δ*ddrB*) and a complementation plasmid expressing *ddrB* under the control of its native promoter (p13421). Due to the high G-C content of *ddrB* (68.25%), and the size of the complementation vector (~11.3 kb) introduction of amino acid substitutions into p13421 is technically challenging; however, a DNA-binding deficient mutant (W66A) was successfully generated and transformed into GY12835.

A plating assay monitoring cell survival following exposure to 254 nm UV-C have been developed utilizing wild-type, Δ*ddrB*, Δ*ddrB* /p13421, and Δ*ddrB* /W66A strains of *D. radiodurans*. Preliminary data from this assay demonstrated a decrease in radioresistance in the strain complemented with DdrB-W66A (Figure 6.2); consistent with observations that W66A decreases DdrB's affinity for ssDNA (Figure 4.7). Moving forward, additional mutants targeting residues involved in higher order oligomerization (E51, R83), 'top' surface DNA binding (R85, K108), and interactions with bases turned in towards the surface of the protein (R87, L97, and Y125) would provide *in vivo* data supporting the mechanism of DdrB mediated annealing outlined in this thesis.

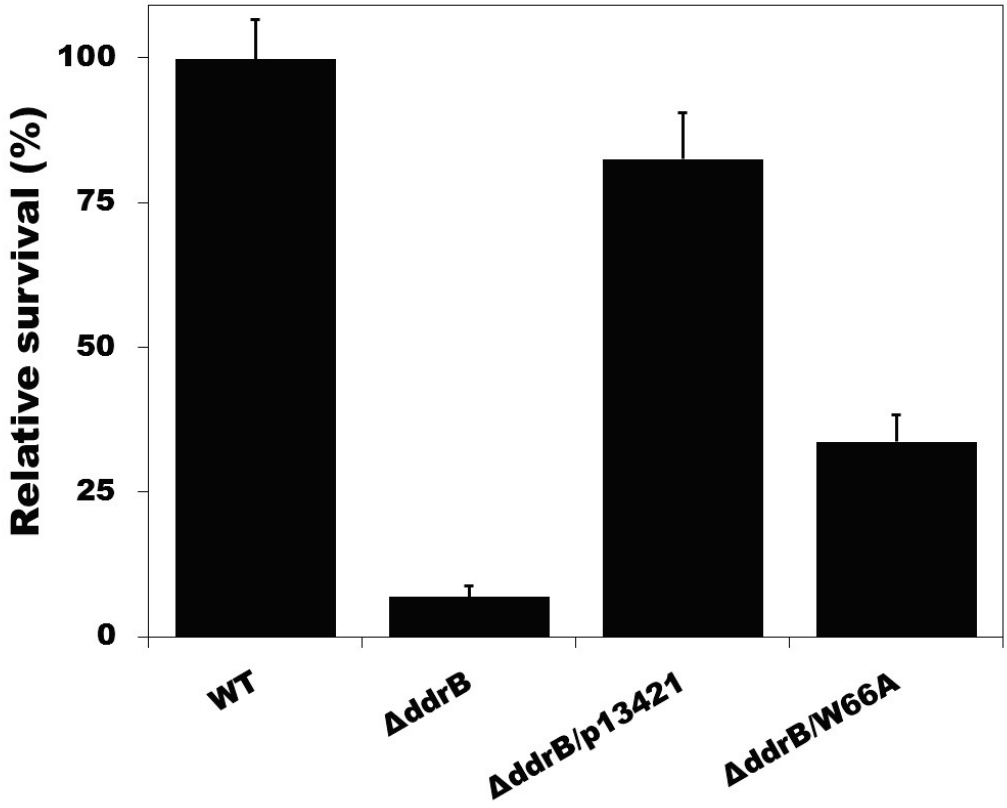

Figure 6.2 – UV survival of ΔddrB/W66A relative to wild-type *D. radiodurans* (error bars represent standard deviation of n=8 trials). Four strains of *D. radiodurans* were exposed to a dose of 240 J/m^2 and their survival rates were assessed relative to the wild-type strain. The ΔddrB deletion strain was reduced to 7±2% relative survival, while complementation with wild-type DdrB restored the ΔddrB strain to 83±8%. Complementation with DdrB-W66A was only able to partially restore the deletion strain (34±5%). Survival frequencies were calculated from an unexposed control experiments and survival of the wild-type strain used as reference 100 was 43±5%.

6.4 Conclusion and significance

DdrB's biological role has only recently begun to be elucidated, rendering any new characterization of the protein extremely informative. The structural data presented in this thesis, in particular, has contributed significantly to determining not only role that DdrB plays in DNA repair, but also the mechanism by which it carries out its function. Together, these three crystal structures represented the discovery of a novel fold for ssDNA binding, an interface contributing to both DNA binding and higher-order oligomerization, and a mechanism for protein mediated single-stranded annealing. Biochemical analysis of an array of DdrB mutants has provided strong support for interpretations of function built upon our analysis of these structures. In addition to contributing significantly to the characterization of DdrB, these findings have also set the stage for future work exploring aspects ranging from mechanical details of DdrB function, to broader questions pertaining to DdrB's biological role in DNA repair. Importantly, mechanistic insight gained from the work presented in this thesis is not restricted to *Deinococcus*, but may also have broader implications applicable to a diverse group of proteins with single-stranded annealing function in both prokaryotes and eukaryotes.

REFERENCES

Adams, P. D., Afonine, P. V., Bunkoczi, G., Chen, V. B., Davis, I. W., Echols, N., Headd, J. J., Hung, L. W., Kapral, G. J., Grosse-Kunstleve, R. W., McCoy, A. J., Moriarty, N. W., Oeffner, R., Read, R. J., Richardson, D. C., Richardson, J. S., Terwilliger, T. C. & Zwart, P. H. (2010) PHENIX: a comprehensive Python-based system for macromolecular structure solution. *Acta Crystallogr. D Biol. Crystallogr.* **66,** 213-221.

Adams, P. D., Grosse-Kunstleve, R. W., Hung, L. W., Ioerger, T. R., McCoy, A. J., Moriarty, N. W., Read, R. J., Sacchettini, J. C., Sauter, N. K. & Terwilliger, T. C. (2002) PHENIX: building new software for automated crystallographic structure determination. *Acta Crystallogr. D Biol. Crystallogr.* **58,** 1948-1954.

Altschul, S. F., Gish, W., Miller, W., Myers, E. W. & Lipman, D. J. (1990) Basic local alignment search tool. *J. Mol. Biol.* **215,** 403-410.

Anderson, A. W., Nordan, H. C., Cain, R. F., Parish, G. & Duggan, D. (1956) Studies on a radioresistant micrococcus. I. Isolation, morphology, cultural characteristics and resistance to gamma radiation. *Food Technol.* **10,** 575-578.

Anderson, D. G. & Kowalczykowski, S. C. (1997) The recombination hot spot chi is a regulatory element that switches the polarity of DNA degradation by the RecBCD enzyme. *Genes Dev.* **11,** 571-581.

Arrage, A. A., Phelps, T. J., Benoit, R. E., Palumbo, A. V. & White, D. C. (1993) Bacterial sensitivity to UV light as a model for ionizing radiation resistance. *Journal of Microbiological Methods.* **18,** 127-136.

Artimo, P., Jonnalagedda, M., Arnold, K., Baratin, D., Csardi, G., de Castro, E., Duvaud, S., Flegel, V., Fortier, A., Gasteiger, E., Grosdidier, A., Hernandez, C., Ioannidis, V., Kuznetsov, D., Liechti, R., Moretti, S., Mostaguir, K., Redaschi, N., Rossier, G., Xenarios, I. & Stockinger, H. (2012) ExPASy: SIB bioinformatics resource portal. *Nucleic Acids Res.* **40,** W597-603.

Bailey, S., Wing, R. A. & Steitz, T. A. (2006) The structure of T. aquaticus DNA polymerase III is distinct from eukaryotic replicative DNA polymerases. *Cell.* **126,** 893-904.

Basu, B. & Apte, S. K. (2012) Gamma radiation-induced proteome of Deinococcus radiodurans primarily targets DNA repair and oxidative stress alleviation. *Mol. Cell. Proteomics.* **11,** M111.011734.

Battista, J. R. (1997) Against all odds: the survival strategies of Deinococcus radiodurans. *Annu. Rev. Microbiol.* **51,** 203-224.

Bentchikou, E., Servant, P., Coste, G. & Sommer, S. (2010) A major role of the RecFOR pathway in DNA double-strand-break repair through ESDSA in Deinococcus radiodurans. *PLoS Genet.* **6,** e1000774.

Bernstein, D. A., Eggington, J. M., Killoran, M. P., Misic, A. M., Cox, M. M. & Keck, J. L. (2004) Crystal structure of the Deinococcus radiodurans single-stranded DNA-binding protein suggests a mechanism for coping with DNA damage. *Proc. Natl. Acad. Sci. U. S. A.* **101,** 8575-8580.

Bjelland, S. & Seeberg, E. (2003) Mutagenicity, toxicity and repair of DNA base damage induced by oxidation. *Mutat. Res.* **531,** 37-80.

Boling, M. E. & Setlow, J. K. (1966) The resistance of Micrococcus radiodurans to ultraviolet radiation. 3. A repair mechanism. *Biochim. Biophys. Acta.* **123,** 26-33.

Bonura, T. & Bruce, A. K. (1974) The repair of single-strand breaks in a radiosensitive mutant of Micrococcus radiodurans. *Radiat. Res.* **57,** 260-275.

Bonura, T. & Smith, K. C. (1975) Enzymatic production of deoxyribonucleic acid double-strand breaks after ultraviolet irradiation of Escherichia coli K-12. *J. Bacteriol.* **121,** 511-517.

Bouthier de la Tour, C., Boisnard, S., Norais, C., Toueille, M., Bentchikou, E., Vannier, F., Cox, M. M., Sommer, S. & Servant, P. (2011) The deinococcal DdrB protein is involved in an early step of DNA double strand break repair and in plasmid transformation through its single-strand annealing activity. *DNA Repair (Amst).* **10**, 1223-1231.

Brooks, B. W. & Murray, R. G. E. (1981) Nomenclature for "Micrococcus radiodurans" and other radiation-resistant cocci: Deinococcaceae fam. Nov. and Deinococcus gen. nov. including five species. *International Journal of Systematic Bacteriology.* **31,** 353-360.

Burrell, A. D., Feldschreiber, P. & Dean, C. J. (1971) DNA-membrane association and the repair of double breaks in x-irradiated Micrococcus radiodurans. *Biochim. Biophys. Acta.* **247,** 38-53.

Chan, K. W., Lee, Y. J., Wang, C. H., Huang, H. & Sun, Y. J. (2009) Single-stranded DNA-binding protein complex from Helicobacter pylori suggests an ssDNA-binding surface. *J. Mol. Biol.* **388,** 508-519.

Chang, X., Yang, L., Zhao, Q., Fu, W., Chen, H., Qiu, Z., Chen, J. A., Hu, R. & Shu, W. (2010) Involvement of recF in 254 nm ultraviolet radiation resistance in Deinococcus radiodurans and Escherichia coli. *Curr. Microbiol.* **61,** 458-464.

Chen, I. & Dubnau, D. (2004) DNA uptake during bacterial transformation. *Nat. Rev. Microbiol.* **2,** 241-249.

Chen, Z., Yang, H. & Pavletich, N. P. (2008) Mechanism of homologous recombination from the RecA-ssDNA/dsDNA structures. *Nature.* **453,** 489-494.

Cole, J. L., Lary, J. W., P Moody, T. & Laue, T. M. (2008) Analytical ultracentrifugation: sedimentation velocity and sedimentation equilibrium. *Methods Cell Biol.* **84,** 143-179.

Cox, M. M. & Battista, J. R. (2005) Deinococcus radiodurans - the consummate survivor. *Nat. Rev. Microbiol.* **3,** 882-892.

Crooke, S. T. & Bradner, W. T. (1976) Mitomycin C: a review. *Cancer Treat. Rev.* **3,** 121-139.

Curth, U., Genschel, J., Urbanke, C. & Greipel, J. (1996) In vitro and in vivo function of the C-terminus of Escherichia coli single-stranded DNA binding protein. *Nucleic Acids Res.* **24,** 2706-2711.

Dalle-Donne, I., Aldini, G., Carini, M., Colombo, R., Rossi, R. & Milzani, A. (2006) Protein carbonylation, cellular dysfunction, and disease progression. *J. Cell. Mol. Med.* **10,** 389-406.

Daly, M. J. (2009) A new perspective on radiation resistance based on Deinococcus radiodurans. *Nat. Rev. Microbiol.* **7,** 237-245.

Daly, M. J., Gaidamakova, E. K., Matrosova, V. Y., Kiang, J. G., Fukumoto, R., Lee, D. Y., Wehr, N. B., Viteri, G. A., Berlett, B. S. & Levine, R. L. (2010) Small-molecule antioxidant proteome-shields in Deinococcus radiodurans. *PLoS One.* **5,** e12570.

Daly, M. J., Gaidamakova, E. K., Matrosova, V. Y., Vasilenko, A., Zhai, M., Leapman, R. D., Lai, B., Ravel, B., Li, S. M., Kemner, K. M. & Fredrickson, J. K. (2007) Protein oxidation implicated as the primary determinant of bacterial radioresistance. *PLoS Biol.* **5,** e92.

Daly, M. J., Gaidamakova, E. K., Matrosova, V. Y., Vasilenko, A., Zhai, M., Venkateswaran, A., Hess, M., Omelchenko, M. V., Kostandarithes, H. M., Makarova, K. S., Wackett, L. P., Fredrickson, J. K. & Ghosal, D. (2004) Accumulation of Mn(II) in Deinococcus radiodurans facilitates gamma-radiation resistance. *Science.* **306,** 1025-1028.

Daly, M. J. & Minton, K. W. (1996) An alternative pathway of recombination of chromosomal fragments precedes recA-dependent recombination in the radioresistant bacterium Deinococcus radiodurans. *J. Bacteriol.* **178,** 4461-4471.

Daly, M. J., Ouyang, L., Fuchs, P. & Minton, K. W. (1994) In vivo damage and recA-dependent repair of plasmid and chromosomal DNA in the radiation-resistant bacterium Deinococcus radiodurans. *J. Bacteriol.* **176,** 3508-3517.

De Bont, R. & van Larebeke, N. (2004) Endogenous DNA damage in humans: a review of quantitative data. *Mutagenesis.* **19,** 169-185.

Dean, C. J., Feldschreiber, P. & Lett, J. T. (1966) Repair of x-ray damage to the deoxyribonucleic acid in Micrococcus radiodurans. *Nature.* **209,** 49-52.

Dean, C. J., Little, J. G. & Serianni, R. W. (1970) The control of post irradiation DNA breakdown in Micrococcus radiodurans. *Biochem. Biophys. Res. Commun.* **39,** 126-134.

Devigne, A., Mersaoui, S., Bouthier de la Tour, C., Sommer, S. & Servant, P. (2013) The PprA protein is required for accurate cell division of gamma-irradiated Deinococcus radiodurans bacteria. *DNA Repair (Amst).* **12,** 265-272.

Dillingham, M. S. & Kowalczykowski, S. C. (2008) RecBCD enzyme and the repair of double-stranded DNA breaks. *Microbiol. Mol. Biol. Rev.* **72,** 642-71.

Driedger, A. A. & Grayston, M. J. (1971) Demonstration of two types of DNA repair in X-irradiated Micrococcus radiodurans. *Can. J. Microbiol.* **17,** 495-499.

Durrant, J. D. & McCammon, J. A. (2011) BINANA: a novel algorithm for ligand-binding characterization. *J. Mol. Graph. Model.* **29,** 888-893.

Eggington, J. M., Haruta, N., Wood, E. A. & Cox, M. M. (2004) The single-stranded DNA-binding protein of Deinococcus radiodurans. *BMC Microbiol.* **4,** 2.

Emsley, P. & Cowtan, K. (2004) Coot: model-building tools for molecular graphics. *Acta Crystallogr. D Biol. Crystallogr.* **60,** 2126-2132.

Erler, A., Wegmann, S., Elie-Caille, C., Bradshaw, C. R., Maresca, M., Seidel, R., Habermann, B., Muller, D. J. & Stewart, A. F. (2009) Conformational adaptability of Redbeta during DNA annealing and implications for its structural relationship with Rad52. *Journal of Molecular Biology.* **391,** 586-598.

Feng, Z., Scott, S. P., Bussen, W., Sharma, G. G., Guo, G., Pandita, T. K. & Powell, S. N. (2011) Rad52 inactivation is synthetically lethal with BRCA2 deficiency. *Proc. Natl. Acad. Sci. U. S. A.* **108,** 686-691.

Flint, D. H., Tuminello, J. F. & Emptage, M. H. (1993) The inactivation of Fe-S cluster containing hydro-lyases by superoxide. *J. Biol. Chem.* **268,** 22369-22376.

French, S. & Wilson, K. (1978) On the treatment of negative intensity observations. *Acta Crystallogr A.* **A34,** 517-525.

Georgescu, R. E., Kim, S. S., Yurieva, O., Kuriyan, J., Kong, X. P. & O'Donnell, M. (2008) Structure of a sliding clamp on DNA. *Cell.* **132,** 43-54.

Grimme, J. M., Honda, M., Wright, R., Okuno, Y., Rothenberg, E., Mazin, A. V., Ha, T. & Spies, M. (2010) Human Rad52 binds and wraps single-stranded DNA and mediates annealing via two hRad52-ssDNA complexes. *Nucleic Acids Research.* **38,** 2917-2930.

Grimsley, J. K., Masters, C. I., Clark, E. P. & Minton, K. W. (1991) Analysis by pulsed-field gel electrophoresis of DNA double-strand breakage and repair in Deinococcus radiodurans and a radiosensitive mutant. *Int. J. Radiat. Biol.* **60,** 613-626.

Gulbis, J. M., Kelman, Z., Hurwitz, J., O'Donnell, M. & Kuriyan, J. (1996) Structure of the C-terminal region of p21(WAF1/CIP1) complexed with human PCNA. *Cell.* **87,** 297-306.

Gutman, P. D., Carroll, J. D., Masters, C. I. & Minton, K. W. (1994) Sequencing, targeted mutagenesis and expression of a recA gene required for the extreme radioresistance of Deinococcus radiodurans. *Gene.* **141,** 31-37.

Gutsche, I., Vujicic-Zagar, A., Siebert, X., Servant, P., Vannier, F., Castaing, B., Gallet, B., Heulin, T., de Groot, A., Sommer, S. & Serre, L. (2008) Complex oligomeric structure of a truncated form of DdrA: a protein required for the extreme radiotolerance of Deinococcus. *Biochim. Biophys. Acta.* **1784,** 1050-1058.

Hamon, L., Pastre, D., Dupaigne, P., Breton, C. L., Le Cam, E. & Pietrement, O. (2007) High-resolution AFM imaging of single-stranded DNA-binding protein-DNA complexes. *Nucleic Acids Res.* **35,** e58.

Hansen, M. T. (1978) Multiplicity of genome equivalents in the radiation-resistant bacterium Micrococcus radiodurans. *J. Bacteriol.* **134,** 71-75.

Harris, D. R., Tanaka, M., Saveliev, S. V., Jolivet, E., Earl, A. M., Cox, M. M. & Battista, J. R. (2004) Preserving genome integrity: the DdrA protein of Deinococcus radiodurans R1. *PLoS Biol.* **2,** e304.

Harsojo, Kitayama, S. & Matsuyama, A. (1981) Genome multiplicity and radiation resistance in Micrococcus radiodurans. *J. Biochem.* **90,** 877-880.

Holm, L., Kaariainen, S., Rosenstrom, P. & Schenkel, A. (2008) Searching protein structure databases with DaliLite v.3. *Bioinformatics.* **24,** 2780-2781.

Hua, Y., Narumi, I., Gao, G., Tian, B., Satoh, K., Kitayama, S. & Shen, B. (2003) PprI: a general switch responsible for extreme radioresistance of Deinococcus radiodurans. *Biochem. Biophys. Res. Commun.* **306,** 354-360.

Imlay, J. A. (2008) Cellular defenses against superoxide and hydrogen peroxide. *Annu. Rev. Biochem.* **77,** 755-776.

Imlay, J. A. (2003) Pathways of oxidative damage. *Annu. Rev. Microbiol.* **57,** 395-418.

Iyer, L. M., Koonin, E. V. & Aravind, L. (2002) Classification and evolutionary history of the single-strand annealing proteins, RecT, Redbeta, ERF and RAD52. *BMC Genomics.* **3,** 8.

Jiao, J., Wang, L., Xia, W., Li, M., Sun, H., Xu, G., Tian, B. & Hua, Y. (2012) Function and biochemical characterization of RecJ in Deinococcus radiodurans. *DNA Repair (Amst).* **11,** 349-356.

Jones, D. T. (1999) Protein secondary structure prediction based on position-specific scoring matrices. *J. Mol. Biol.* **292,** 195-202.

Joshi, B., Schmid, R., Altendorf, K. & Apte, S. K. (2004) Protein recycling is a major component of post-irradiation recovery in Deinococcus radiodurans strain R1. *Biochem. Biophys. Res. Commun.* **320,** 1112-1117.

Kabsch, W. (1976) A solution for the best rotation to relate two sets of vectors. *Acta Crystallogr A.* **32,** 922-923.

Kagawa, W., Kurumizaka, H., Ishitani, R., Fukai, S., Nureki, O., Shibata, T. & Yokoyama, S. (2002) Crystal Structure of the Homologous-Pairing Domain from the Human Rad52 Recombinase in the Undecameric Form. *Mol. Cell.* **10,** 359-371.

Kawabata, T. (2003) MATRAS: A program for protein 3D structure comparison. *Nucleic Acids Res.* **31,** 3367-3369.

Khairnar, N. P., Kamble, V. A. & Misra, H. S. (2008) RecBC enzyme overproduction affects UV and gamma radiation survival of Deinococcus radiodurans. *DNA Repair (Amst).* **7,** 40-47.

Kidane, D., Carrasco, B., Manfredi, C., Rothmaier, K., Ayora, S., Tadesse, S., Alonso, J. C. & Graumann, P. L. (2009) Evidence for different pathways during horizontal gene transfer in competent Bacillus subtilis cells. *PLoS Genet.* **5,** e1000630.

Kim, J. I. & Cox, M. M. (2002) The RecA proteins of Deinococcus radiodurans and Escherichia coli promote DNA strand exchange via inverse pathways. *Proc. Natl. Acad. Sci. U. S. A.* **99,** 7917-7921.

Kitayama, S., Asaka, S. & Totsuka, K. (1983) DNA double-strand breakage and removal of cross-links in Deinococcus radiodurans. *J. Bacteriol.* **155,** 1200-1207.

Kong, X. P., Onrust, R., O'Donnell, M. & Kuriyan, J. (1992) Three-dimensional structure of the beta subunit of E. coli DNA polymerase III holoenzyme: a sliding DNA clamp. *Cell.* **69,** 425-437.

Kota, S., Kumar, C. V. & Misra, H. S. (2010) Characterization of an ATP-regulated DNA-processing enzyme and thermotolerant phosphoesterase in the radioresistant bacterium Deinococcus radiodurans. *Biochem. J.* **431,** 149-157.

Kowalczykowski, S. C., Dixon, D. A., Eggleston, A. K., Lauder, S. D. & Rehrauer, W. M. (1994) Biochemistry of homologous recombination in Escherichia coli. *Microbiol. Rev.* **58,** 401-465.

Kozmin, S. G., Sedletska, Y., Reynaud-Angelin, A., Gasparutto, D. & Sage, E. (2009) The formation of double-strand breaks at multiply damaged sites is driven by the kinetics of excision/incision at base damage in eukaryotic cells. *Nucleic Acids Res.* **37,** 1767-1777.

Krisko, A. & Radman, M. (2010) Protein damage and death by radiation in Escherichia coli and Deinococcus radiodurans. *Proc. Natl. Acad. Sci. U. S. A.* **107,** 14373-14377.

Krissinel, E. & Henrick, K. (2007) Inference of macromolecular assemblies from crystalline state. *J. Mol. Biol.* **372,** 774-797.

Kusano, K., Takahashi, N. K., Yoshikura, H. & Kobayashi, I. (1994) Involvement of RecE exonuclease and RecT annealing protein in DNA double-strand break repair by homologous recombination. *Gene.* **138,** 17-25.

Laue, T. M., Shah, B. D., Ridgeway, T. M. & Pelletier, S. L. (1992). *Computer-Aided Interpretation of Analytical Sedimentation Data for Proteins.* edited by S. Harding & A. Rowe, pp. 90-125. Cambridge: Royal Society of Chemistry.

Lee, B. & Richards, F. M. (1971) The interpretation of protein structures: estimation of static accessibility. *J. Mol. Biol.* **55,** 379-400.

Leslie, G. W. A. & Powell, H. R. (2007) Processing diffraction data with mosflm. *Evolving methods for macromolecular crystallography.* **245,** 41-51.

Lett, J. T., Feldschreiber, P., Little, J. G., Steele, K. & Dean, C. J. (1967) The repair of x-ray damage to the deoxyribonucleic acid in Micrococcus radiodurans: a study of the excision process. *Proc. R. Soc. Lond. B. Biol. Sci.* **167,** 184-201.

Levin-Zaidman, S., Englander, J., Shimoni, E., Sharma, A. K., Minton, K. W. & Minsky, A. (2003) Ringlike structure of the Deinococcus radiodurans genome: a key to radioresistance? *Science.* **299,** 254-256.

Liu, Y., Zhou, J., Omelchenko, M. V., Beliaev, A. S., Venkateswaran, A., Stair, J., Wu, L., Thompson, D. K., Xu, D., Rogozin, I. B., Gaidamakova, E. K., Zhai, M., Makarova, K. S., Koonin, E. V. & Daly, M. J. (2003) Transcriptome dynamics of

Deinococcus radiodurans recovering from ionizing radiation. *Proc. Natl. Acad. Sci. U. S. A.* **100,** 4191-4196.

Lloyd, R. G. & Buckman, C. (1985) Identification and genetic analysis of sbcC mutations in commonly used recBC sbcB strains of Escherichia coli K-12. *J. Bacteriol.* **164,** 836-844.

Luscombe, N. M., Laskowski, R. A. & Thornton, J. M. (1997) NUCPLOT: a program to generate schematic diagrams of protein-nucleic acid interactions. *Nucleic Acids Res.* **25,** 4940-4945.

Mackay, V. & Linn, S. (1976) Selective inhibition of the dnase activity of the recBC enzyme by the DNA binding protein from Escherichia coli. *J. Biol. Chem.* **251,** 3716-3719.

Makarova, K. S., Aravind, L., Wolf, Y. I., Tatusov, R. L., Minton, K. W., Koonin, E. V. & Daly, M. J. (2001) Genome of the extremely radiation-resistant bacterium Deinococcus radiodurans viewed from the perspective of comparative genomics. *Microbiol. Mol. Biol. Rev.* **65,** 44-79.

Makarova, K. S., Omelchenko, M. V., Gaidamakova, E. K., Matrosova, V. Y., Vasilenko, A., Zhai, M., Lapidus, A., Copeland, A., Kim, E., Land, M., Mavrommatis, K., Pitluck, S., Richardson, P. M., Detter, C., Brettin, T., Saunders, E., Lai, B., Ravel, B., Kemner, K. M., Wolf, Y. I., Sorokin, A., Gerasimova, A. V., Gelfand, M. S., Fredrickson, J. K., Koonin, E. V. & Daly, M. J. (2007) Deinococcus geothermalis: the pool of extreme radiation resistance genes shrinks. *PLoS One.* **2,** e955.

Makharashvili, N., Koroleva, O., Bera, S., Grandgenett, D. P. & Korolev, S. (2004) A novel structure of DNA repair protein RecO from Deinococcus radiodurans. *Structure.* **12,** 1881-1889.

Markillie, L. M., Varnum, S. M., Hradecky, P. & Wong, K. K. (1999) Targeted mutagenesis by duplication insertion in the radioresistant bacterium Deinococcus radiodurans: radiation sensitivities of catalase (katA) and superoxide dismutase (sodA) mutants. *J. Bacteriol.* **181,** 666-669.

Mattimore, V. & Battista, J. R. (1996) Radioresistance of Deinococcus radiodurans: functions necessary to survive ionizing radiation are also necessary to survive prolonged desiccation. *J. Bacteriol.* **178,** 633-637.

McGuffin, L. J., Bryson, K. & Jones, D. T. (2000) The PSIPRED protein structure prediction server. *Bioinformatics.* **16,** 404-405.

Minton, K. W. (1994) DNA repair in the extremely radioresistant bacterium Deinococcus radiodurans. *Mol. Microbiol.* **13,** 9-15.

Minton, K. W. & Daly, M. J. (1995) A model for repair of radiation-induced DNA double-strand breaks in the extreme radiophile Deinococcus radiodurans. *Bioessays.* **17,** 457-464.

Misra, H. S., Khairnar, N. P., Kota, S., Shrivastava, S., Joshi, V. P. & Apte, S. K. (2006) An exonuclease I-sensitive DNA repair pathway in Deinococcus radiodurans: a major determinant of radiation resistance. *Mol. Microbiol.* **59,** 1308-1316.

Mitchel, R. E. (1978) The radiation-releasable cell wall nuclease of Micrococcus radiodurans. Purification and properties of the native enzyme. *Biochim. Biophys. Acta.* **524,** 362-372.

Moeller, R., Douki, T., Rettberg, P., Reitz, G., Cadet, J., Nicholson, W. L. & Horneck, G. (2010) Genomic bipyrimidine nucleotide frequency and microbial reactions to germicidal UV radiation. *Arch. Microbiol.* **192,** 521-529.

Morris, G. M., Huey, R., Lindstrom, W., Sanner, M. F., Belew, R. K., Goodsell, D. S. & Olson, A. J. (2009) AutoDock4 and AutoDockTools4: Automated docking with selective receptor flexibility. *J. Comput. Chem.* **30,** 2785-2791.

Mortensen, U. H., Lisby, M. & Rothstein, R. (2009) Rad52. *Current Biology.* **19,** R676-R677.

Moseley, B. E. & Evans, D. M. (1983) Isolation and properties of strains of Micrococcus (Deinococcus) radiodurans unable to excise ultraviolet light-induced pyrimidine dimers from DNA: evidence for two excision pathways. *J. Gen. Microbiol.* **129,** 2437-2445.

Murakami, M., Narumi, S., Satoh, K., Furukawa, A. & Hayata, I. (2006) Analysis of interaction between DNA and Deinococcus radiodurans PprA protein by atomic force microscopy. *Biochim. Biophys. Acta.* **1764,** 20-23.

Muskavitch, K. M. & Linn, S. (1982) A unified mechanism for the nuclease and unwinding activities of the recBC enzyme of Escherichia coli. *J. Biol. Chem.* **257,** 2641-2648.

Narumi, I., Satoh, K., Cui, S., Funayama, T., Kitayama, S. & Watanabe, H. (2004) PprA: a novel protein from Deinococcus radiodurans that stimulates DNA ligation. *Mol. Microbiol.* **54,** 278-285.

Narumi, I., Satoh, K., Kikuchi, M., Funayama, T., Kitayama, S., Yanagisawa, T., Watanabe, H. & Yamamoto, K. (1999) Molecular analysis of the Deinococcus radiodurans recA locus and identification of a mutation site in a DNA repair-deficient mutant, rec30. *Mutat. Res.* **435,** 233-243.

Norais, C., Servant, P., Bouthier de la Tour, C., Coureux, P. D., Ithurbide, S., Vannier, F., Guerin, P. P., Dulberger, C. L., Satyshur, K. A., Keck, J. L., Armengaud, J., Cox, M. M. & Sommer, S. (2013) The Deinococcus radiodurans DR1245 protein, a DdrB partner homologous to YbjN proteins and reminiscent of type III secretion system chaperones. *PloS one.* **8,** e56558.

Norais, C. A., Chitteni-Pattu, S., Wood, E. A., Inman, R. B. & Cox, M. M. (2009) DdrB protein, an alternative Deinococcus radiodurans SSB induced by ionizing radiation. *J. Biol. Chem.* **284,** 21402-21411.

Otwinowski, Z. & Minor, W. (1997). *Processing of X-Ray Diffraction Data Collected in Oscillation Mode,* edited by C. W. J. Carter & R. M. Sweet, pp. 307-326. New York: Academic Press.

Pardo, B., Gomez-Gonzalez, B. & Aguilera, A. (2009) DNA repair in mammalian cells: DNA double-strand break repair: how to fix a broken relationship. *Cell Mol. Life Sci.* **66,** 1039-1056.

Parsons, C. A., Baumann, P., Van Dyck, E. & West, S. C. (2000) Precise binding of a single-stranded DNA termini by human Rad52 protein. *EMBO J.* **19,** 4175-4181.

Passy, S. I., Yu, X., Li, Z., Radding, C. M. & Egelman, E. H. (1999) Rings and filaments of beta protein from bacteriophage lambda suggest a superfamily of recombinant proteins. *Proc. Natl. Acad. Sci. U. S. A.* **96,** 4279-4284.

Patel, S. S. & Picha, K. M. (2000) Structure and function of hexameric helicases. *Annu. Rev. Biochem.* **69,** 651-697.

Pestryakov, P. E. & Lavrik, O. I. (2008) Mechanisms of single-stranded DNA-binding protein functioning in cellular DNA metabolism. *Biochemistry (Mosc).* **73,** 1388-1404.

Pfeifer, G. P. (1997) Formation and processing of UV photoproducts: effects of DNA sequence and chromatin environment. *Photochem. Photobiol.* **65,** 270-283.

Ploquin, M., Bransi, A., Paquet, E. R., Stasiak, A. Z., Stasiak, A., Yu, X., Cieslinska, A. M., Egelman, E. H., Moineau, S. & Masson, J. Y. (2008) Functional and structural basis for a bacteriophage homolog of human Rad52. *Current Biology.* **18,** 1142-1146.

Poteete, A. R., Sauer, R. T. & Hendrix, R. W. (1983) Domain structure and quaternary organization of the bacteriophage P22 Erf protein. *J. Mol. Biol.* **171,** 401-418.

Potts, M. (1994) Desiccation tolerance of prokaryotes. *Microbiol. Rev.* **58,** 755-805.

Raghunathan, S., Kozlov, A. G., Lohman, T. M. & Waksman, G. (2000) Structure of the DNA binding domain of E. coli SSB bound to ssDNA. *Nat. Struct. Biol.* **7,** 648-652.

Repar, J., Cvjetan, S., Slade, D., Radman, M., Zahradka, D. & Zahradka, K. (2010) RecA protein assures fidelity of DNA repair and genome stability in Deinococcus radiodurans. *DNA Repair (Amst).* **9,** 1151-1161.

Roberts, V.A., Pique, M.E., Hsu, S., Li, S., Siupphaug, G., Rambo, R.P., Jamison, J.W., Liu, T., Lee, J.H., Tainer, J.A., Ten Eyck, L.F. & Woods, V.L. Jr. (2012) Combining H/D exchange mass spectroscopy and computational docking reveals extended DNA-binding surface on uracil-DNA glycosylase. *Nucleic Acids Research*. **40,** 6070-6081.

Roche, B., Aussel, L., Ezraty, B., Mandin, P. & Barras, F. (2013) Iron/sulfur proteins biogenesis in prokaryotes: Formation, regulation and diversity. *Biochim. Biophys. Acta.* **1827**, 455-469.

Rothernberg, E., Grimme, J. M. & Ha, T. (2008) Human Rad52-mediated homology search and annealing occurs by continuous interactions between overlapping nucleoprotein complexes. *Proc. Natl. Acad. Sci. U. S. A.* **105,** 20274-20279.

Saff, E. & Kuijlaars, A. (1997) Distributing many points on a sphere. *The Mathematical Intelligencer.* **19,** 5-11.

Sancar, A., Williams, K. R., Chase, J. W. & Rupp, W. D. (1981) Sequences of the ssb gene and protein. *Proc. Natl. Acad. Sci. U. S. A.* **78,** 4274-4278.

Schuck, P. (2003) On the analysis of protein self-association by sedimentation velocity analytical ultracentrifugation. *Anal. Biochem.* **320,** 104-124.

Schuck, P. (2000) Size-distribution analysis of macromolecules by sedimentation velocity ultracentrifugation and lamm equation modeling. *Biophys. J.* **78,** 1606-1619.

Servant, P., Jolivet, E., Bentchikou, E., Mennecier, S., Bailone, A. & Sommer, S. (2007) The ClpPX protease is required for radioresistance and regulates cell division after gamma-irradiation in Deinococcus radiodurans. *Mol. Microbiol.* **66,** 1231-1239.

Shashidhar, R., Kumar, S. A., Misra, H. S. & Bandekar, J. R. (2010) Evaluation of the role of enzymatic and nonenzymatic antioxidant systems in the radiation resistance of Deinococcus. *Can. J. Microbiol.* **56,** 195-201.

Shereda, R. D., Kozlov, A. G., Lohman, T. M., Cox, M. M. & Keck, J. L. (2008) SSB as an organizer/mobilizer of genome maintenance complexes. *Crit. Rev. Biochem. Mol. Biol.* **43,** 289-318.

Shi, I., Hallwyl, S. C., Seong, C., Mortensen, U., Rothstein, R. & Sung, P. (2009) Role of the Rad52 amino-terminal DNA binding activity in DNA strand capture in homologous recombination. *J. Biol. Chem.* **284,** 33275-33284.

Shukla, M., Chaturvedi, R., Tamhane, D., Vyas, P., Archana, G., Apte, S., Bandekar, J. & Desai, A. (2007) Multiple-stress tolerance of ionizing radiation-resistant bacterial isolates obtained from various habitats: correlation between stresses. *Curr. Microbiol.* **54,** 142-148.

Singleton, M. R., Wentzell, L. M., Liu, Y., West, S. C. & Wigley, D. B. (2002) Structure of the single-strand annealing domain of human RAD52 protein. *Proc. Natl. Acad. Sci. U. S. A.* **99,** 13492-13497.

Slade, D., Lindner, A. B., Paul, G. & Radman, M. (2009) Recombination and replication in DNA repair of heavily irradiated Deinococcus radiodurans. *Cell.* **136,** 1044-1055.

Slade, D. & Radman, M. (2011) Oxidative stress resistance in Deinococcus radiodurans. *Microbiol. Mol. Biol. Rev.* **75,** 133-191.

Song, L., Hobaugh, M. R., Shustak, C., Cheley, S., Bayley, H. & Gouaux, J. E. (1996) Structure of staphylococcal alpha-hemolysin, a heptameric transmembrane pore. *Science.* **274,** 1859-1866.

Sugawara, N., Ira, G. & Haber, J. E. (2000) DNA length dependence of the single-strand annealing pathway and the role of Saccharomyces cerevisiae RAD59 in double-strand break repair. *Mol. Cell Biol.* **20,** 5300-5309.

Sugiman-Marangos, S. & Junop, M. (2012) Crystallization of the DdrB-DNA complex from Deinococcus radiodurans. *Acta Crystallogr F.* **68,** 1534-1537.

Sugiman-Marangos, S. & Junop, M. S. (2010) The structure of DdrB from Deinococcus: a new fold for single-stranded DNA binding proteins. *Nucleic Acids Res.* **38,** 3432-3440.

Sugiyama, T., Kantake, N., Wu, Y. & Kowalczykowski, S. C. (2006) Rad52-mediated DNA annealing after Rad51-mediated DNA strand exchange promotes second ssDNA capture. *EMBO J.* **25,** 5539-5548.

Suhrer, S. J., Wiederstein, M., Gruber, M. & Sippl, M. J. (2009) COPS--a novel workbench for explorations in fold space. *Nucleic Acids Res.* **37,** W539-544.

Sweet, D. M. & Moseley, B. E. (1976) The resistance of Micrococcus radiodurans to killing and mutation by agents which damage DNA. *Mutat. Res.* **34,** 175-186.

Tanaka, M., Earl, A. M., Howell, H. A., Park, M. J., Eisen, J. A., Peterson, S. N. & Battista, J. R. (2004) Analysis of Deinococcus radiodurans's transcriptional response to ionizing radiation and desiccation reveals novel proteins that contribute to extreme radioresistance. *Genetics.* **168,** 21-33.

Tanaka, M., Narumi, I., Funayama, T., Kikuchi, M., Watanabe, H., Matsunaga, T., Nikaido, O. & Yamamoto, K. (2005) Characterization of pathways dependent on the uvsE, uvrA1, or uvrA2 gene product for UV resistance in Deinococcus radiodurans. *J. Bacteriol.* **187,** 3693-3697.

Theobald, D. L., Mitton-Fry, R. M. & Wuttke, D. S. (2003) Nucleic acid recognition by OB-fold proteins. *Annu. Rev. Biophys. Biomol. Struct.* **32,** 115-133.

Thresher, R. J., Markhov, A. M., Hall, S. D., Kolodner, R. & Griffith, J. D. (1995) Electron microscopic visualization of RecT protein and its complexes with DNA. *J. Mol. Biol.* **254,** 364-371.

Tian, B., Wu, Y., Sheng, D., Zheng, Z., Gao, G. & Hua, Y. (2004) Chemiluminescence assay for reactive oxygen species scavenging activities and inhibition on oxidative damage of DNA in Deinococcus radiodurans. *Luminescence.* **19,** 78-84.

Timmins, J., Leiros, I. & McSweeney, S. (2007) Crystal structure and mutational study of RecOR provide insight into its mode of DNA binding. *EMBO J.* **26,** 3260-3271.

Tolun, G., Makhov, A. M., Ludtke, S. J. & Griffith, J. D. (2013) Details of ssDNA annealing revealed by an HSV-1 ICP8-ssDNA binary complex. *Nucleic Acids Res.* **41,** 5927-5937.

Tsang, S. S., Muniyappa, K., Azhderian, E., Gonda, D. K., Radding, C. M., Flory, J. & Chase, J. W. (1985) Intermediates in homologous pairing promoted by recA protein. Isolation and characterization of active presynaptic complexes. *J. Mol. Biol.* **185,** 295-309.

Udupa, K. S., O'Cain, P. A., Mattimore, V. & Battista, J. R. (1994) Novel ionizing radiation-sensitive mutants of Deinococcus radiodurans. *J. Bacteriol.* **176,** 7439-7446.

Varghese, A. J. & Day, R. S.,3rd. (1970) Excision of cytosine-thymine adduct from the DNA of ultraviolet-irradiated Micrococcus radiodurans. *Photochem. Photobiol.* **11,** 511-517.

Vukovic-Nagy, B., Fox, B. W. & Fox, M. (1974) The release of a deoxyribonucleic acid fragment after x-irradiation of Micrococcus radiodurans. *Int. J. Radiat. Biol. Relat. Stud. Phys. Chem. Med.* **25,** 329-337.

Weiner, J. H., Bertsch, L. L. & Kornberg, A. (1975) The deoxyribonucleic acid unwinding protein of Escherichia coli. Properties and functions in replication. *J. Biol. Chem.* **250,** 1972-1980.

Weng, M. W., Zheng, Y., Jasti, V. P., Champeil, E., Tomasz, M., Wang, Y., Basu, A. K. & Tang, M. S. (2010) Repair of mitomycin C mono- and interstrand cross-linked DNA adducts by UvrABC: a new model. *Nucleic Acids Res.* **38,** 6976-6984.

White, O., Eisen, J. A., Heidelberg, J. F., Hickey, E. K., Peterson, J. D., Dodson, R. J., Haft, D. H., Gwinn, M. L., Nelson, W. C., Richardson, D. L., Moffat, K. S., Qin, H., Jiang, L., Pamphile, W., Crosby, M., Shen, M., Vamathevan, J. J., Lam, P., McDonald, L., Utterback, T., Zalewski, C., Makarova, K. S., Aravind, L., Daly, M. J.,

Minton, K. W., Fleischmann, R. D., Ketchum, K. A., Nelson, K. E., Salzberg, S., Smith, H. O., Venter, J. C. & Fraser, C. M. (1999) Genome sequence of the radioresistant bacterium Deinococcus radiodurans R1. *Science.* **286,** 1571-1577.

Winn, M. D., Ballard, C. C., Cowtan, K. D., Dodson, E. J., Emsley, P., Evans, P. R., Keegan, R. M., Krissinel, E. B., Leslie, A. G., McCoy, A., McNicholas, S. J., Murshudov, G. N., Pannu, N. S., Potterton, E. A., Powell, H. R., Read, R. J., Vagin, A. & Wilson, K. S. (2011) Overview of the CCP4 suite and current developments. *Acta Crystallogr D Biol Crystallogr.* **67,** 235-242.

Wu, Y., Sugiyama, T. & Kowalczykowski, S. C. (2006) DNA annealing mediated by Rad52 and Rad59 proteins. *J. Biol. Chem.* **281,** 15541-15449.

Xu, G., Lu, H., Wang, L., Chen, H., Xu, Z., Hu, Y., Tian, B. & Hua, Y. (2010) DdrB stimulates single-stranded DNA annealing and facilitates RecA-independent DNA repair in Deinococcus radiodurans. *DNA Repair (Amst).* **9,** 805-812.

Xu, G., Wang, L., Chen, H., Lu, H., Ying, N., Tian, B. & Hua, Y. (2008) RecO is essential for DNA damage repair in Deinococcus radiodurans. *J. Bacteriol.* **190,** 2624-2628.

Xu, W., Shen, J., Dunn, C. A., Desai, S. & Bessman, M. J. (2001) The Nudix hydrolases of Deinococcus radiodurans. *Mol. Microbiol.* **39,** 286-290.

Yamada, M., Satoh, K. & Narumi, I. (2010) Purification, crystallization and preliminary X-ray diffraction analysis of DNA damage response A protein from Deinococcus radiodurans. *Acta Crystallogr F.* **66,** 1614-1616.

Yang, Y., Wang, H. & Erie, A. (2003) Quantitative characterization of biomolecular assemblies and interactions using atomic force microscopy. *Methods.* **29,** 175-187.

Yang, J. M. & Tung, C. H. (2006) Protein structure database search and evolutionary classification. *Nucleic Acids Res.* **34,** 3646-3659.

Yuan, M., Chen, M., Zhang, W., Lu, W., Wang, J., Yang, M., Zhao, P., Tang, R., Li, X., Hao, Y., Zhou, Z., Zhan, Y., Yu, H., Teng, C., Yan, Y., Ping, S., Wang, Y. & Lin, M. (2012) Genome sequence and transcriptome analysis of the radioresistant bacterium Deinococcus gobiensis: insights into the extreme environmental adaptations. *PLoS One.* **7,** e34458.

Zahradka, K., Slade, D., Bailone, A., Sommer, S., Averbeck, D., Petranovic, M., Lindner, A. B. & Radman, M. (2006) Reassembly of shattered chromosomes in Deinococcus radiodurans. *Nature.* **443,** 569-573.

Zhao, H., Ghirlando, R., Piszczek, G., Curth, U., Brautigam, C. A. & Schuck, P. (2013) Recorded scan times can limit the accuracy of sedimentation coefficients in analytical ultracentrifugation. *Anal. Biochem.* **437,** 104-108.

Zhao, H. & Shuck, P. (2012) Global multi-method analysis of affinities and cooperativity in complex systems of macromolecular interactions. *Analytical Chemistry.* **84**, 9513-9519.

Zhou, Q., Zhang, X., Xu, H., Xu, B. & Hua, Y. (2007) A new role of Deinococcus radiodurans RecD in antioxidant pathway. *FEMS Microbiol. Lett.* **271,** 118-125.

Zhu, Z. Y. & Karlin, S. (1996) Clusters of charged residues in protein three-dimensional structures. *Proc. Natl. Acad. Sci. U. S. A.* **93,** 8350-8355.

Zimmerman, J. M. & Battista, J. R. (2005) A ring-like nucleoid is not necessary for radioresistance in the Deinococcaceae. *BMC Microbiol.* **5,** 17.

APPENDIX

Table A.1 – Data collection and model refinement statistics for the un-optimized "overlapping" substrate complex ($DdrB_{Dr}$/AS1-AS2).

Data Collection		**Model and refinement**	
Space group	$P3_221$	Resolution (Å)[a]	46.00 - 2.85 (2.93 – 2.85)
Unit cell parameters		R_{work}/R_{free} (%)	24.8/28.1
a,b,c (Å)	76.8, 76.8, 254.8	$Reflections_{observed}$	21,024
Molecules in ASU	7	$Reflections_{Rfree}$	1,986
Resolution range (Å)[a]	50.00 – 2.85 (2.90 - 2.85)	No. atoms	
Observed reflections	197,203	Protein	5,186
Unique reflections[a]	21,100 (1,023)	DNA	469
Redundancy[a]	9.3 (7.8)	Water	58
Completeness (%)[a]	100.0 (100.0)	R.m.s.d. bond	
I/σ(I)[a]	16.5 (2.5)	Lengths (Å)	0.010
R_{meas} (%)[a]	11.8 (87.9)	Angles (°)	1.811
Wilson B Factor (Å^2)	76.9	Average B Factor (Å^2)	58.54

[a] Statistics for the highest resolution shell are shown in parentheses.

Table A.2 List of all constructs

Plasmid (MJ#)	Construct	Comments	Plasmid (MJ#)	Construct	Comments
4606	Dgeo2628	6H-M-T	4972	$DR0070_{Y125A}$	6H-T, CO
4607	$Dgeo2628_{26-302}$	6H-T	4973	$DR0070_{R132A}$	6H-T, CO
4608	Dgeo0295	6H-T	4974	$DR0070_{R135A}$	6H-T, CO
4615	$Dgeo0295_{1-113}$	6H-T	4975	$DR0070_{A147C}$	6H-T, CO
4724	SSB_{Dg}	6H-T, NE	5005	DR0070	pJET, CO
4726	$DR0070_{W66A}$	6H-T, CO	5006	$DR0070_{E51A}$	pJET, CO
4728	$DR0070_{R64A}$	6H-T, CO	5007	$DR0070_{W66A}$	pJET, CO
4730	DR0070	6H-T, CO	5008	$DR0070_{R83A}$	pJET, CO
4733	SSB_{Dr}	6H-T, NE	5009	$DR0070_{Y125A}$	pJET, CO
4735	$0295_{R83/85/93Q}$	6H-T, CO	5010	p13421 (P.S.)	SV
4737	$Dgeo0295_{1-172}$	6H-T	5011	DR0070	SV, CO, NE
4738	$Dgeo0295_{R64Q}$	6H-T	5012	$DR0070_{E51A}$	SV, CO, NE
4739	$Dgeo0295_{W66A}$	6H-T	5013	$DR0070_{W66A}$	SV, CO, NE
4740	$Dgeo0295_{R83Q}$	6H-T	5014	$DR0070_{R83A}$	SV, CO, NE
4741	$Dgeo0295_{R85Q}$	6H-T	5029	$DR0070_{Y125A}$	SV, CO, NE
4742	$Dgeo0295_{R93Q}$	6H-T	5030	$DR0070_{E51/86A}$	6H-T, CO
4747	$DR0070_{1-125}$	6H-T, NE	5031	$DR0070_{E51/86/88A}$	6H-T, CO
4748	$DR0070_{1-144}$	6H-T	5032	$DR0070_{E51/86/D91A}$	6H-T, CO
4749	$DR0070_{1-174}$	6H-T	5033	$DR0070_{L95A}$	6H-T, CO
4783	$DR0070_{1-140}$	6H-T, NE	5034	$DR0070_{L95/97A}$	6H-T, CO
4958	$DR0070_{Q47A}$	6H-T, CO	5035	$DR0070_{L87A/Y125A}$	6H-T, CO
4959	$DR0070_{E51A}$	6H-T, CO	5036	$DR0070_{R85A}$	SV, CO, NE
4960	$DR0070_{R64A}$	6H-T, CO	5037	$DR0070_{K102A}$	SV, CO, NE
4961	$DR0070_{R83A}$	6H-T, CO	5038	$DR0070_{R85A}$	pJET, CO
4962	$DR0070_{R85A}$	6H-T, CO	5039	$DR0070_{K102A}$	pJET, CO
4963	$DR0070_{E86A}$	6H-T, CO	5047	DR0069	pJET
4964	$DR0070_{E88A}$	6H-T, CO	5048	DR0069-70	SV, CO, NE
4965	$DR0070_{D91A}$	6H-T, CO	5049	$DR0069\text{-}70_{E51A}$	SV, CO, NE
4966	$DR0070_{R93A}$	6H-T, CO	5050	$DR0069\text{-}70_{W66A}$	SV, CO, NE
4967	$DR0070_{K94A}$	6H-T, CO	5051	$DR0069\text{-}70_{R83A}$	SV, CO, NE
4968	$DR0070_{K96A}$	6H-T, CO	5052	$DR0069\text{-}70_{R85A}$	SV, CO, NE
4969	$DR0070_{K102A}$	6H-T, CO	5053	$DR0069\text{-}70_{K102A}$	SV, CO, NE
4970	$DR0070_{R105A}$	6H-T, CO	5054	$DR0069\text{-}70_{Y125A}$	SV, CO, NE
4971	$DR0070_{K108A}$	6H-T, CO			

Abbreviations – 6His-tag-Maltose binding protein-TEV cleavage site (6H-M-T), 6His-tag-TEV cleavage site (6H-T), no expression (NE), codon optimized (CO), *E.coli/D. radiodurans* shuttle vector (SV), pJET1.2 blunt cloning vector (pJET), PprA from *D. geothermalis* (Dgeo2628), DdrB from *D. geothermalis* (Dgeo0295), and *D. radiodurans* (DR0070). MJ5010 was a generous gift from Dr. Pascale Servant.

Peer-reviewed publications by S.N. Sugiman-Marangos

Sugiman-Marangos, S., Peel, J., Weiss, Y., Ghirlando, R. & Junop, M.S. (2013) Crystal structure of the DdrB/ssDNA complex from *Deinococcus radiodurans* reveals a DNA binding surface involving higher-order oligomeric states. *Nucleic Acids Research*, in press.

Sugiman-Marangos, S. & Junop, M. (2012) Crystallization of the DdrB-DNA complex from *Deinococcus radiodurans*. *Acta Crystallogr. Sect. F.* **68**, 1534-1537.

Stone, C.B., **Sugiman-Marangos, S.**, Bulir, D.C., Clayden, R.C., Leighton, T.L., Slootstra, J.W., Junop, M.S. & Mahony, J.B. (2012) Structural characterization of a novel *Chlamydia pneumonia* type III secretion-associated protein Cpn0803. *PLoS One.* **7**, e30220.

Jackson, S., **Sugiman-Marangos, S.**, Cheung, K. & Junop, M. (2011) Crystallization and preliminary diffraction analysis of truncated human pleckstrin. *Acta Crystallogr. Sect. F.* **67**, 412-416.

Sugiman-Marangos, S. & Junop, M.S. (2010) The structure of DdrB from *Deinococcus*: a new fold for single-stranded DNA binding proteins. *Nucleic Acids Res.* **38,** 3432-3440.

Taylor, P.L., **Sugiman-Marangos, S.**, Zhang, K., Valvano, M.A., Wright, G.D. & Junop, M.S. (2010) Structural and kinetic characterization of the LPS biosynthetic enzyme D-alpha,beta-D-heptose-1,7-bisphosphate phosphatase (GmhB) from *Escherichia coli*. *Biochemistry.* **49,** 1033-1041.

Gao, B., **Sugiman-Marangos, S.**, Junop, M.S. & Gupta, R.S. (2009) Structural and phylogenetic analysis of a conserved actinobacteria-specific protein (ASP1;SCO1997) from *Streptomyces coelicolor*. *BMC Struct. Biol.* **9,** 40.

Submitted and in-review

Neal, J., **Sugiman-Marangos, S.**, VanderVere-Carozza, P., Wagner, M., Turchi, J., Lees-Miller, S., Junop, M.S. & Meek, K. (2013) Unraveling the complexities of DNA-PK autophosphorylation. Submitted to *Molecular and Cellular Biology* on July 2, 2013.

Fowler, C.C., **Sugiman-Marangos, S.**, Junop, M.S., Brown, E.D. & Li, Y. (2013) Exploring intermolecular interactions of a substrate-binding protein using a riboswitch-based sensor. Submitted to *The Journal of Biological Chemistry* on January 21, 2013.

List of PDB depositions by S.N. Sugiman-Marangos

4IQZ – The structure of a large insert in RNA polymerase (RpoC) subunit from *E. coli* (2013).

4IPU, 4IPV – Crystal structure of *P. aeruginosa* (PAO1) type IV minor pilin FimU (2013).

4HQB – Crystal structure of DdrB from *D. radiodurans* bound to ssDNA (2012).

3Q9D – Crystal structure of Cpn0803 from *C. pneumoniae* (2011).

4EXW – Crystal structure of DdrB from *D. geothermalis* (2010).

3L1U – Crystal structure of Calcium-bound GmhB from *E. coli* (2010).

3L1V – Crystal structure of GmhB from *E. coli* in complex with calcium and phosphate (2010).

3E35 – Actinobacteria-specific protein of unknown function, SCO1997 (2009).

HOLD – Crystal structure of DdrB from *D. radiodurans* with ssDNA bound to the 'top' face of the pentamer.

HOLD –Structure of pathogenicity island-2 T3SS ATPase (SsaN) from *Salmonella*.

HOLD – Crystal structures of GmhA from *E. coli* in complex with 3 novel inhibitors.

HOLD – Crystal structure of HldA from *B. cenocepacia.*

HOLD – Crystal structure of NeuB from *N. meningitis*.

HOLD – Crystal structure of SCO1662 from *S. coelicolor*.

HOLD – Crystal structure of HldE C-terminal domain from *C. rodentium*.

HOLD – Crystal structure of SCO3367 from *S. coelicolor*.